Fatigue Testing and Design of Large Diameter Shear Studs Used in Highway Bridges

by

Daniel Lee Mundie

A thesis submitted to the Graduate Faculty of
Auburn University
in partial fulfillment of the
requirements for the Degree of
Master of Science

Auburn, AL
August 6, 2011

Keywords: Studs, shear strength, push-out test, fatigue tests

Copyright 2011 by Daniel Lee Mundie

Approved by

Hassan H. Abbas, Chair, Assistant Professor of Civil Engineering
J. Michael Stallings, Professor of Civil Engineering
G. Ed Ramey, Professor Emeritus of Civil Engineering

Abstract

Headed studs are commonly used to transfer shear forces along the interface of the steel beam and concrete deck in composite highway bridge girders. Typical stud diameters used in composite bridge design are less than 1". Because of the need for bridge decks to be replaced quickly, using fewer studs with larger diameter (1¼") would be beneficial in accelerating the construction. Before being put into use, these large diameter studs must be tested to ensure that they perform adequately and meet current fatigue design provisions in AASHTO LRFD (2007).

An experimental test program was carried out that tested a total of 24 push-out specimens. Twelve specimens had shear studs with a large diameter of 1¼", and the other twelve had shear studs with a standard diameter of $^{7}/_{8}$". Shear stress ranges of 18, 22, and 26 ksi were used. Based on the research presented in this thesis, the 1¼"-diameter studs performed equally as well as the $^{7}/_{8}$"-diameter studs and can safely be designed using the current fatigue design provisions of AASHTO LRFD (2007).

Acknowledgements

First of all I would like to thank the Alabama Department of Transportation (ALDOT), the Auburn University Highway Research Center (HRC), and FabArc Steel Supply for their financial support of this research. I would also like to thank my advisory committee consisting of Dr. Hassan H. Abbas, Dr. G. Ed Ramey, and Dr. J. Michael Stallings for their continuous guidance, support, and knowledge that they have shared with me throughout this research. Thanks to the large number of both graduate and undergraduate assistants who assisted me in pouring concrete and setting up each test in the lab.

Next, I would like to thank my parents, Don and Lynn Mundie, and my in-laws, Temple and Jenny Anderson for encouraging and supporting me in my graduate studies. A special thanks goes out to my loving and beautiful wife, Katie Anderson Mundie, for always being there for me and being my biggest supporter by far. She is the best mother to my children that I could ever ask for, and she always believes in me and knows that I can do anything I put my mind to.

Table of Contents

List of Tables

List of Figures

Chapter 1 INTRODUCTION

1.1 Overview

Highway bridges that are composed of a concrete deck on top of steel girders are often designed to achieve composite action, meaning that under a given load the steel girder and concrete deck act as a single unit rather than acting independently. This composite action is typically achieved by using shear connectors. Although steel channels have been used in the past as shear connectors, the term shear connectors is now generally accepted to mean headed studs attached to steel beams using a drawn-arc stud welding process (Champney and Hsu 2009). Standard diameter studs usually refers to those with a diameter less than or equal to 1" while large diameter studs usually refers to those with a diameter greater than 1". Studs used in composite bridges are usually either ¾" or $^{7}/_{8}$" in diameter. In bridges with high shear, up to four $^{7}/_{8}$" headed studs may be required across the flange in order to meet design requirements (Badie et al. 2002). Figure 1-1 illustrates that for certain bridges the number of required studs can be rather large leading to the congested appearance shown in the figure. The use of 1¼"-diameter studs has been recently proposed as a means of reducing the number of shear studs (Badie et al. 2002). The cross-sectional area of a single 1¼"-diameter stud is approximately equal to the cross-sectional area of two $^{7}/_{8}$"-diameter studs or three ¾"-diameter studs.

There are many advantages to using 1¼" shear studs as opposed to either of the smaller diameter studs, the most important of which is saving time and labor. Since there will be fewer shear studs, there will be less shop or field welding required during the fabrication process. In situations where the concrete deck has deteriorated and rehabilitation is necessary, having a large

number of shear studs could slow down the process of removing the old deck. In situations of new construction, the number of studs required would be significantly reduced. Lastly, if large diameter studs are used, there will be fewer studs welded across the flange which would increase the safety of construction workers in the field by reducing the risk of tripping. Currently, the use of 1¼"-diameter studs is not allowed by the AASHTO LRFD Bridge Design Specifications (AASHTO 2007), primarily due to the lack of design criteria.

Figure 1-1 Welded Shear Studs on Cooper River Bridge (Champney and Hsu 2009)

1.2 Motivation

The Alabama Department of Transportation (ALDOT) maintains interstate bridges in the state of Alabama that have large numbers of annual average daily traffic (AADT). Some of the concrete decks of these bridges are in need of being replaced, but ALDOT wants to minimize the interruption of traffic as much as possible. When performing rapid deck replacement, having 1¼"-diameter studs in the existing deck would make deck removal easier. For new bridge

construction, using 1¼"-diameter studs would require about half as many studs therefore increasing the speed of construction. Before these large diameter studs can be implemented, fatigue testing must be done to determine design criteria of the new 1¼"-diameter shear studs.

1.3 Research Objectives

The objectives of this research project were as follows:

- Generate experimental data that can be used to assess the fatigue life for 1¼"-diameter stud-type shear connectors
- Propose fatigue design criteria for 1¼"-diameter shear studs

1.4 Tasks

In order to achieve the objectives of this research, the following tasks were carried out:

1. Review previous research related to fatigue of shear connectors
2. Develop a test plan
3. Design and fabricate test specimens
4. Develop instrumentation, monitoring, and loading plans
5. Perform the tests
6. Analyze the test data
7. Propose design recommendations for large diameter shear studs

1.5 Scope and Approach

The research described in this thesis is limited to welded, headed stud shear connectors as applied to highway bridge structures. The thesis does not include information or research on the use of steel channels or non-headed studs as shear connectors.

It was determined that in order to get a fair comparison between $^{7}/_{8}$"-diameter and 1¼"-diameter studs, both should be tested in the same test program under the same conditions. Although standard test setups have been proposed for fatigue testing of shear connectors, there are always slight differences in the test programs. By testing both standard and large diameter studs in the same test program, a fair comparison could be made.

1.6 Thesis Organization

This thesis is organized into six chapters. Chapter 1 gives an introduction, lays out the objectives of this research, and explains the approach to be used to accomplish the objectives. Chapter 2 provides a background on fatigue in general and how it relates to steel structures, gives an overview of the purpose and use of shear studs, and reviews similar test programs that have been carried out to quantify the fatigue life of shear studs. Chapter 3 details the test program that was used including test matrix, specimen fabrication, instrumentation, and testing procedure used in the experimental program. Chapter 4 presents the results that were gathered as a result of testing including relative slip data as well as pictures documenting the various failure modes that were seen in the different tests. Chapter 5 consists of analysis of the results in the context of a stress range vs. number of cycles relationship, commonly referred to as an S-N curve. This chapter also includes a comparison of the test data with other design codes. Chapter 6 provides a

summary of the research findings, conclusions that were made, and recommendations for design criteria of the 1¼"-diameter shear studs.

Chapter 2 BACKGROUND AND LITERATURE REVIEW

2.1 Overview

The following chapter will give an overview of the phenomenon of fatigue in steel with an emphasis on how it applies to stud shear connectors. It will give an overview of the purpose of shear studs and how they can be used to make a steel-concrete composite member behave more efficiently. Next, a comparison of fatigue design criteria will be made between the AASHTO LRFD Bridge Design Specifications (AASHTO 2007), the Eurocode 4 (CEN 2005), the Japanese Society of Civil Engineers (JSCE 2009), and the BS 5400 (BSI 1980).

This chapter will also give a comprehensive literature review of test data on the fatigue life of stud shear connectors. All of the results that will be reviewed in this section were performed on push-out test specimens. Push-out specimens are smaller in size and are a much simpler and cheaper way to test shear studs than testing full size composite beams. They consist of a short steel section with shear studs that were welded using a drawn-arc welding process of a stud gun to attach the studs. Concrete slabs are then poured occasionally on one but most often both sides of the steel section to represent the concrete deck in a bridge girder. These push-out specimens have been shown to give conservative results compared to full scale beam tests and therefore have a built in safety factor when using these results for design (Slutter and Fisher 1966). Figure 2-1 is taken from Eurocode 4 (CEN 2005) and gives recommendations on the geometry that can be used for push-out tests.

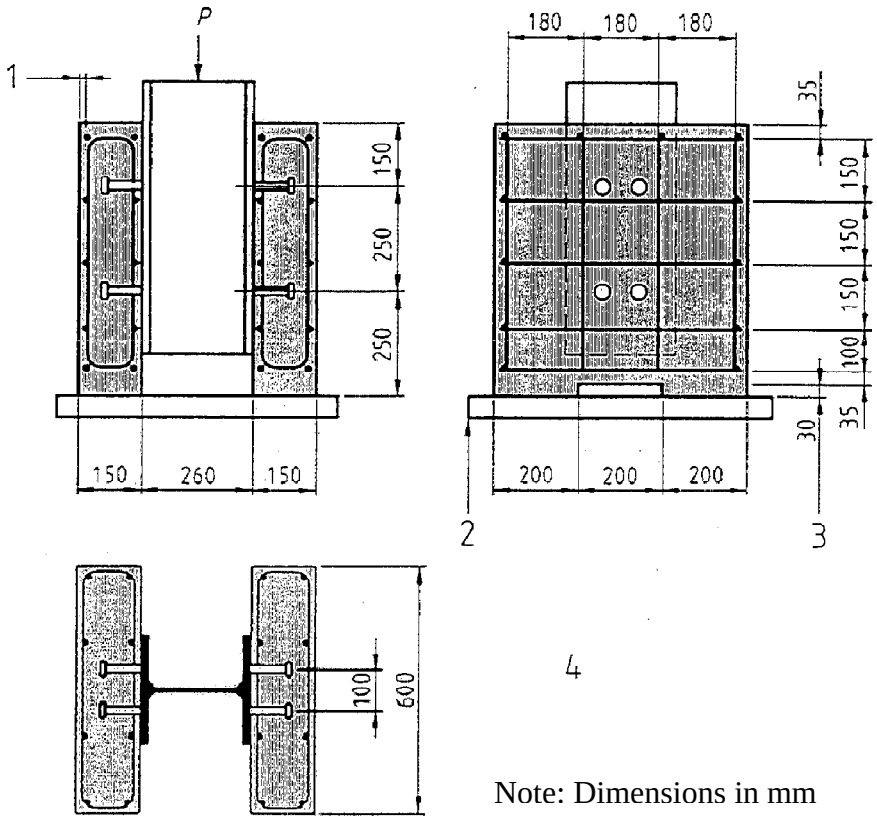

Note: Dimensions in mm

Key

1 cover 15 mm

2 bedded in mortar or gypsum

3 recess optional

4 reinforcement: ribbed bars ϕ 10 mm resulting in a high bond with $450 \leq f_{sk} \leq 550$ N/mm^2
steel section: HE 260 B or 254 x 254 x 89 kg. UC

Figure 2-1 Standard Push-Out Specimen Geometry (Eurocode 4 (CEN 2005))

2.2 Fatigue of Steel

Fatigue in metals is a process by which cracks initiate and grow under cyclic loading. If the crack is allowed to propagate for a long duration, failure of the member can occur when the remaining effective area of the component has been reduced enough so that it is unable to carry the internal forces being imposed on the system (Fisher et al. 1998). Different materials behave differently under cyclic loading, but fatigue has become a major concern for steel structures.

Steel bridges are the most common civil engineering structures that are susceptible to fatigue cracking. Early steel bridges were designed and fabricated by using mechanical fasteners such as rivets which were later followed by the use of high-strength bolts. Fatigue cracking was rare not only because these connection details had small initial imperfections, but the number of cycles seen by these early bridges was very low compared to the present. When welding became a more common form of steel fabrication in the 1950's, fatigue became an increasingly larger problem for two reasons. The welding process produces a much more severe initial defect than does mechanical fastening, and connecting the materials by means of welding gave the possibility of the fatigue crack propagating uninhibited through to the next element (Fisher et al. 1998). Fatigue is broken down into three stages of crack initiation, crack propagation, and failure which will be elaborated on in this chapter.

2.2.1 Crack Initiation

Laboratory tests have shown that all fatigue cracks start at an initial defect or discontinuity. Although the surface of a steel component may look flawless before cyclic loading begins, there are many flaws that may lie within the weld itself. This can include but is not limited to partial penetration, lack of fusion, porosities, microflaws at the weld toe, and inclusions around a weld repair. Complete elimination of these types of flaws is not practical and therefore it must be the responsibility of the welder/fabricator as well as the inspector to minimize these conditions.

2.2.2 Crack Propagation

Once the fatigue crack has been initiated, the propagation stage begins. This is when the crack front grows under each subsequent load cycle. The crack front is initially sharp and therefore causes very high stress concentrations at that point and plastic deformations occur locally at that location (Fisher et al. 1998). As the crack front grows with every cycle, evidence of the crack growth is left behind in the form of striations, or microscopic lines that can be used to determine the initiation point as well as the direction of propagation.

The crack propagation stage is the most important when determining how often to inspect steel structures for fatigue cracks. By documenting the size of the crack and the crack length, inspectors can get some insight into how much longer the structure can be in service before some rehabilitation must be performed. To determine the amount of time between inspections, the cracks are assumed to be the largest possible that are still undetectable. The amount of time for that crack to grow to a point where the strength of the structure is compromised is used as the inspection period (Bro and Westberg 2004).

2.2.3 Failure

Failure usually occurs in one of two ways. The first is when the reduction of the cross-sectional area by crack propagation leaves a small enough area that the load cannot be carried by the remaining uncracked section alone. This usually results in yielding of the remaining material (Fisher et al. 1998). Evidence of this type of failure can be seen when looking at the fracture surface. The smooth dull colored region of the fracture surface is due to fatigue cracks whereas the bright shiny and irregular surface is due to the ductile, forced failure at the end of the test (Bro and Westberg 2004). The second failure mode is a brittle failure that occurs when a crack

reaches a critical size under certain conditions such as material toughness, temperature, and loading rate.

2.3 Shear Studs

Since the idea and invention of cold formed headed shear connector studs in 1955 by R.C. Singleton of Nelson Stud Welding, headed studs have almost completely taken the place of other shear connectors, such as channels, as the method used in composite construction (Champney and Hsu 2009). The idea behind using shear studs is to reduce the amount of slip between the concrete slab and steel beam. Without shear studs, the concrete and steel have a tendency to deform independently resulting in what is known as slip as shown in Figure 2-2. In composite construction, the interaction between steel and concrete can be classified as non-composite, full composite, or partial composite action. These three scenarios are described in more detail below.

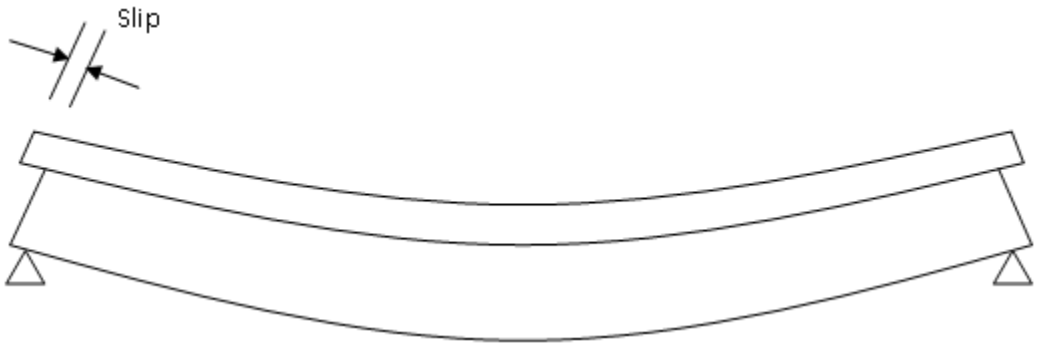

Figure 2-2 Independent Deformation of Two Materials

2.3.1 Non-Composite

A beam that consists of concrete and steel used together but has no means of positively connecting the two materials is commonly referred to as non-composite. An advantage of this type of construction is that a large amount of time and money could be saved by not designing,

purchasing, and installing hundreds or thousands of shear studs on the top of the beam flanges. However, one of the most significant disadvantages is that the concrete must resist tension forces and the steel must resist compression forces, neither of which are ideal situations for each material individually. Because of this disadvantage, it is possible that a thicker concrete slab as well as a larger steel beam might have to be designed which increases the total weight of the structure. A typical strain diagram for non-composite beams can be seen in Figure 2-3.

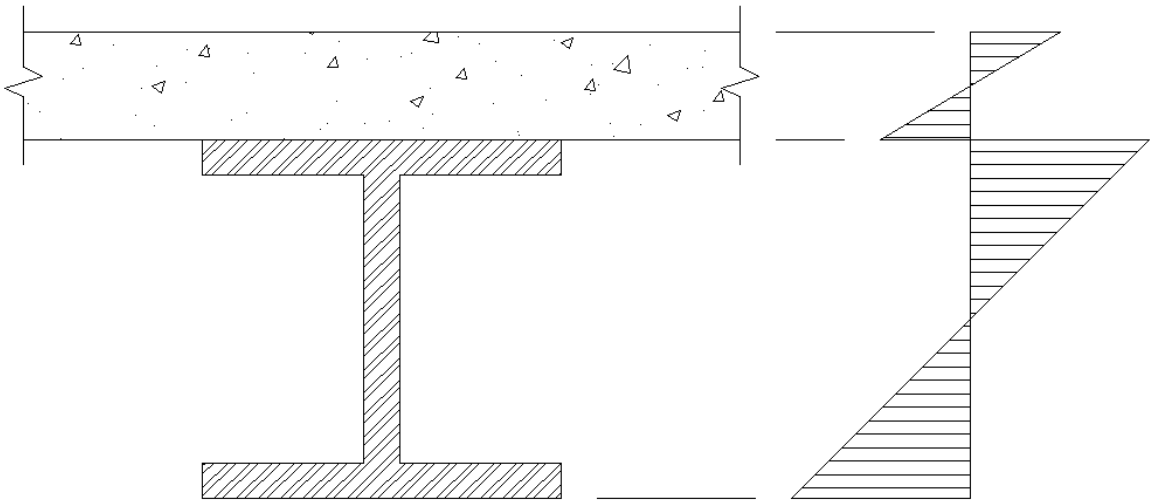

Figure 2-3 Strain Diagram for Non-Composite Action

2.3.2 Full Composite Action

Full composite action is achieved when a sufficient number of shear studs are provided to prevent the concrete slab and steel girder from slipping relative to each other. This results in the best situation for both materials where the majority of the concrete is resisting compressive forces, and the majority of the steel girder is resisting the tension forces. Full composite action results in improved strength and stiffness over non-composite construction, and hence lighter girder weight. The strain diagram in Figure 2-4 shows that when full composite action is achieved, there is no discontinuity of strain at the interface between the steel and concrete. The

AASHTO LRFD Bridge Design Specifications (AASHTO 2007) recommends the use of full composite action in design.

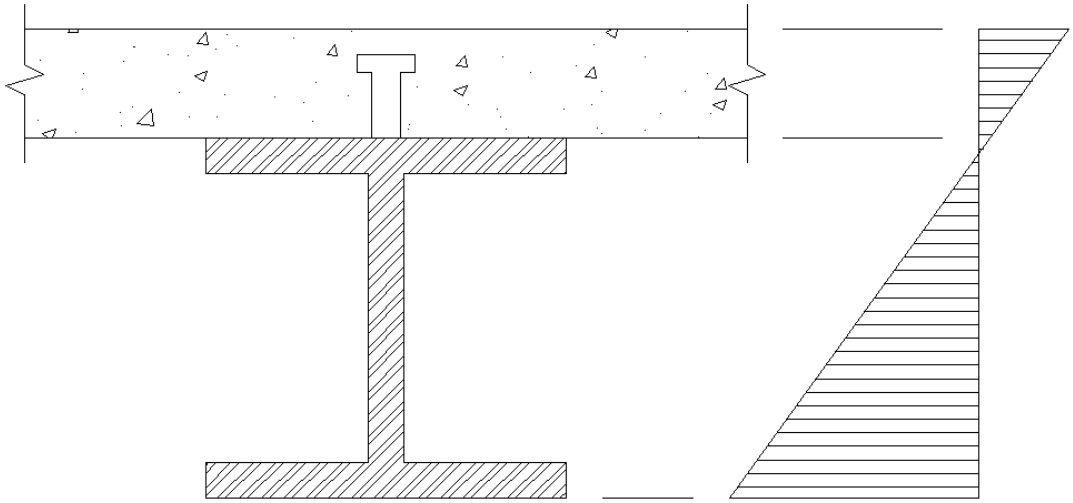

Figure 2-4 Strain Diagram for Full Composite Action

2.3.3 Partial Composite Action

Partial composite action is achieved when the number of shear studs used to connect the concrete slab and steel girder is less than the number required to achieve full composite action. With this type of composite design, the slip between the two materials is not completely prevented, although the magnitude of that slip is not as large as that seen in non-composite construction. The AASHTO LRFD Bridge Design Specifications (AASHTO 2007) does not allow the use of partial composite action in design.

2.4 Review of Fatigue Design Provisions Worldwide

Although the purpose and goal for each country is to build safe, economical structures that will last for the duration of their design life, the codes and equations used to achieve these goals can differ greatly. The most common way to determine design criteria for shear studs is by using empirical data gathered from experiments. These results are most commonly shown on

what is known as an S-N curve where S represents the stress range on the y-axis and N represents the number of cycles on the x-axis. Although AASHTO (2007) gives a semi-log relationship between number of cycles and stress range, most other design codes give equations that are based on a log-log relationship which has now become more common. This section will review fatigue design criteria for shear studs according to the AASHTO LRFD Bridge Design Specifications (AASHTO 2007), the Eurocode 4 (CEN 2005), the Japanese Society of Civil Engineers (JSCE 2009), and the BS 5400 (BSI 1980).

2.4.1 AASHTO LRFD Bridge Design Specifications (AASHTO 2007)

The AASHTO LRFD Bridge Design Specifications (AASHTO 2007) bases most of its design on the research done by Slutter and Fisher (1966) at Lehigh University. They chose to develop equations that used the range of live load shear force (Z_r) rather than the stress range as other codes have done.

The following equation is used to determine the live load shear force (Z_r):

$$Z_r = \alpha d^2 \geq 2.75 d^2 \qquad (2\text{-}1)$$

where

$$\alpha = 34.5\text{-}4.28 \log N \qquad (2\text{-}2)$$

AASHTO (2007) provides a constant amplitude fatigue limit (CAFL) of 3.5 ksi, a stress range below which no propagation of fatigue cracks is expected. AASHTO (2007) also has some geometry requirements that give limitations on dimensions and spacing of studs. These are as follows:

1) Ratio of height to diameter of stud should not be less than 4.0

2) Center-to-center pitch of shear connectors shall not exceed 24" and shall not be less than six times the stud diameter
3) Stud shear connectors shall not be closer than 4.0 stud diameters center-to-center transverse to the longitudinal axis of the supporting member
4) The clear distance between the edge of the top flange and the edge of the nearest shear connector shall not be less than 1"
5) The cover over the top of the shear connectors should not be less than 2" and the shear connectors should penetrate at least 2" into the concrete deck.

2.4.2 Eurocode 4 (CEN 2005)

Eurocode 4 (CEN 2005) is focused on the design of composite steel and concrete structures and part 2 of that codes focuses on design of bridges. Eurocode 4 (CEN 2005) differs from AASHTO (2007) in that it gives design criteria based on the stress range and not the range of live load shear force. Another difference is that Eurocode 4 does not include a constant amplitude fatigue limit (CAFL).

For automatically welded headed studs used with normal weight concrete, the fatigue life curve is given as:

$$(\Delta\tau_R)^m N_R = (\Delta\tau_c)^m N_c \quad (2\text{-}3)$$

where:

$\Delta\tau_R$ = the fatigue shear strength related to the cross-sectional area of the shank of the stud, using the nominal diameter d of the shank

$\Delta\tau_c$ = the reference value at $N_c = 2 \times 10^6$ cycles with $\Delta\tau_c$ equal to 13.1 ksi

m = the slope of the fatigue strength curve with the value m = 8

N_R = the number of stress-range cycles

Equation 2-3 can be rewritten in the following linear log-log form:

$$\log N = 21.935 - 8\log S_r \quad (2\text{-}4)$$

and is graphically represented in Figure 2-5.

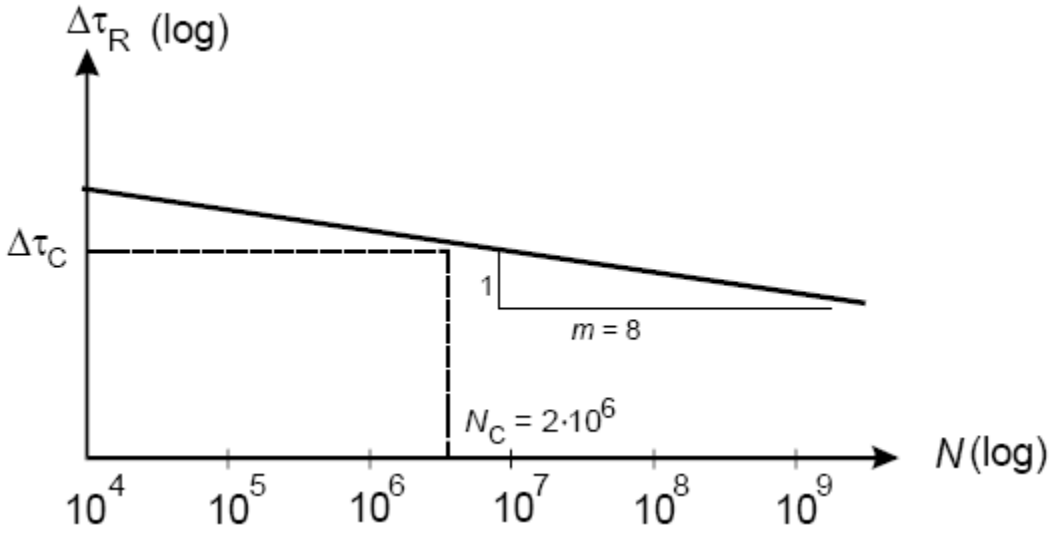

Figure 2-5 Graphical Representation of Equation 2-4 (taken from Eurocode 4 (CEN 2005))

Similar to the AASHTO (2007), Eurocode 4 (CEN 2005) has limitations on the geometry and the dimensions of the studs as well as their location. These constraints are taken directly from Eurocode 4 (CEN 2005) and are stated as follows:

1) The overall height of a stud should be not less than 3d, where d is the diameter of the shank.
2) The head should have a diameter of not less than 1.5d and a depth of not less than 0.4d.
3) For elements in tension and subjected to fatigue loading, the diameter of a welded stud should not exceed 1.5 times the thickness of the flange to which it is welded,

unless test information is provided to establish the fatigue resistance of the stud as a shear connector. This applies also to studs directly over a web.

4) The spacing of studs in the direction of the shear force should be not less than 5d; the spacing in the direction transverse to the shear force should be not less than 2.5d in solid slabs and 4d in other cases.
5) Except when the studs are located directly over the web, the diameter of a welded stud should be not greater than 2.5 times the thickness of that part to which it is welded, unless test information is provided to establish the resistance of the stud as a shear connector.

2.4.3 Japanese Society of Civil Engineers (JSCE 2009)

The Japanese Society of Civil Engineers (JSCE 2009) differs from both the AASHTO (2007) and Eurocode 4 (CEN 2005) when designing for fatigue of shear connectors in that it takes into account the static strength of the shear connectors. Included in the equation for the static strength are the height of the stud and the compressive strength of the concrete. Neither AASHTO (2007) nor Eurocode 4 (CEN 2005) take these parameters into consideration. Another difference that is seen in the JSCE (2009) is that the design equations are dependent on which direction the concrete was poured relative to the shear connectors. Four different concrete casting configurations are given and are designated as shown in Figure 2-6.

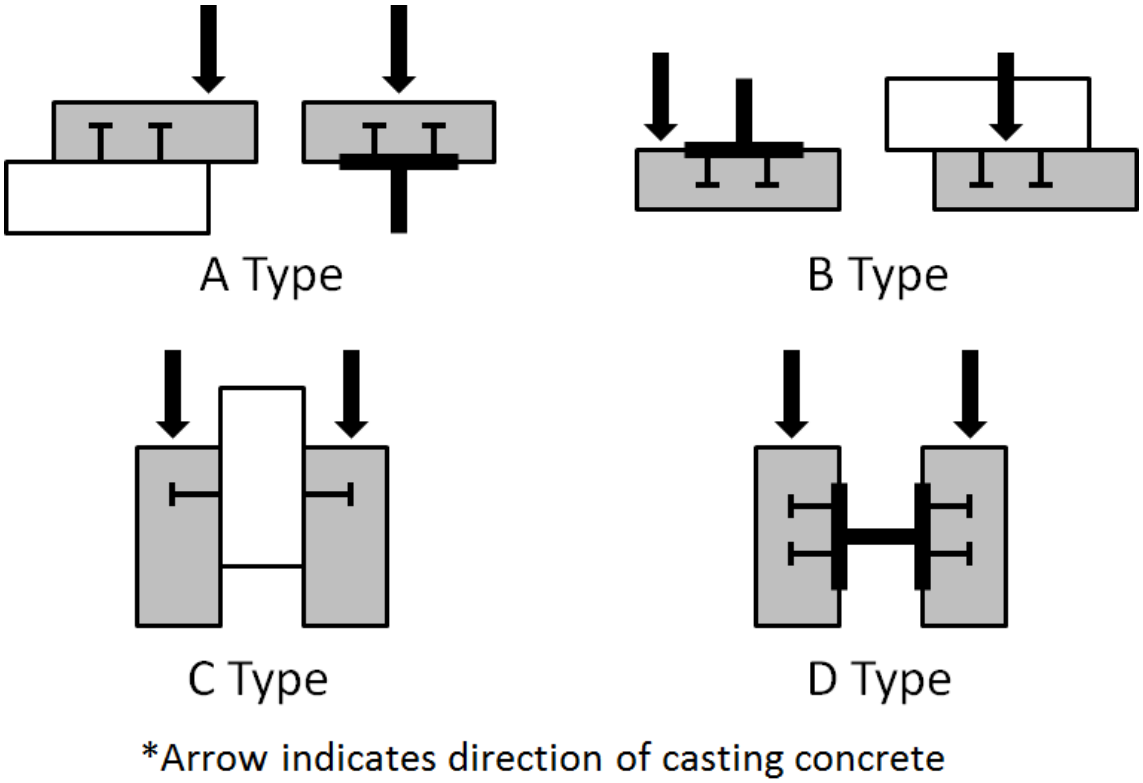

Figure 2-6 Casting Configurations for JSCE (2009)

The following equations have been developed to determine the fatigue resistance of shear studs:

For Types A,C, and D:

$$V_{srd}/V_{sud} = 0.99N^{-0.105} \quad (2\text{-}5)$$

For Type B:

$$V_{srd}/V_{sud} = 0.93N^{-0.105} \quad (2\text{-}6)$$

where

$$V_{sud} = (31A_{ss}\sqrt{\left(\frac{h_{ss}}{d_{ss}}\right)f'_{cd}} + 10000)/\gamma_b \quad (2\text{-}7)$$

A_{ss} = Cross-sectional area of stud (mm^2)

h_{ss} = Height of a stud

d_{ss} = Shank diameter of a stud

V_{srd} = Design shear resistance when fatigue is considered (shear force amplitude)

V_{sud} = Design shear resistance of stud (N)

f'_{cd} = Design compressive strength of concrete (N/mm^2)

N = Number of cycles representing fatigue life or fatigue resistance

γ_b = Member factor, generally taken as 1.0

According to the JSCE (2009), both of the equations given for the fatigue resistance of shear connectors are applicable for studs of shank diameters ranging from $^1/_2$" to 1¼", heights from 2" to 6", tensile strength ranges from 58 ksi to 80 ksi, and concrete strengths from 2900 psi to 7900 psi.

2.4.4 BS 5400 (BSI 1980)

The BS 5400 (BSI 1980) is focused on steel, concrete, and composite structures and Part 10 is specifically the code of practice for fatigue. Much like other fatigue design, the BS 5400 (BSI 1980) bases its design on an S-N curve. This code is different from other codes with the exception of the JSCE (2009) in that the fatigue strength is dependent on the static strength of the shear studs, which in turn is a function of the stud dimensions and the compressive strength of the concrete. The static strength is incorporated into the fatigue design due to the way that stresses in the weld metal of shear studs are computed. Instead of calculating the stress based on the load and the nominal diameter of the stud, it is calculated as follows in the BS-5400: Part10 (BSI 1980):

$$stress\ in\ weld = \frac{longitudinal\ shear\ load\ on\ stud}{appropriate\ nomial\ static\ strength\ (from\ Part\ 5)} * 61.7ksi \qquad (2\text{-}8)$$

Equation 2-8 refers the designer to the BS 5400: Part 5 (BSI 2005) which has a table that gives the nominal static strengths of shear connectors for different concrete strengths. This table is also limited to studs with diameters ranging from ½" to 1" and is shown in Figure 2-7.

Type of connector		Connector material	Nominal static strengths in kN per connector for concrete strengths f_{cu}, N/mm^2			
			20	30	40	50
Headed studs (see Figure 1a)		Material with a characteristic yield stress of 385 N/mm^2, minimum elongation of 18 % and a characteristic tensile strength of 495 N/mm^2				
Diameter mm	Overall height mm					
25	100		139	154	168	183
22	100		112	126	139	153
19	100		90	100	109	119
19	75		78	87	96	105
16	75		66	74	82	90
13	65		42	47	52	57
Bars with hoops (see Figure 1b and Figure 1c)		Grade S275 of BS EN 10025				
50 mm × 40 mm × 200 mm bar			697	830	963	1096
25 mm × 25 mm × 200 mm bar			348	415	482	548
Channels (see Figure 1d)		Grade S275 of BS EN 10025				
127 mm × 64 mm × 14.90 kg × 150 mm			351	397	419	442
102 mm × 51 mm × 10.42 kg × 150 mm			293	337	364	390
76 mm × 38 mm × 6.70 kg × 150 mm			239	283	305	326
Friction grip bolts		BS 4395-1	see Clause **10**			

NOTE 1 f_{cu} is the specified characteristic cube strength at 28 days.

NOTE 2 Strengths for concrete of intermediate grade may be obtained by linear interpolation.

NOTE 3 For bars (see Figure 1b and Figure 1c), and channels (see Figure 1d) of lengths different from those quoted above, the capacities are proportional to the lengths for lengths greater than 100 mm.

NOTE 4 For stud connectors of overall height greater than 100 mm, the nominal static strength should be taken as the values given for 100 mm high connectors, unless the static strength is determined from push-out tests in accordance with **5.3.2.4.**

Figure 2-7 Static Strength of Shear Studs (BS 5400: Part 5 (BSI 1980))

Once Equation 2-8 is used to determine the stress in the weld, the stress range can be determined based on the given loads. This stress range can then be used with the fatigue design curve equation given in the BS 5400: Part 10 (BSI 1980) which is as follows:

$$LogN = LogK_2 - mLog\sigma_r \quad (2\text{-}9)$$

where

N = number of cycles

K_2 = 2.08×10^{22} (for shear connector detail)

m = 8.0 (for shear connector detail)

σ_r = Stress range determined from Equation 2-8

2.5 Previous Research

Although a large amount of research and testing has been performed on the fatigue resistance of shear studs in composite bridge decks, only recently have these studies been expanded to test with larger diameter shear studs. While the cross-sectional area of two $^7/_8$"-diameter shear studs in approximately the same as that of a single 1¼"-diameter stud, there may be other factors that are involved in determining the fatigue resistance of the shear studs. The following chronological presentation of previous research of fatigue of shear studs dates back to the 1960's and continues to the present time. The following subsections will go through experiments and test results from previous test programs.

2.5.1 Slutter and Fisher (1966)

The scope of their test program was to determine the fatigue strength of shear connectors for steel and concrete composite beams. A total of 56 push-out specimens were tested which

included 35 using $^{3}/_{4}$"-diameter studs, 9 using $^{7}/_{8}$"-diameter studs, and 12 using 4 in., 5.4-lb channel connectors. Any results from specimens using channel connectors will be ignored as the main focus of this thesis is headed stud connectors. A test matrix was designed to evaluate two controlled variables -- the stress range and minimum stress level.

All push-out specimens were tested until failure occurred. Failure usually took place in one of two manners. The first and most common was for the crack to form at the weld and continue to propagate into and through the beam flange resulting in a concave depression left on the beam flange. In the second type of failure, the crack formed in the weld and propagated through the weld. This type of failure was usually the result of insufficient weld penetration (Slutter and Fisher 1966). The results from the ¾"-diameter studs and $^{7}/_{8}$"-diameter studs can be seen in Figure 2-8 and Figure 2-9, respectively.

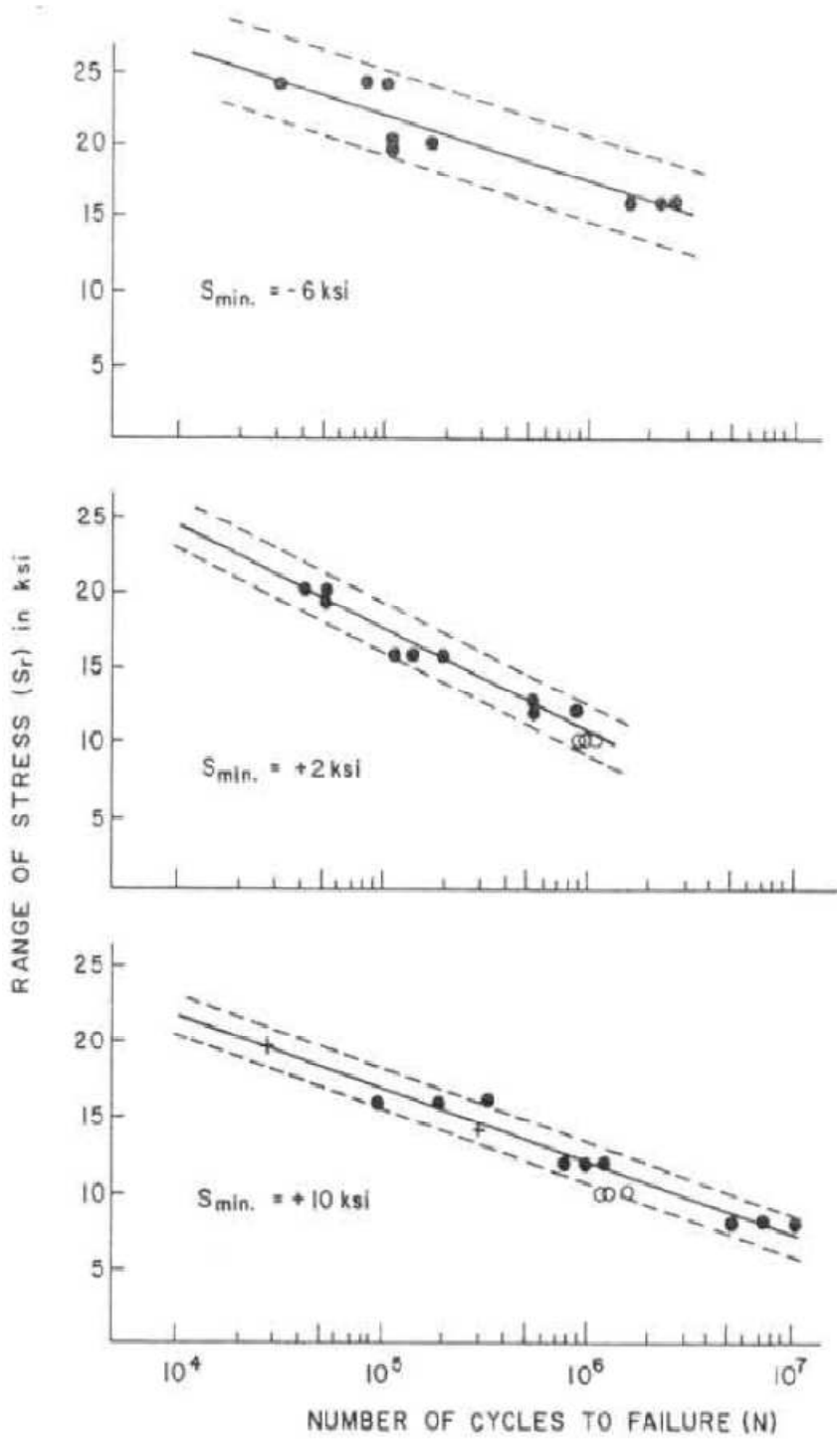

Figure 2-8 Results from ¾"-Diameter Stud Tests (Slutter and Fisher 1966)

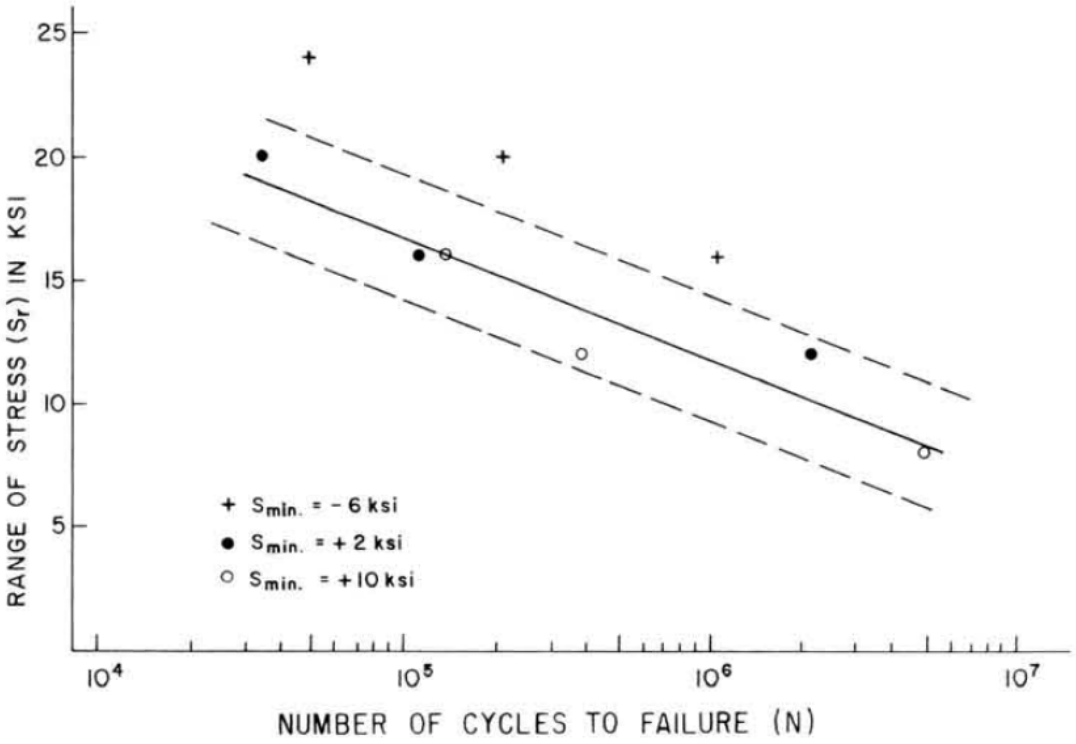

Figure 2-9 Results from $^7/_8$"-Diameter Stud Tests (Slutter and Fisher 1966)

By controlling two variables simultaneously, Slutter and Fisher were able to determine whether minimum stress, the stress range, or both had an impact on the fatigue life. After analyzing the experimental data, it was determined that the overall stress range had the largest effect on the fatigue life and that it was independent of the minimum stress level.

After performing a regression analysis on the their test data, Slutter and Fisher developed the following semi-log relationship for fatigue life.

$$logN = 8.072 - 0.1753\, S_r \tag{2-10}$$

Slutter and Fisher also used their test results to come up with design criteria to be used when designing composite bridge decks. The spacing, or pitch of shear stud connectors was given as

$$P = \frac{\Sigma Z_r}{H_r} \tag{2-11}$$

where

H_r = range of horizontal shear per inch of beam length at beam-slab interface

Z_r = allowable range of horizontal shear for the connector

P = spacing of shear connectors

H_r and V_r in the preceding equation are computed as follows:

$$H_r = \frac{VQ}{I} \tag{2-12}$$

$$Z_r = \alpha d_s^2 \tag{2-13}$$

where

V = shear in kips acting on the composite section

Q = statical moment of the transformed compressive concrete area about the neutral axis of the composite section

I = moment of inertia of the composite section

α = 13,800 for 100,000 cycles, 10,600 for 500,000 cycles, and 7,850 for 2,000,000 cycles

d_s = diameter of stud in inches

This procedure is currently being used to design shear studs by the AASHTO (2007).

2.5.2 Mainstone and Menzies (1967)

Mainstone and Menzies tested the fatigue resistance of three different types of shear connectors including headed shear studs, steel channels, and steel bars. Since this paper is focused on the fatigue resistance of headed shear studs, the other two types of connectors will be ignored. The shear studs that they tested were ¾"-diameter by 4 in. “Cromparc” headed studs welded to the top of a steel flange using an electric-arc welding process which utilizes a stud

welding gun to automatically “shoot” the studs onto the steel beam resulting in a fairly repeatable weld.

The main objective of this test program was to develop a relationship between the maximum stress on a shear connector and its fatigue life at different ratios of maximum to minimum stress levels. This was accomplished by fabricating push-out specimens as well as some full-scale composite beams, but this review will be limited to that of the push-out specimens only.

The concrete slabs of the push-out specimens were cast in the horizontal position as would be done in a bridge deck. This complicated matters by having to cast each slab of the push-out specimens on consecutive days. The concrete used for these specimens was composed of river gravel and ordinary Portland cement and was designed so that the compressive strength at time of testing would be approximately 5000 psi. The flange of the steel beam was greased prior to casting the concrete in order to prevent the natural bond between the concrete and steel flange from forming. The concrete was then cured under moist sacks for three days, after which it was cured at 65 degrees Fahrenheit and 64% relative humidity until it was tested.

The minimum and maximum stress, stress range, ratio of minimum to maximum stress, and number of cycles to failure are shown in Table 2-1.

Table 2-1 Tabulated Results from Mainstone and Menzies (1967)

Specimen	S_{min} (ksi)	S_{max} (ksi)	S_r (ksi)	Ratio S_{min}/S_{max}	Number of Cycles to Failure
S1	2.2635	22.64	20.4	0.1	76,000
S2	1.8108	18.11	16.3	0.1	439,000
S7	1.8108	18.11	16.3	0.1	1,940,000
S9	2.4899	24.90	22.4	0.1	42,000
S10	15.166	30.33	15.2	0.5	1,700,000
S12	16.977	33.95	17.0	0.5	679,000
S20	18.674	37.35	18.7	0.5	669,000
S23	28.86	38.48	9.6	0.75	657,000
S24	31.407	41.88	10.5	0.75	9,200
S25	19.806	39.61	19.8	0.5	13,300
S27	19.806	39.61	19.8	0.5	8,970
S28	19.24	38.48	19.2	0.5	6,000
S30	31.407	41.88	10.5	0.75	13,100
S31	30.558	40.74	10.2	0.75	8,600
S32	29.709	39.61	9.9	0.75	165,000
S33	19.806	39.61	19.8	0.5	106,000

The test program completed by Mainstone and Menzies (1967) did not focus much on stress range as being the main variable in the fatigue tests, but instead their tests focused on the ratio between the maximum and minimum stresses. There is some scatter in the data, but this was mainly attributed to the differences in concrete strength. When the failure occurs in the weld of the stud, the stresses must be influenced by the deformation of the concrete which is related to the strength of the concrete (Mainstone and Menzies 1967).

2.5.3 Roderick and Ansourian (1976)

The test program that Roderick and Ansourian performed was mainly focused on testing composite beams under repeated loading, but they also tested seven push-out specimens, four under constant amplitude loading and three under programmed loading. For this review, only the push-out specimens tested under constant amplitude loading will be discussed.

Each of their push-out specimens had four ¾"-diameter studs welded in pairs on the outside of each flange. The studs were 3.9" tall and were embedded into a 5.1" concrete slab on

each side of the flange. Hot forged steel with an average yield stress of 40.6 ksi was used for the studs. Of the four push-out specimens, three were tested under a constant stress range of 20.4 ksi while the other was tested under a constant stress range of 21.7 ksi. These stress ranges were chosen for the purpose of having a quick failure of the specimen. Loading frequencies of 13.3, 2.67, 3, and 0.5 Hz were used for the four tests.

The results from these four push-out tests can be seen in Table 2-2. Because only a few constant amplitude fatigue tests were carried out, there was not sufficient data to produce a curve for stress range vs. number of cycles, or S-N curve. Instead, the results from these tests were compared with those of Slutter and Fisher (1966) done in the United States as well as Mainstone and Menzies (1967) in the United Kingdom (Roderick and Ansourian 1967).

According to the mean regression line developed by Slutter and Fisher (1966), there is a semi-log relationship between stress range and number of cycles. The equation for this line is $logN = 8.072 - 0.1753\,S_r$ where N is the number of cycles and S_r in the stress range in ksi. By using this regression line and the given stress ranges tested by Roderick and Ansourian (1976), the expected number of cycles would be 32,600 for R1-R3 and 18,160 for R4. The results from this test program showed fatigue lives much greater than what was predicted by Slutter and Fisher's equation.

Table 2-2 Tabulated Results from Roderick and Ansourian (1976)

Specimen	S_{min} (ksi)	S_{max} (ksi)	S_r (ksi)	Cycles to Failure
R1	2.3	22.6	20.3	616,000
R2	2.3	22.6	20.3	194,110
R3	2.3	22.6	20.3	190,460
R4	0.9	22.6	21.7	49,300

Although these test results did not match well with those done by Slutter and Fisher (1966), they did coincide much better with those done by Mainstone and Menzies (1967) which

shows a relationship between maximum nominal stress on the stud and fatigue life. The graphical comparison from these tests can be seen in Figure 2-10 and Figure 2-11

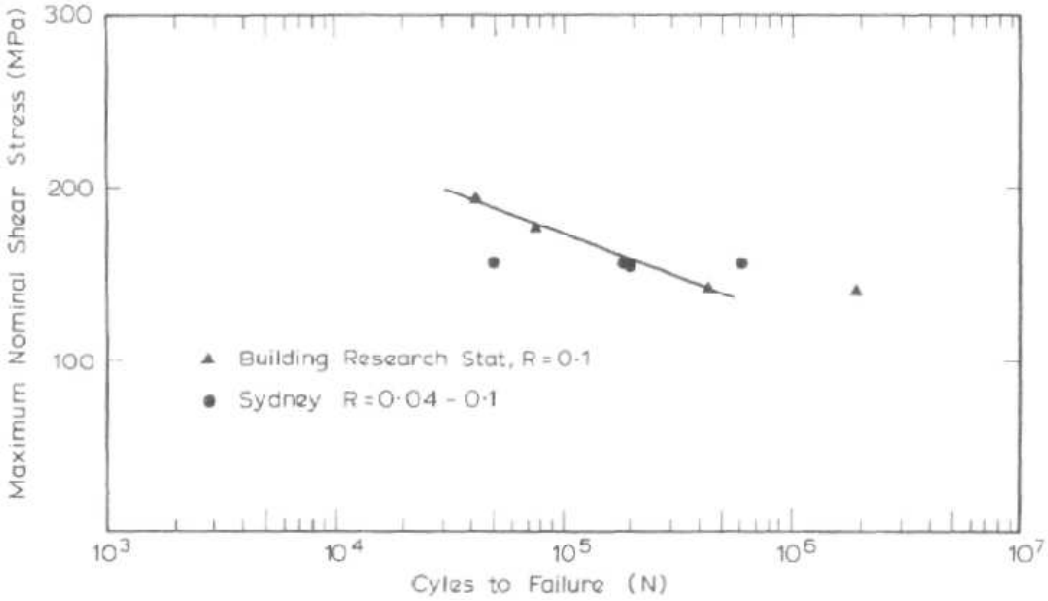

Figure 2-10 Comparison of Roderick and Ansourian (1976) to Mainstone and Menzies (1967)

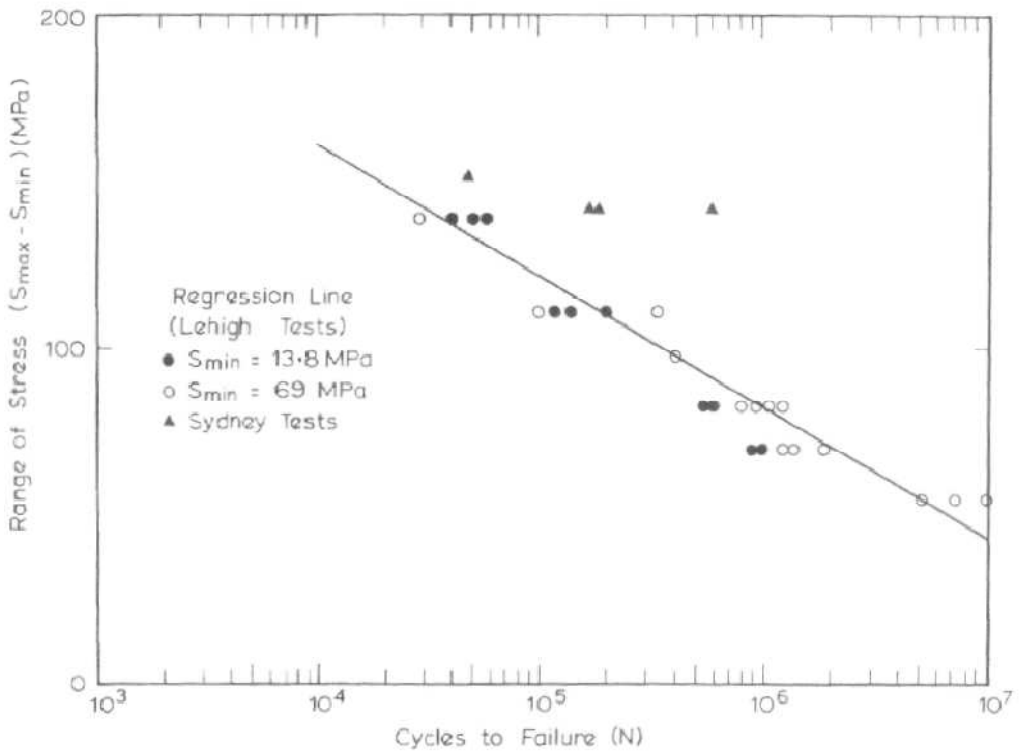

Figure 2-11 Comparison of Roderick and Ansourian (1976) to Slutter and Fisher (1966)

2.5.4 Hallam (1976)

Because of the differences between American design codes and British design codes, Hallam's experimental test program was undertaken to help resolve these differences as well as investigate the behavior of shear studs subjected to variable amplitude cyclic loads (Hallam 1976).

His test program consisted of 18 push-out specimens that were each tested until the maximum load in a fatigue cycle was large enough to statically fail the shear studs on at least one side. All specimens used ¾"-diameter by 3" studs. Thirteen were tested under constant amplitude cyclic loads, four were tested under variable amplitude cyclic loads, and a single specimen was tested under static loading. For the purposes of this review, only the specimens tested under constant amplitude cyclic loading will be considered.

All of the push-out specimens of Hallam's test program were fabricated in order to closely simulate the condition that would be experienced by the shear studs in a composite beam. In order to prevent bending stress at the base of the studs, a rod was cast in the specimen at the base of the concrete to prevent the slab from separating from the steel section. The steel section was oiled at the interface where it met the concrete slab to attempt to prevent natural bond of the concrete and steel. This would ensure that all of the force being transferred was being transferred through the stud and not as frictional forces along the steel section. Since concrete compressive strength was another factor to be investigated, the concrete strengths of the slabs ranged from 3300 psi to 8800 psi (Hallam 1976).

For all of the cyclic load tests, the following procedure was followed:

1) Specimen was loaded statically up to the maximum load that would be used in the dynamic test and then the load was reduced to zero.
2) Cyclic loading (constant amplitude or variable amplitude) was carried out until one pair of studs failed. Relative slip between concrete and steel section was measured periodically.
3) The concrete slab on the failed side of the specimen was removed and a precast slab was attached so that testing could continue.
4) Cyclic loading was continued until failure of the other pair of studs occurred.

Table 2-3 gives the results from the thirteen constant amplitude fatigue tests. The number of cycles given in the table is for failure of the first pair of studs. As stated earlier, the specimen was reset so that the pair of studs on the other side of the specimen could be failed, but this is not included in this table of values.

Table 2-3 Tabulated Results from Hallam (1976)

Specimen	f'c psi	S_{max} (ksi)	S_{min} (ksi)	S_r (ksi)	N Cycles to Failure
1	8750	14.4	0.6	13.8	1,303,669
2	8430	14.4	1.2	13.2	823,970
3	8430	14.4	1.2	13.2	652,300
4	5110	25.3	1.2	24.1	52,801
5	5110	25.3	1.2	24.1	58,630
6	4820	14.9	1.2	13.7	3,170,000
7	4820	14.9	1.2	13.7	5,140,000
8	4760	11.8	0.7	11.1	21,391,000
9	4760	11.8	0.7	11.7	24,305,000
10	4400	22.5	1.2	21.3	61,700
11	4400	22.5	1.2	21.3	110,000
12	3310	17.1	1.2	15.9	148,700
13	3310	17.1	1.2	15.9	182,600

One of the most important conclusions made by Hallam was the difference in failure modes. Three types of failure modes, which Hallam called A, B, and C, were apparent. Mode A consisted of the crack being initiated at the top of the weld collar, defined as the location where the weld meets the stud material, and propagating along the stud-weld interface. For failure mode B, the crack formed at the weld toe, defined as the location where the weld meets the base material, and propagated back and forth between the weld material and the base material. Failure mode C formed at the same location as mode B, but the crack propagated down through the flange of the base material and left a large concave depression in the top of the flange after failure (Hallam 1976).

Based on all of the failures seen in the studs, Hallam made the following conclusions:

1) The high maximum stress cases usually caused failure mode A
2) The low maximum stress cases usually caused failure mode C
3) The mid range maximum stress cases caused failure modes A and B

At the time of this test program, the only other significant testing of shear studs under constant amplitude loading was done by Slutter and Fisher (1966) and Mainstone and Menzies (1967).

To compare these results to those of Slutter and Fisher, Hallam needed the concrete strength of Slutter and Fisher's test specimens. Slutter and Fisher did not give concrete strength of individual push-out specimens, but instead gave the mean concrete strengths for each batch of concrete. Therefore, Hallam made the assumption that the concrete strength of each specimen was equal to the mean concrete strength of each concrete batch. When this comparison was carried out, the results were similar to that of Slutter and Fisher.

When comparing data to Mainstone and Menzies (1967), Hallam agreed with the conclusions made that concrete strength, minimum stress, and stress range were variables that needed to be considered when determining the fatigue life. Interestingly, although their conclusions were the same, Mainstone and Menzies' results gave much longer fatigue lives than those found by Hallam.

2.5.5 Oehlers (1990)

The main objective of the research done by Oehlers was to formulate an equation that would take into account the reduction in static strength of shear studs due to previous cyclic loading. A graphical representation of the relationship between static and fatigue strength was introduced by Oehlers and is shown in Figure 2-12. The graph in Figure 2-12 shows that design codes assume that even after cyclic loading, the static strength of shear studs is the same as it was initially. Only when the number of cycles reaches the value corresponding to the fatigue life, does the static strength of the shear studs reduce drastically.

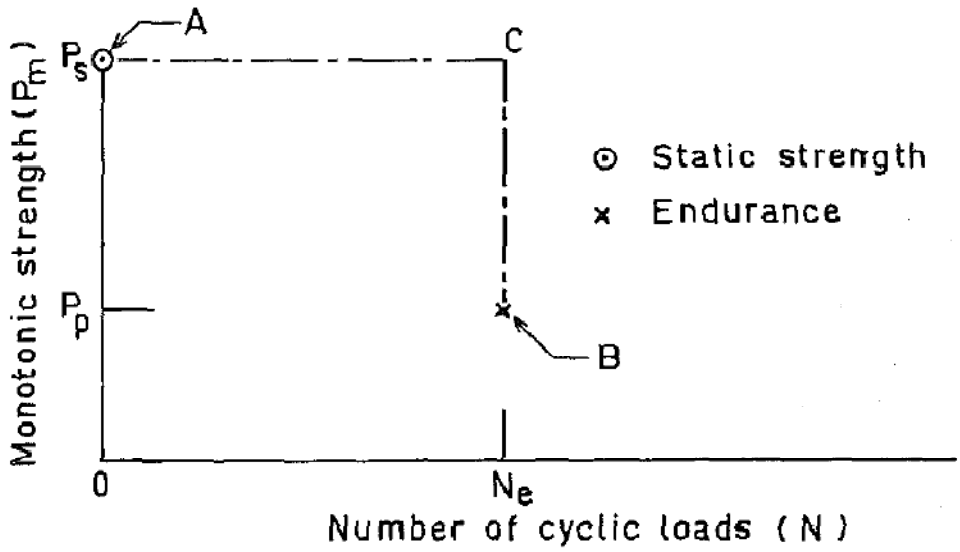

Figure 2-12 Graphical Representation of Design Criteria (Oehlers 1990)

In his test program, Oehlers tested fourteen push-out specimens. Three were tested under static loading, six under fatigue loading, and five were tested for residual strength after cyclic loading. For the purposes of this literature review, only push-out specimens tested under fatigue loading will be investigated.

When fabricating the push-out specimens for his test program, Oehlers welded the studs to a steel plate and cast the concrete slabs in the horizontal position at the same time and from a single batch of concrete. Wax was applied to the steel-concrete interface to prevent bond, therefore reducing the friction between the two materials. The concrete was allowed to cure for a long period of time until the strength leveled off. The steel plates were bolted to steel I-sections to form the push-out specimen.

The shear studs used by Oehlers were ½"-diameter by 3" tall and had an ultimate tensile strength of approximately 66.5 ksi. Since the concrete slabs were allowed to cure for a long time, the compressive strength of approximately 7100 psi was assumed to be the same for all tests.

Since the relationship between fatigue life and stress range was not being directly investigated, the stress ranges of the fatigue tests were all the same and were selected to equal 25% of the average static capacity of the specimen. This gave a stress range of 15.5 ksi for all fatigue tests. The variable that was changed in the fatigue tests was the maximum stress or maximum load and conclusions were drawn about whether this affected the fatigue life.

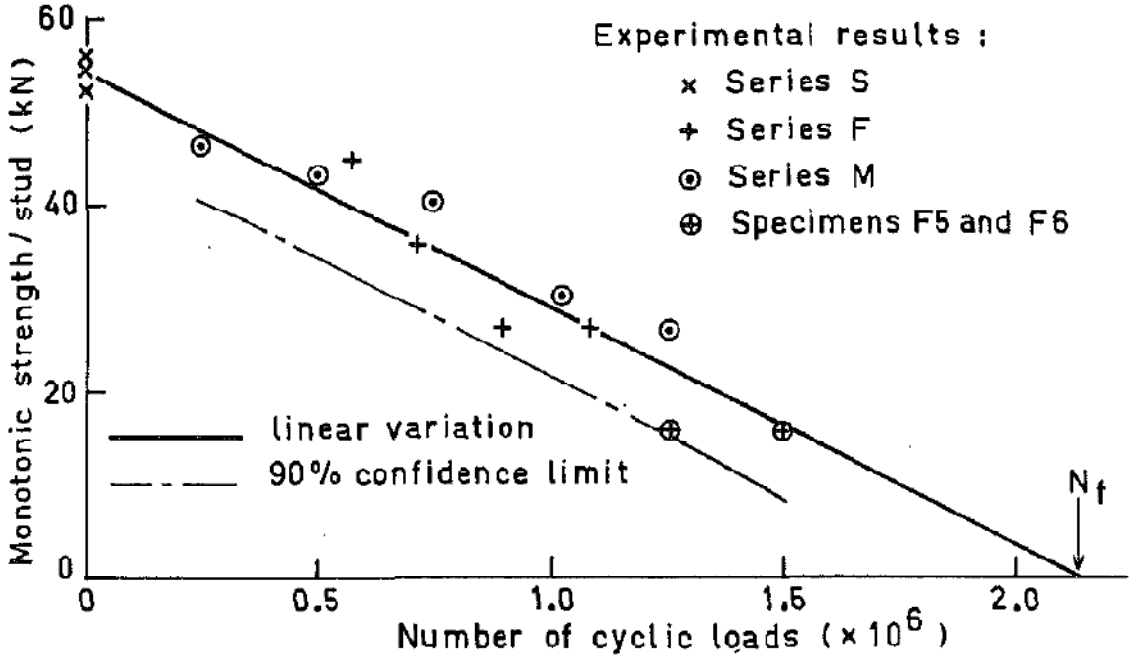

Figure 2-13 Graphical Results from Oehlers (1990)

The results from all of Oehlers' push-out tests are shown in Figure 2-13. Series S are from static test, series F are from constant amplitude fatigue tests, and series M are from residual strength tests. By looking at series F data alone, Oehlers saw a clear relationship that a higher maximum load per stud resulted in a reduced fatigue life (1990). This conclusion is important because it shows that stress range of the shear stud may not be the only factor governing the fatigue life of the stud as some previous research had concluded.

2.5.6 Roberts and Dogan (1997)

Although the main objective of this test program was to evaluate the fatigue resistance of tension plate shear connectors when being used in SCSS or steel-concrete-steel sandwich beam construction, six push-out tests using 0.39"-diameter studs were also performed for comparison to the beam tests. Only the fatigue tests on push-out specimens will be considered in this review.

It must be mentioned that there were some differences in this push-out specimen compared to those in other test programs. Instead of using a wide flange steel section to weld the shear studs to, Roberts and Dogan used a 200×100×8 RHS (rectangular hollow section). Also, instead of using a bed of mortar or gypsum at the base of the concrete slabs, they used soft wooden boards in order to achieve a uniform bearing surface.

Instrumentation consisted of measuring the load from the actuator using a load cell and slip between steel section and concrete slab using a displacement transducer that was fixed to the steel and reacted off of steel plates attached to the concrete slab. For each test specimen, the load was initially increased to approximately 40 kips to seat the specimen as well as eliminate any adhesion that still existed between the concrete and steel interface. The load was then cycled sinusoidally until failure with the exception of stopping intermittently to record load and slip measurements.

Failure of the push-out specimens was initiated by a fatigue crack which then propagated through the heat affected zone of the shear stud. In Figure 2-14, which shows the load vs. slip plot for PS6, the increase in slip with increasing number of cycles is indicative of the fatigue crack propagating through the stud resulting in a reduction in stiffness of the specimen until failure occurs (Roberts and Dogan 1997). The results from the six push-out specimens are given in Table 2-4.

Table 2-4 Tabulated Results from Roberts and Dogan (1997)

Specimen	S_r (ksi)	Number of Cycles at Failure
PS1	20.8	128,367
PS2	9.2	18,477,755
PS3	13.9	1,528,187
PS4	18.5	279,102
PS5	11.5	3,920,083
PS6	25.4	47,024

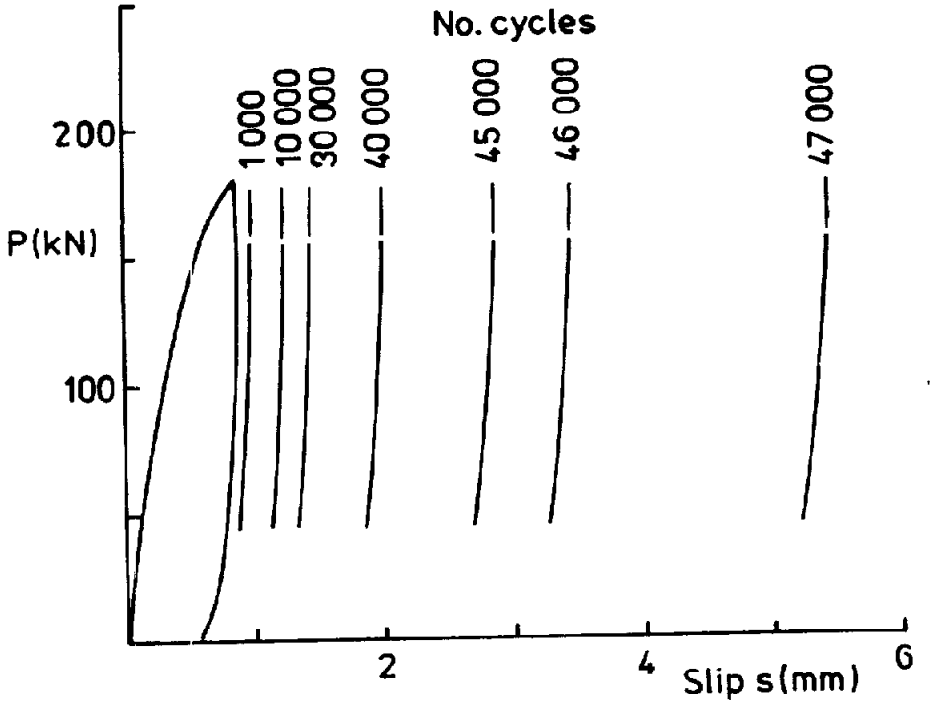

Figure 2-14 Load vs. Slip Plot for PS6 (Roberts and Dogan 1997)

At the time of this test program, Eurocode 3 (CEN 1993) was the most current design code in Europe and was therefore used for comparison with the experimental data. When this comparison was made, it showed that the experimental data gave longer fatigue lives than what was given by Eurocode 3 (CEN 1993). Therefore it was concluded that the design curve provided a conservative evaluation of the fatigue strength of headed shear studs (Roberts and Dogan 1997).

2.5.7 Badie et al. (2002)

The test program carried out by Badie et al. (2002) was focused on comparing the fatigue life of 1¼"-diameter shear studs with $^{7}/_{8}$"-diameter shear studs under static loading as well as fatigue loading. To be able to compare these results, the researchers first had to validate acceptable welding quality of the large diameter studs.

A study was performed in collaboration with stud manufacturers to determine a grade of steel as well as the factors that affect the quality of welding used for the large diameter studs. They discovered that SAE (Society of Automotive Engineering) 1008 or 1018 could be used. After many welding trials, they also determined that the slope of the chamfer, amount of flux, and power supply all affected the quality of the weld. In order to achieve a quality weld, a steep chamfer was created, the amount of flux was tripled, and the amperage was increased to 2400 which was about 400-600 more than that required for a $^{7}/_{8}$"-diameter shear stud (Badie et al. 2002).

After determining that quality welds could be achieved by making the adjustments mentioned above, the experimental testing could begin. Twenty push-out specimens were fabricated for ultimate strength, and twenty-five were fabricated for fatigue testing. The push-out specimen used in this test program was different from the typical push-out specimens for fatigue tests. Instead of having studs and concrete slabs on both sides of the steel section, they were only placed on one side of the steel section. Also, for the fatigue tests, instead of using a wide flange beam, a steel plate was used. The researchers mentioned that the eccentricity from this test setup affected the results, but they chose not to change the setup to eliminate the eccentricity (Badie et al. 2002).

The procedure for conducting cyclic fatigue testing consisted of slowly loading the specimen with a monotonic load up to the maximum fatigue load and then reducing the load to eliminate any residual slip. The load was applied again while the load and slip were recorded. Cyclic loading was then applied at a rate of 2 Hz until failure of the specimen occurred. The number of cycles as well as mode of failure can be seen in Table 2-5 taken from Badie et al. (2002).

Table 2-5 Tabulated Results from Badie et al. (2002)

31.8 mm (1 $\frac{1}{4}$ in.) stud specimen			22.2 mm (7/8 in.) stud specimen		
Specimen	Cycles$\times 10^6$	Type of Failure	Specimen	Cycles$\times 10^6$	Type of Failure
LS-5[a]-25A[b]	0.049	Stud failure	SS-5-25	0.027	Stud failure
LS-5-25B	0.050	Stud failure	—	—	—
LS-5-23A	0.074	Stud failure	SS-5-23	0.060	Stud failure
LS-5-21	0.094	Stud failure	SS-5-21	0.285	Stud failure
LS-5-20	0.554	Stud failure	SS-5-20	0.189	Stud failure
LS-5-19	0.567	Concrete crushing	SS-5-19	0.157	Stud failure
LS5-18A	0.166	Concrete crushing	SS-5-18	0.935	Stud failure
LS5-18B	2.533	Stud failure	—	—	—
LS5-17	1.636	Base plate failure	SS-5-17	0.400	Concrete crushing
LS-5-16	1.372	Base plate failure	SS-5-16	2.452	Stud failure
LS-5-15	2.000	No failure	SS-5-15	0.600	Stud failure
LS-5-14	2.594	No failure	SS-5-14	2.000	No failure
LS-5-10A	4.680	No failure	SS-5-10	2.500	No failure
LS-5-10B	6.708	No failure	—	—	—

[a]Minimum applied shear stress on stud (ksi).

[b]Applied shear stress range on stud (ksi).

Much like the research done by Slutter and Fisher (1966), these researchers chose to plot the data as a semi-log relationship. They came up with a different design curve for each of the two size studs that were tested. The equations, reformulated for English units are:

1¼"-diameter studs $$S_r = 51.49 - 5.81Log(N) \quad (2\text{-}14)$$

$^7/_8$"-diameter studs $$S_r = 51.15 - 5.92Log(N) \quad (2\text{-}15)$$

These equations were further altered to put them in the same form as the equation given in the AASHTO LRFD Bridge Design Specifications (1998). This gives the following equations for English units:

1¼"-diameter studs $\alpha = 40.44 - 4.56Log(N)$ (2-16)

$^{7}/_{8}$"-diameter studs $\alpha = 40.17 - 4.65Log(N)$ (2-17)

To make the difference in these equations more visible, the equations developed by these researchers were plotted on the same graph as the equations from the AASHTO Standard Specifications for Highway Bridges (1996) as well as the AASHTO LRFD Bridge Design Specifications (1998). Figure 2-15 is taken from Badie et al. (2002).

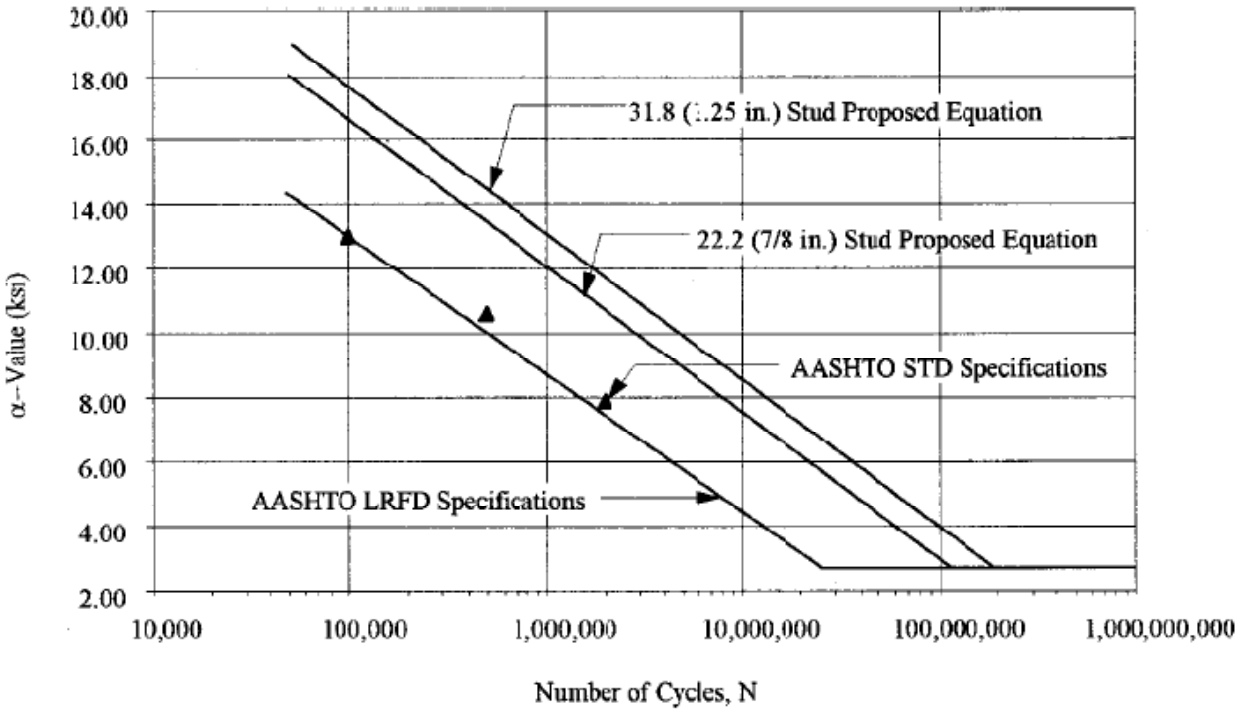

Figure 2-15 Comparison of Results and AASHTO (1998) Equations (Badie et al. 2002)

Based on the results from this test program, the following conclusions were made by Badie et al. (2002):

1) The α-values given in AASHTO (1998) give conservative results when computing the range of horizontal shear force for both size shear studs.

2) By using the equations presented by Badie et al. (2002), the number of required shear studs used could be reduced by approximately 30% therefore reducing the initial cost as well as costs for future deck replacement.
3) Using 1¼"-diameter shear studs spaced at 6" in a single line over the web of the girder will be sufficient to provide full composite action for the majority of bridges while also increasing safety of construction workers walking on top of the beam flanges.
4) The equation for the 1¼"-diameter studs might be too conservative for any stress ranges below 16 ksi because no failure was observed even after testing to approximately 7 million cycles.

2.5.8 Lee et al. (2005)

The main focus of this test program was to investigate the use of large diameter shear studs which are classified in this paper as those studs with diameters larger than 1". This investigation was done by means of push-out and beam tests under static as well as cyclic loading. The results were compared to design equation in Eurocode 4 (CEN 1997) and AASHTO LRFD Bridge Design Specifications (2004). Due to the scope of this thesis, only cyclic testing of push-out specimens will be included.

Much like the research done by Badie et al. (2002), these researchers were concerned with the material properties as well as the welding conditions and quality of welds for large diameter studs since experience with this size stud is limited. So that the comparison between standard diameter and large diameter studs could be made, the same steel was used so that proper strength and ductility could be achieved. The tensile yield stress, ultimate stress, and elongation of the studs were 51.2 ksi, 61.8 ksi, and 34% respectively (Lee et al. 2005). Welding trials were

carried out and determined that a modified stud chamfer, a power source with minimum of 2400 amperage, and increasing the welding time to 1.3 seconds gave a quality weld.

Dimensions for push-out specimens given in Eurocode 4 (CEN 1997) were used so that results from this test program could be compared to those from other test programs. The slabs were cast in the horizontal position as is done in composite beam construction and were air-cured. The flanges were greased at the interface to prevent bond between the concrete and steel (Lee et al. 2005).

For purposes of determining concrete compressive strength, four concrete specimens were made at the time of casting the slabs. One set of these were cured using standard methods in a moist-cure room while the other set was cured alongside the push-out specimens.

For the fatigue tests, a 225 kip capacity hydraulic testing machine was used. Longitudinal slip between the concrete slab and steel section were measured constantly using four LVDTs with accuracy of 0.001 mm. Figure 2-16 taken from Lee et al. (2005) shows a picture of the typical setup for this test program.

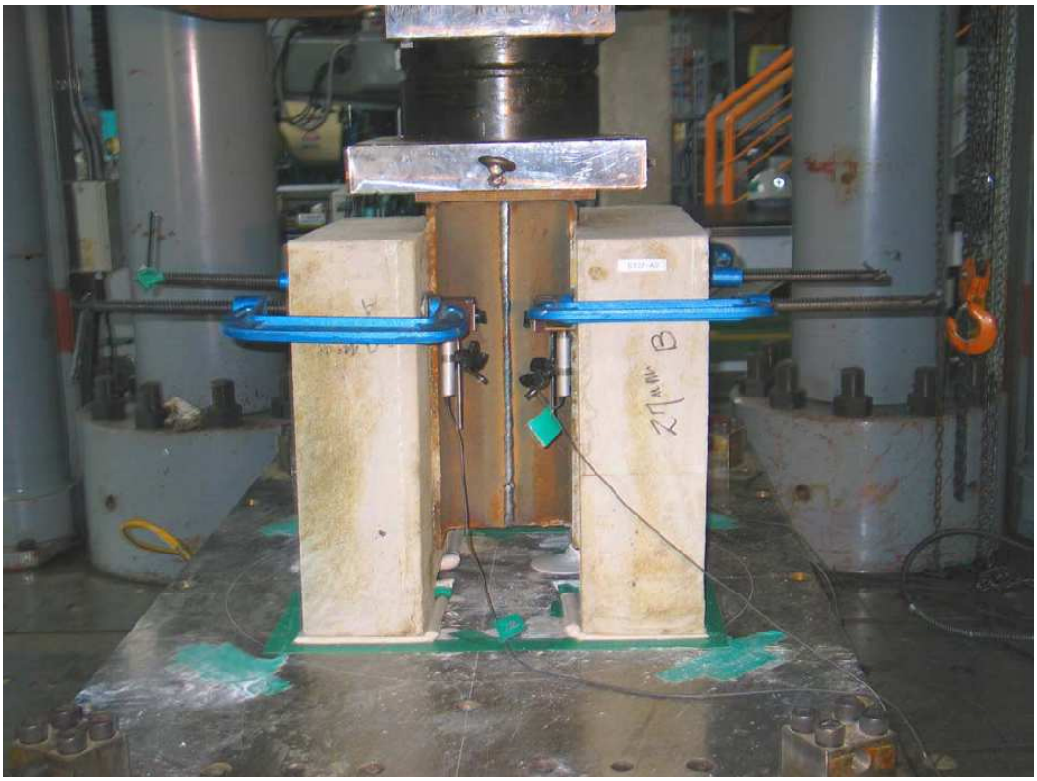

Figure 2-16 Typcial Set-up (Lee et al. 2005)

As is normal practice in fatigue testing of push-out specimens, cyclic loading was continued at a constant load range until the area of the shear studs had been reduced enough by fatigue crack propagation that the peak load in a single cycle was large enough to completely shear off the remaining studs. Table 2-6 shows the results from the fatigue testing.

Table 2-6 Tabulated Results from Lee et al. (2005)

Specimen	S_r (ksi)	Number of Cycles at Failure
FT25-A1	14.5	2,133,970
FT25-A2	21.8	44,827
FT25-A3	24.7	60,000
FT25-B1	18.9	687,209
FT25-B2	21.8	61,063
FT25-B3	25.7	5,320
FT27-A1	18.6	142,641
FT27-A2	21.8	22,488
FT27-A3	24.7	13,766
FT30-A1	18.9	75,484
FT30-A2	21.8	10,436
FT30-A3	22.7	19,333

Lee et al. (2005) plotted their results based on a log-log relationship between the stress range and number of cycles and performed a linear regression analysis so that their data could be compared to the design curves given by Eurocode 4 (CEN 1997) and AASHTO (2004). This comparison is shown in Figure 2-17. When comparing the data points to the design curve from Eurocode 4 (CEN 1997), eight of the twelve points fall below the design curve. When comparing the data points to the design curve from AASHTO (2004), one of the twelve points fall below the design curve. Based on this comparison, it was concluded that the fatigue life of large diameter studs was slightly lower than that of standard diameter studs and therefore the current design codes need to be modified for large-diameter studs (Lee et al. 2005).

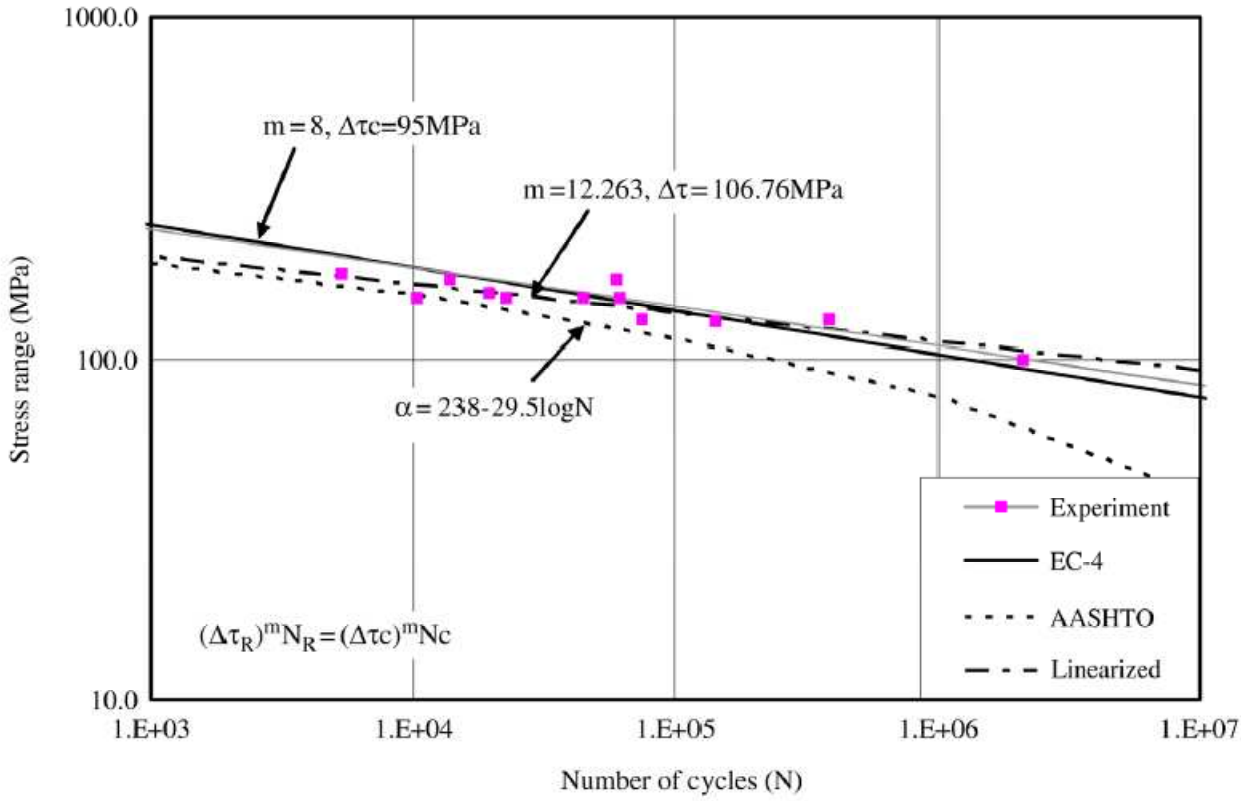

Figure 2-17 Comparison of Test Data and Design Codes (Lee et al. 2005)

2.5.9 Ahn et al. (2007)

Due to the introduction of a new steel-concrete bridge deck system, this test program was carried out to obtain data to support the design and safety of $^{5}/_{8}$"-diameter studs used in the new system (Ahn et al. 2007). Fifteen push-out specimens were fabricated according to the suggested dimensions given in Eurocode 4 (CEN 2005). Three were tested statically, nine were tested in fatigue, and three were used for residual testing. For this review, only those tested in fatigue will be considered.

So that the concrete slabs could be poured with the same concrete mix and in the horizontal position at the same time, steel plates were used and were later bolted and held vertically to create the push-out specimen. The shear studs used in this test were made from

SS400 grade steel which had a yield stress of 50.9 ksi, ultimate stress of 61.2 ksi, and an elongation of 34%. The slabs were cast with concrete with a nominal strength of 4300 psi. After concrete cylinders were made for compressive strength determination, one set was cured alongside the specimens while the other set was cured under standard curing conditions.

Four LVDTs were used to measure the relative slip between the concrete and steel to which the studs were welded. While running the fatigue tests, cycling was set at 6 Hz. To monitor the relative displacement and stiffness variation, a load of 34 kips was applied at increments of every 50,000 cycles until failure occurred. The results from fatigue tests are shown in Table 2-7.

Table 2-7 Tabulated Results from Ahn et al. (2007)

Specimen	S_r (ksi)	Number of Cycles	Failure Mode
ST-F-A1	14.5	2,120,000	Shank Failure
ST-F-A2		2,535,490	Shank Failure
ST-F-A3		2,828,560	Shank Failure
ST-F-B1	18.3	656,880	Shank Failure
ST-F-B2		735,740	Shank Failure
ST-F-B3		1,300,800	Shank Failure
ST-F-C1	21.8	231,580	Shank Failure
ST-F-C2		274,440	Shank Failure
ST-F-C3		161,430	Shank Failure

Figures 2-18 – 2-20 taken from Ahn et al. (2007) show the relative slip plotted against the load for the three given stress ranges. These plots show that there is an increase in the relative slip with increasing number of cycles. The stud bears against the concrete and causes high bearing stresses in the concrete at the base of the stud. Due to deformations in the concrete at this point, the concrete began crushing at which point the shear stud was also allowed to deform. This pattern continued gradually until just before failure when the relative slip increased sharply (Ahn et al. 2007).

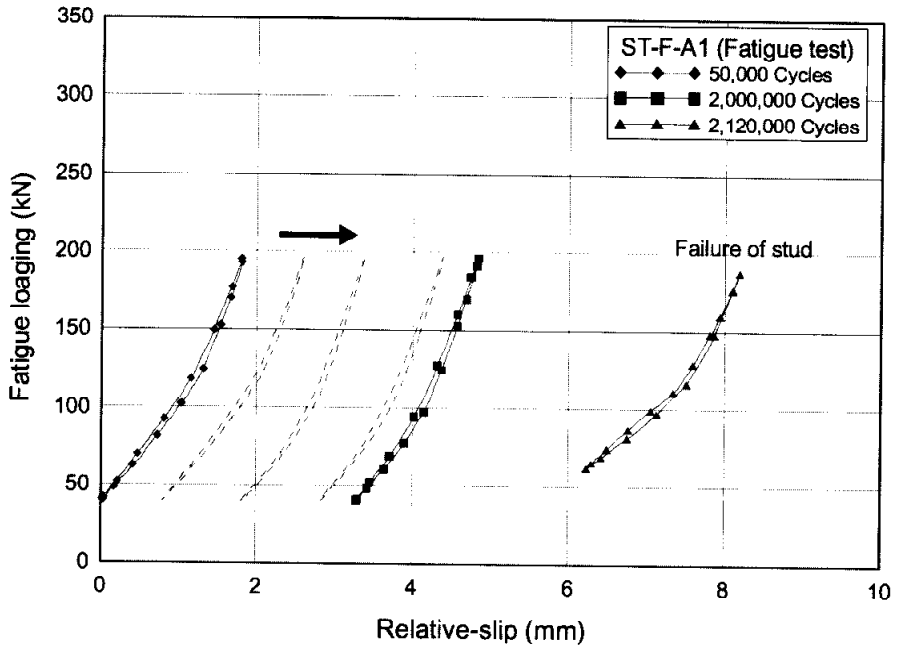

Figure 2-18 Load vs. Slip for 14.5 ksi Stress Range (Ahn et al. 2007)

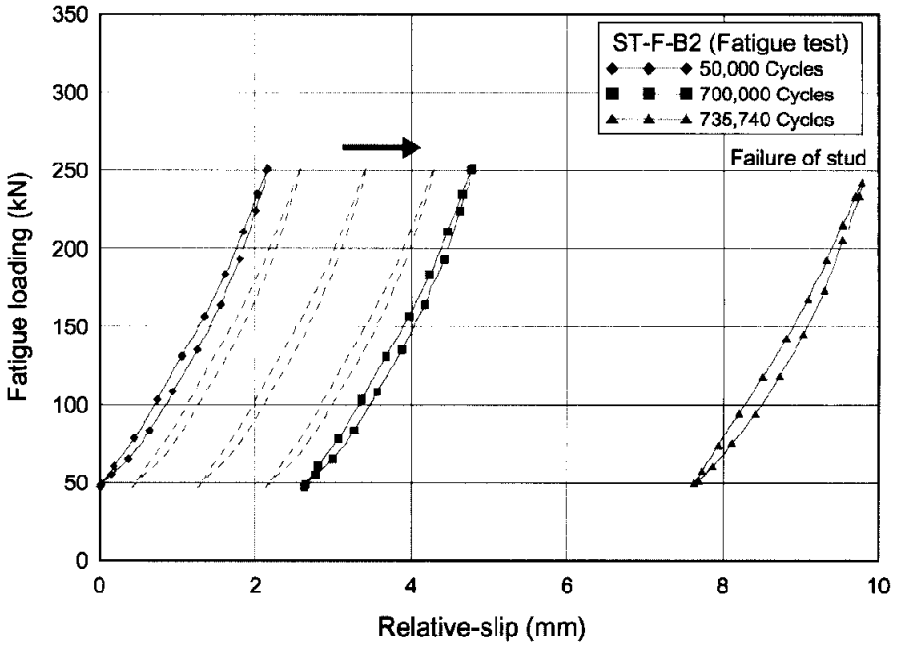

Figure 2-19 Load vs. Slip for 18.3 ksi Stress Range (Ahn et al. 2007)

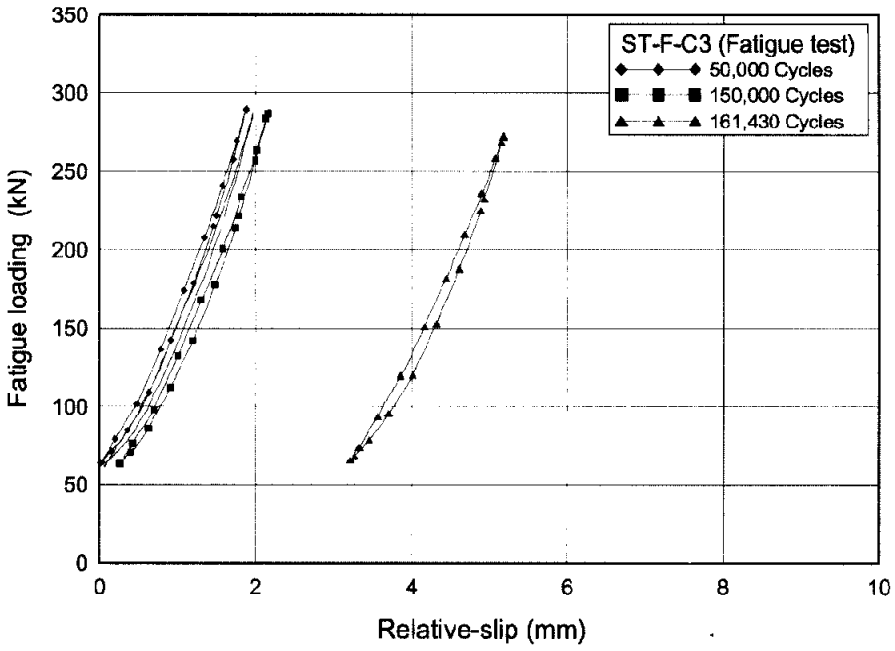

Figure 2-20 Load vs. Slip for 21.8 ksi Stress Range (Ahn et al. 2007)

Another interesting observation made in this test program was how a reduction of the initial static stiffness could be used to define failure of the specimen. The researchers claim that fatigue damage does not occur until the stiffness variation decreases to 0.95 at which point the damage occurs and rapidly accelerates the failure. In the case of the 14.5 ksi stress range, it was determined that fatigue damage did not occur until approximately 1,500,000 cycles. After this point, the stiffness variation continued to decrease until it was 0.95 or less and failure occurred (Ahn et al. 2007). The plots for variation of stiffness are shown on normal and log scales in Figures 2-21 and 2-22 respectively.

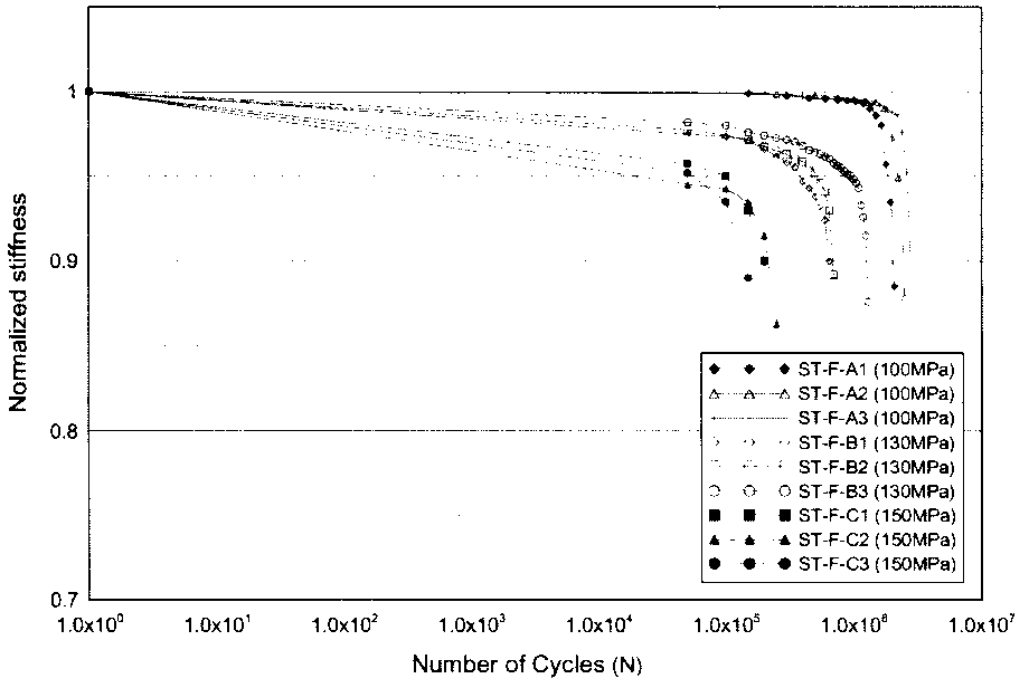

Figure 2-21 Log Scale of Stiffness Variation (Ahn et al. 2007)

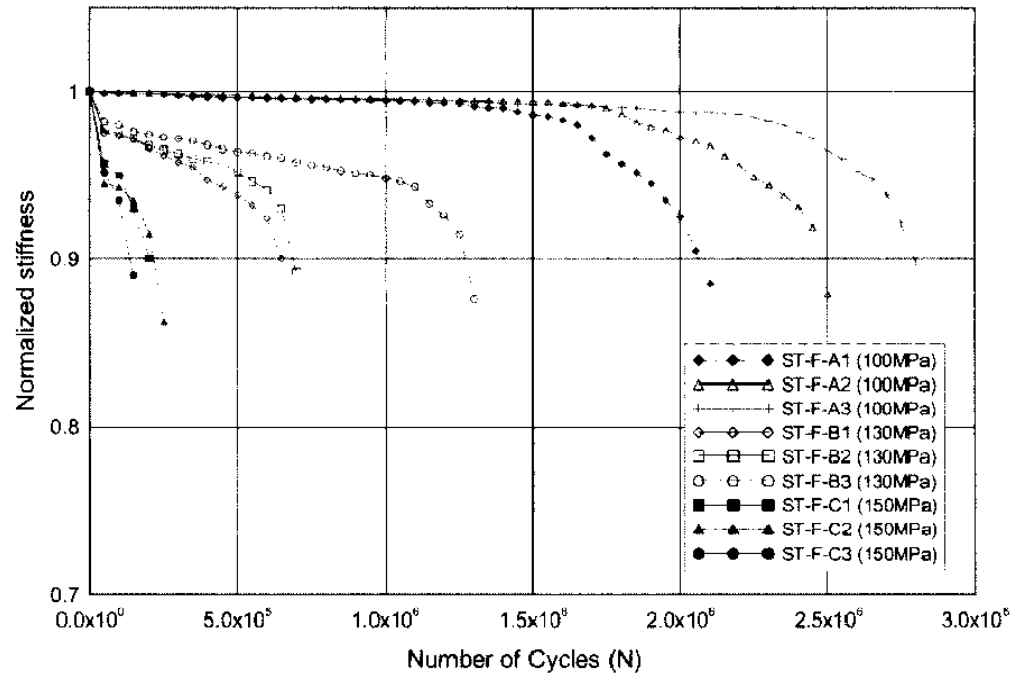

Figure 2-22 Normal Scale of Stiffness Variation (Ahn et al. 2007)

The results from this test program were compared to the Eurocode 4 (CEN 1997), AASHTO (2004), and Japanese Society of Steel Construction (JSSC 1995). After performing a linear regression analysis of the test data, a slope of 7.5 and a mean value of fatigue strength at 2 million cycles was determined to be 15.5 ksi. When this information was compared to the three previously mentioned design codes, the $^{5}/_{8}$"-diameter shear connectors satisfied all of the design codes.

2.5.10 Hanswille et al. (2007)

Although previous experimental research has been done on the residual strength of headed stud shear connectors, these researchers wanted to add a comprehensive study to this data. The main purpose of this test program was to determine fatigue life and show a possible reduction in static strength due to cyclic loading.

A total of 71 push-out specimens were fabricated for this test program, but the only tests that will be covered here are the twelve corresponding to constant amplitude cyclic loading. Similar to other tests of this type, the specimens were fabricated according to the standard given in Eurocode 4 (CEN 2005). In order to simultaneously cast both slabs in the horizontal position from the same concrete batch, the steel section was cut down the middle of the web and welded back together after the concrete had cured. The bottoms of the concrete slabs were restrained laterally by using steel angles. The purpose of this was to prevent additional tensile forces on the studs as well as make the behavior more like that in an actual bridge (Hanswille et al. 2007).

For cyclic testing, a load frequency of 3 Hz was used. This was run constantly with the exception of being stopped intermittently so that slip and stiffness could be measured. This was done by loading the specimen monotonically while recording load from the load cell, ram

displacement, longitudinal displacement between concrete slab and steel using 2 LVDTs, and also the uplift of the slabs.

Because using materials from different sources or different batches could skew the test results, care was taken to make sure that all steel sections, headed studs, and steel reinforcing bars came for the same batches respectively. The mean yield stress and ultimate stress of the steel section were 48.9 ksi and 65.0 ksi respectively. The mean yield stress and ultimate stress of the shear studs were 63.9 ksi and 76.6 ksi respectively.

During fatigue tests, failure was defined as when the strength of the studs was reduced so that the peak load in a fatigue cycle caused failure of the specimen. The results from constant amplitude fatigue testing are shown in Table 2-8. Although there were thirteen push-out specimens tested under constant amplitude cyclic loading, these were done in five series with three specimens in the first four series and a single specimen in the fifth series. Instead of giving results from each of the thirteen, only the averages from each series were reported. For series S1, S2, S3, and S4, the number of cycles to failure represents the average of three tests. For series S5E, the number of cycles to failure represents the average a single test.

Table 2-8 Tabulated Results for Hanswille et al. (2007)

Series	S_r (ksi)	Number of Cycles
S1	15.64	6,200,000
S2	17.55	1,200,000
S3	19.17	5,100,000
S4	13.81	3,500,000
S5E	18.02	6,400,000

The researchers from this test program performed a comprehensive investigation of the failure modes of their push-out specimens in order to determine exactly how failure was initiated as well as how it progressed throughout the test. After failure, both concrete slabs were completely removed from the specimen, and in many cases the steel section was cut into slices

so that metallurgical investigations could be carried out on the shear stud failure surfaces. The fracture surfaces on the studs consisted of the typical dull fatigue fracture surface caused by crack propagation and a bright or shiny surface that corresponded to the forced fracture at the very end of the cyclic testing (Hanswille et al. 2007). The two main failure modes were denoted as Mode A and Mode B failures. Mode A failure consisted of crack initiation at the base of the shank between the shank and weld collar and propagation continued horizontally through the shank. Mode B failure consisted of crack initiation either at the previously mentioned location or at the weld toe and propagation continued down through the flange of the steel section. It was noted that the peak load in the cyclic testing had an influence on whether or not the failure had a tendency to be Mode A or Mode B. In the cases of high peak loads such as in series S2 and S4, only Mode A failures were observed. In the cases of low peak loads such as in series S1, S3, and S5E, Mode B failures were typically observed. The researchers also pointed out that in some cases both failure modes were observed in the same stud therefore giving two cracks that were propagating simultaneously (Hanswille et al. 2007).

2.6 S-N Curve of All Previous Data

All of the data from the research explained previously is compiled into a single S-N curve on a log-log plot in Figure 2-23 so that it can be viewed and compared simultaneously. Design curves for AASHTO (2007) and Eurocode 4 (CEN 2005) are also shown so that these can also be compared to the experimental data from which they were derived.

Although design according to the BS 5400 (BSI 1980) and JSCE (2009) were evaluated earlier in this chapter, these two code equations are not included in Figure 2-23 because of their dependence on parameters other than just the stress range. Since the data points presented come

from many test programs with various concrete strengths, showing the design curves for the BS 5400 (BSI 1980) and JSCE (2009) would not give a good comparison to the test results.

There is a noticeable scatter in the data in Figure 2-23 that is consistent with fatigue testing of push-out specimens and fatigue testing in general. This is one of the characteristics of fatigue testing that makes coming up with design equations quite difficult. The equation needs to be conservative enough to cover the scatter of the data but not so conservative that large amounts of time and money are wasted with over-designing the structure. Another interesting observation seen in this figure is the difference in design codes. Since the equation from the Eurocode 4 (CEN 2005) was based on a log-log relationship, this is shown as a straight line in the figure. On the other hand, since the design equation for AASHTO (2007) was derived based on a semi-log relationship, this plot is shown as a curved line in the figure with a CAFL or constant amplitude fatigue limit of 3.5 ksi, a value below which no fatigue propagation is expected. Because of its curved shape, the design equation given by AASHTO (2007) gives extremely conservative results compared to the design equation given by Eurocode 4 (CEN 2005).

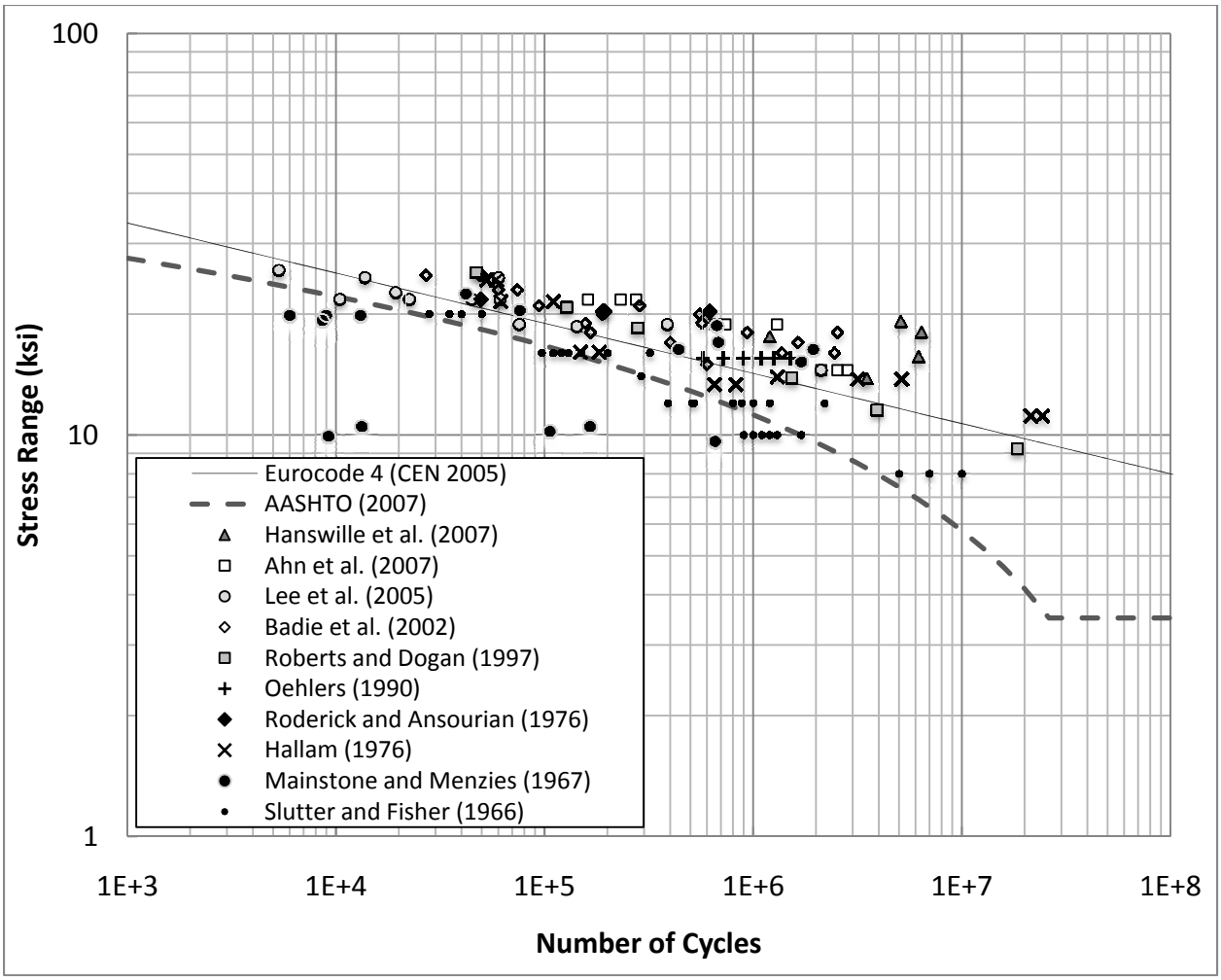

Figure 2-23 S-N Curve of All Previous Research

Chapter 3 TEST PROGRAM

3.1 Overview

This chapter is dedicated to presenting the details of the test program. It will provide the details used in the development of the test matrix and specimen design, document the fabrication of the push-out specimens, describe the typical test setup and instrumentation plan, and lastly it will explain the loading protocol as well as the post-failure procedure that was used for the test program.

3.2 Specimen Identification

The specimen identification scheme shown in Figure 3-1was used in the test program and will be used throughout this thesis to help identify the various test specimens.

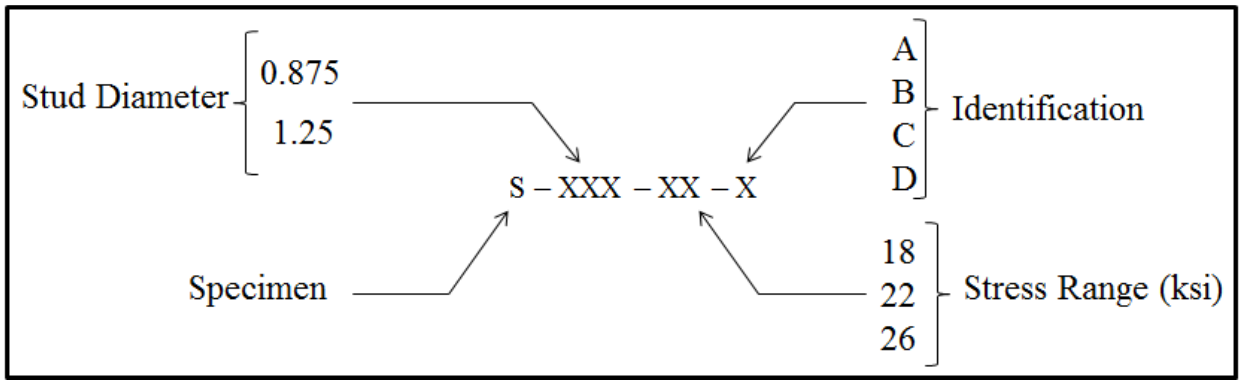

Figure 3-1 Specimen Identification

3.3 Test Matrix

Four shear stress ranges were originally selected for the test program, namely, 22, 18, 14, and 10 ksi, but after carrying out the 22 and 18 ksi stress ranges, it became evident that it would be impractical to test at the 14 and 10 ksi stress ranges due to time constraints on the project. Therefore it was chosen to test at a 26 ksi stress range which in turn would shorten the amount of time to complete the testing. Also, instead of only testing six specimens at each stress range, the remaining specimens were spread out over the three stress ranges so that there would be eight specimens for each stress range. By increasing the number of tests for each stress range, the wide scatter of the data would become more apparent.

Since the push-out specimens were cast with three separate batches of concrete over a period of six weeks and the concrete compressive strengths were not exactly the same, the decision to place one specimen from each concrete batch in each stress range and stud size group was made. This was done so that if concrete strength did affect the fatigue life, it would only impact the scatter of the data and it would not affect the slope of the S-N curve drastically.

It is important to note how the load range applied to the push-out specimen was converted to a stress range. The following equation was used to calculate the stress range (S_r):

$$S_r = \frac{P_{max} - P_{min}}{(\#\ of\ studs) * (\pi * d^2/4)} \quad (3\text{-}1)$$

where

P_{max} = Maximum fatigue load

P_{min} = Minimum fatigue load

d = Diameter of stud

It was decided to keep the minimum stress the same for all specimens at 5 ksi which gives a close approximation to the stress related to the permanent dead load on a composite

bridge. Since the area of the 1¼"-diameter stud is not exactly twice the area of the $^{7}/_{8}$"-diameter stud, the load ranges for the two stud size specimens were not exactly the same but very close. Information regarding the test matrix and specimen details can be seen in Table 3-1.

Table 3-1 Test Matrix

Specimen ID	Min. Stress (ksi)	Max. Stress (ksi)	S_r (ksi)	Concrete Mix
S-0.875-22-A	5	27	22	Mix 3
S-0.875-22-B	5	27	22	Mix 2
S-0.875-22-C	5	27	22	Mix 1
S-0.875-22-D	5	27	22	Mix 1
S-1.25-22-A	5	27	22	Mix 3
S-1.25-22-B	5	27	22	Mix 2
S-1.25-22-C	5	27	22	Mix 1
S-1.25-22-D	5	27	22	Mix 2
S-0.875-18-A	5	23	18	Mix 2
S-0.875-18-B	5	23	18	Mix 3
S-0.875-18-C	5	23	18	Mix 1
S-0.875-18-D	5	23	18	Mix 1
S-1.25-18-A	5	23	18	Mix 2
S-1.25-18-B	5	23	18	Mix 3
S-1.25-18-C	5	23	18	Mix 1
S-1.25-18-D	5	23	18	Mix 2
S-0.875-26-A	5	31	26	Mix 2
S-0.875-26-B	5	31	26	Mix 3
S-0.875-26-C	5	31	26	Mix 1
S-0.875-26-D	5	31	26	Mix 1
S-1.25-26-A	5	31	26	Mix 3
S-1.25-26-B	5	31	26	Mix 2
S-1.25-26-C	5	31	26	Mix 1
S-1.25-26-D	5	31	26	Mix 2

3.4 Material Properties

Material properties of all three concrete mixes and steel materials used in this test program can be found either in this section or in Appendix A.

3.4.1 Concrete Properties

Due to the large number of push-out specimens to be manufactured, pouring of concrete was done in three pours over a six week time period. All concrete was supplied by Couch Ready Mix USA in Opelika, AL. The concrete mix proportions supplied by the concrete batch plant for each of the three mixes can be seen in Table 3-2. Because the exact amount of water added after leaving the batch plant is unknown, the water proportions in this table are not exact. In order to determine the compressive strength of the concrete, thirty-six 4×8 cylinders were made from each concrete mix. For each concrete mix, eighteen of these cylinders were stored in a moist-cure room while the remaining eighteen cylinders were allowed to cure under the same laboratory conditions as the push-out specimens. Compression tests were performed at 7 days, 14 days, 28 days, 3 months, and 6 months for both the moist-cured cylinders and lab-cured cylinders. Three cylinders were tested at each age, and the average compressive strength was determined. By doing this, a plot of average compressive strength vs. time could be constructed so that the concrete strength would be known at any given time or curing condition.

Table 3-2 Concrete Mix Proportions

	Mix 1	Mix 2	Mix 3
#57 Limestone	1919 lb/yd^3	1919 lb/yd^3	1910 lb/yd^3
Sand	1280 lb/yd^3	1293 lb/yd^3	1280 lb/yd^3
Cement	496 lb/yd^3	496 lb/yd^3	496 lb/yd^3
C Ash	124 lb/yd^3	126 lb/yd^3	124 lb/yd^3
Water*	92.75 lb/yd^3	163 lb/yd^3	144 lb/yd^3
ADVA 140M	---	12 oz/yd^3	12 oz/yd^3
Darex II AFA	1.0 oz/yd^3	1.667 oz/yd^3	1.667 oz/yd^3
Daratard 37	24.5 oz/yd^3	12 oz/yd^3	50 oz/yd^3

*Actual amount of water is not known

Figures 3-2 through 3-4 give a graphical representation of the relationship of average compressive strength of concrete with time for mixes 1, 2, and 3 respectively, and these values are tabulated in Table 3-3. Even though the test cylinders were cured alongside the push-out

specimens, the strengths could still differ because of differences in surface area to volume ratios as well as other factors. For this reason, actual values for concrete strength at the time of testing are not given, but should be assumed to be somewhere between that of the air-cured cylinders and the moist-cured cylinders.

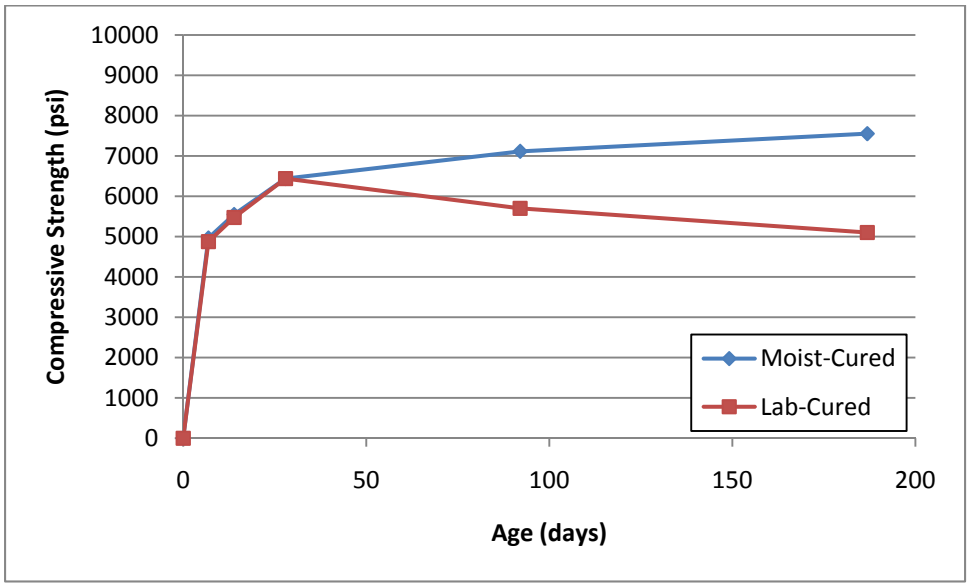

Figure 3-2 Compressive Strength of Concrete Mix 1

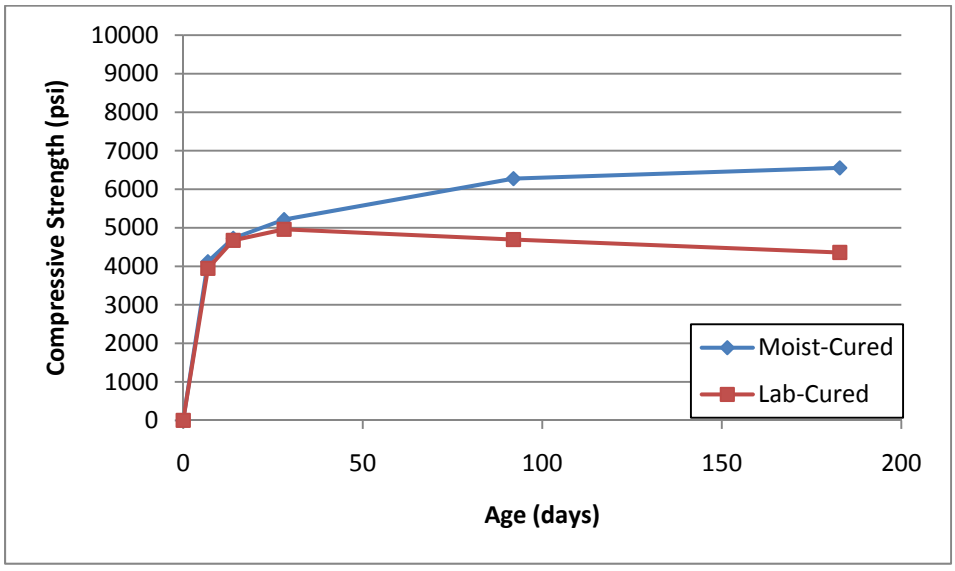

Figure 3-3 Compressive Strength of Concrete Mix 2

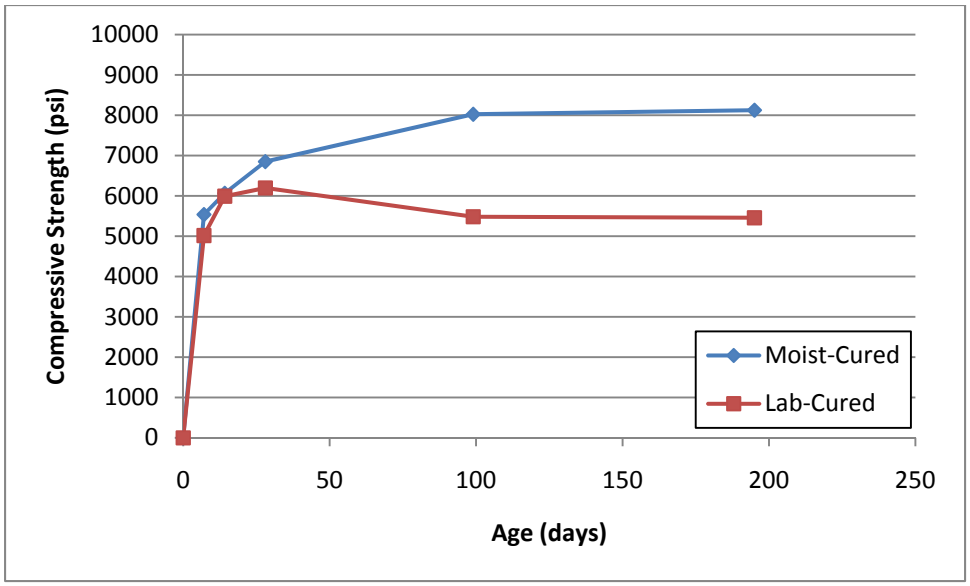

Figure 3-4 Compressive Strength of Concrete Mix 3

Table 3-3 Compressive Strength of Concrete Mixes

	Mix 1		Mix 2		Mix 3	
	Lab-Cured	Moist-Cured	Lab-Cured	Moist-Cured	Lab-Cured	Moist-Cured
7 Day	4875	4964	3946	4119	5017	5539
14 Day	5475	5549	4675	4726	5992	6065
28 Day	6439	6439	4960	5212	6198	6851
3 Month	5700	7115	4695	6277	5483	8025
6 Month	5103	7553	4359	6556	5457	8126

3.4.2 Steel Properties

There were various steel components used in this test program which consisted of wide flange beams, a steel plate that studs were welded to for performing the bend test, steel reinforcement in concrete slab, and the cold-formed headed shear studs. The properties and characteristics of each of these will be described in this section.

The wide flange beam used in each push-out specimen consisted of a 26" long W10×60 of ASTM A992 Gr. 50 steel. The mill report and chemical composition of this steel can be found in Appendix A. To perform the bend test, the studs were welded to a piece of ¾"-thick

steel plate with similar properties to the W10×60. The mill report for this steel is also found in Appendix A.

Slab reinforcement for concrete slabs consisted of #4 Grade 60 rebar. All reinforcement was cut, bent, and tied together in the Auburn University Concrete Laboratory. Bar chairs were tied onto the outside of the reinforcement cages in order to achieve at least a 1" cover to all reinforcement. Spacing and layout of reinforcement cages can be seen in Figures 3-5 and 3-6.

The cold-formed shear studs were provided by Tru-Weld Stud Welding in Medina, OH. The properties for the studs such as yield stress, ultimate stress, and elongation are provided here, and other properties such as chemical composition and large diameter stud dimensions can be found in Appendix A. The $^{7}/_{8}$"-diameter studs had a yield stress, ultimate stress, and elongation of 57.0 ksi, 70.7 ksi, and 29.7% respectively. The 1¼"-diameter studs had a yield stress, ultimate stress, and elongation of 52.8 ksi, 68.1 ksi, and 25.0% respectively.

3.5 Design of Push-Out Specimen

In order to design the test specimen, previous research and other test programs were examined with the goal of having a similar design so that these test results could be compared to other results that have been produced in the past. Many past researchers used a push-out specimen similar to the standard given in Eurocode 4 (CEN 2005), therefore these guidelines along with code requirements in AASHTO (2007) were used to come up with the $^{7}/_{8}$" stud specimen design shown in Figure 3-5 and the 1¼" stud specimen design shown in Figure 3-6.

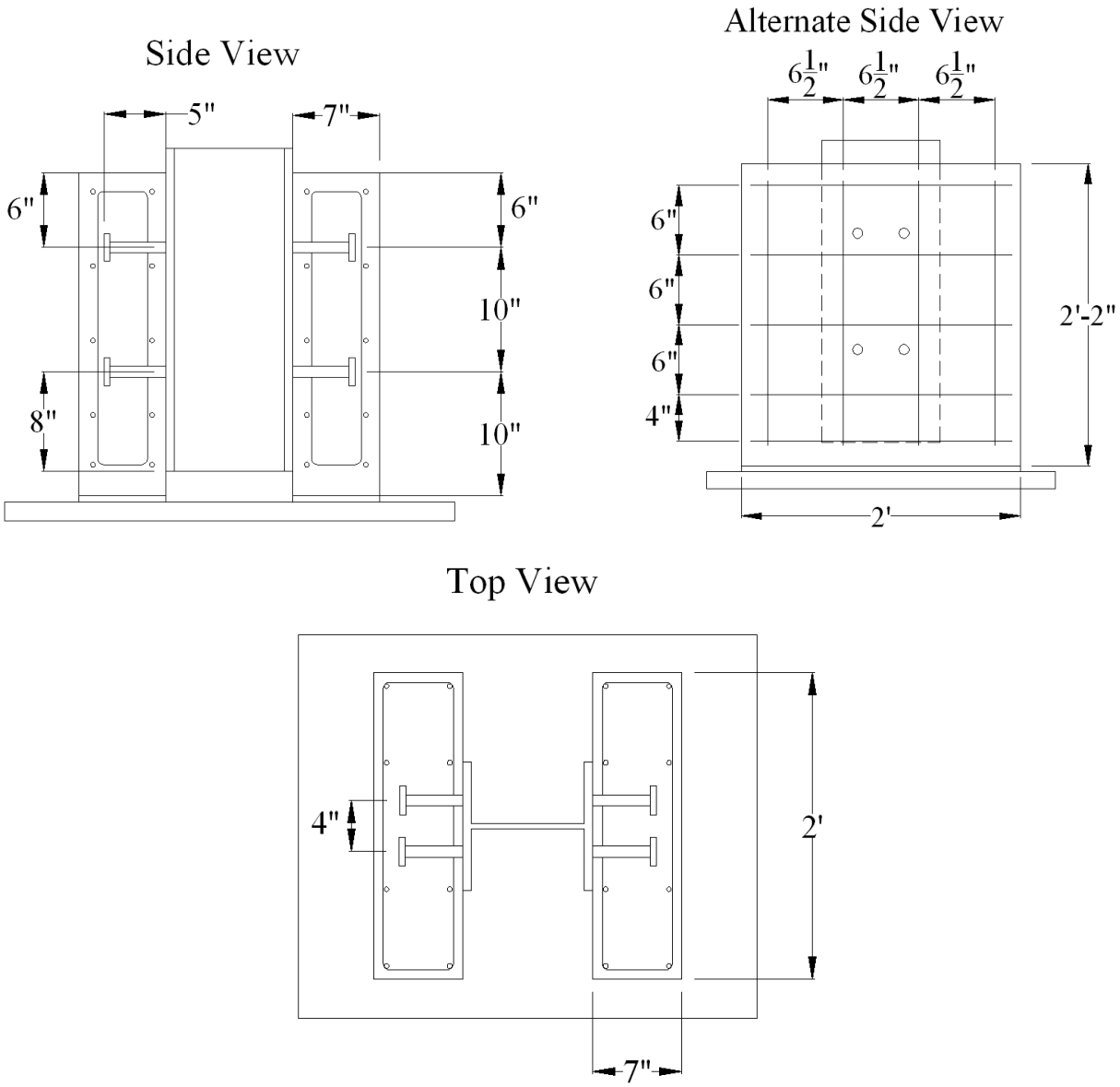

Figure 3-5 Design of $^{7}/_{8}$"-Diameter Push-out Specimen

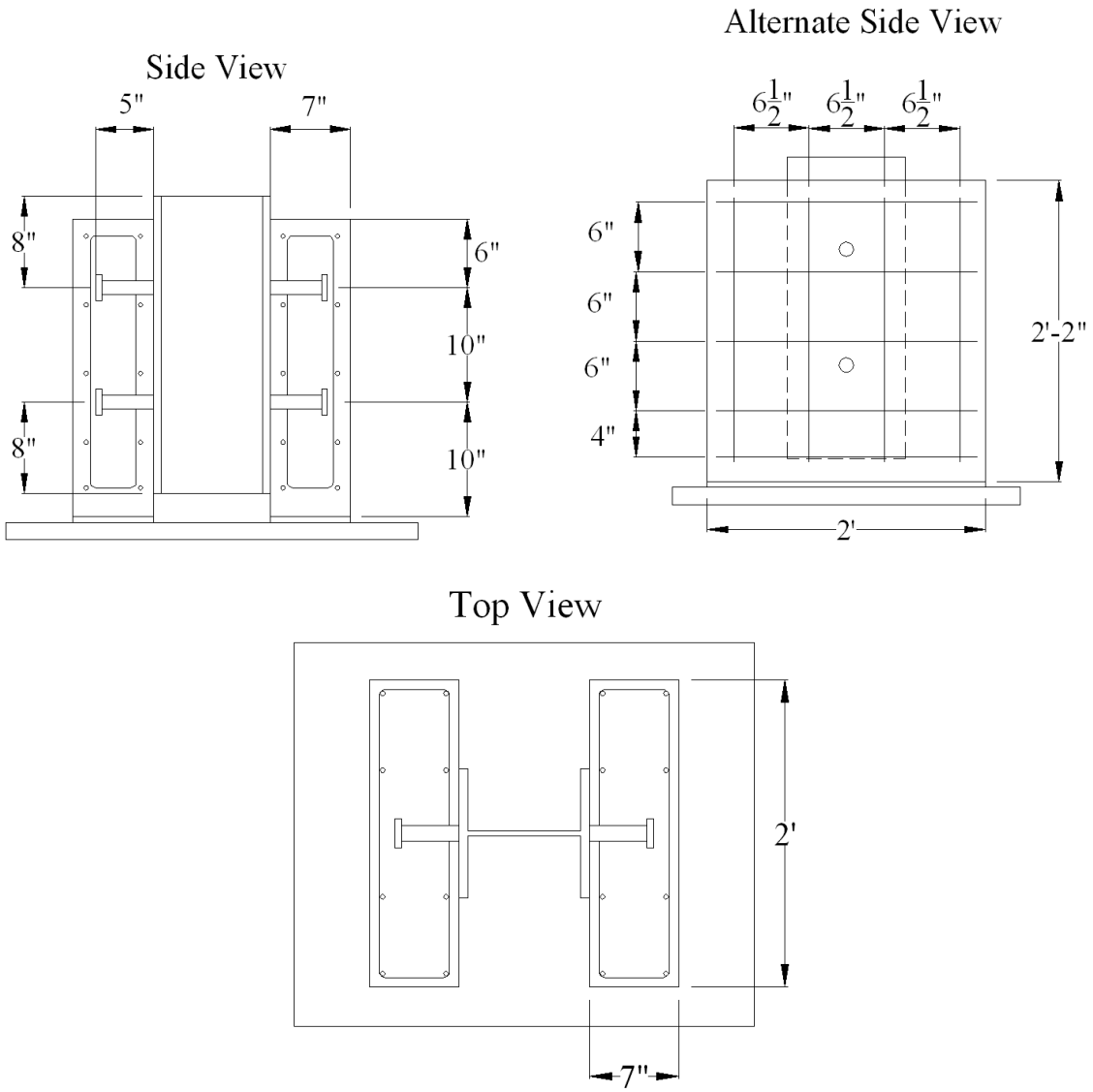

Figure 3-6 Design of 1¼"-Diameter Push-out Specimen

3.6 Manufacturing of Test Specimens

This section describes the process and procedure that was used to fabricate the push-out specimens used in this test. This includes building plywood formwork for casting the concrete slabs, steel fabrication and welding that was performed on the wide flange beams, and the procedure that was followed for casting the concrete slabs.

3.6.1 Concrete Slab Formwork

The wooden formwork used to cast the concrete slabs was built and constructed in the Auburn University Concrete Laboratory out of 2×4's, 2×6's, and ¾" plywood. The plywood was already coated with a single coat of oil, but two coats of polyurethane were additionally applied to any part of the formwork that would be in contact with concrete in an attempt to preserve the formwork for future castings. The formwork was constructed in a way that could be easily disassembled and reassembled to facilitate the next concrete pour.

3.6.2 Steel Fabrication and Welding

At the time of stud welding, the Auburn University Concrete Laboratory did not have sufficient welding capabilities to weld the shear studs to the steel sections. Therefore the welding of all shear studs was done at FabArc Steel Supply Inc., a steel fabricator in Oxford, AL using a drawn-arc welding process shown in Figure 3-7. All stud welding was done with a Pro-Weld Arc 3000 welder and a Pro Weld H.D. Arc Gun AG.900. For the $^{7}/_{8}$"-diameter studs, a current of 1891 amps and 1.012 second weld time were used. For the 1¼"-diameter studs, a current of 2707 amps and 1.812 second weld time was used. To ensure quality welds, studs were welded to a plate of similar steel properties as the W10×60's that were to be used, and then bent 90°. This was done to satisfy the bend test method given in section 7.6.6.1 in AASHTO/AWS D1.5: 2008. The result of this bend test can be seen in Figure 3-8. Although one of the bent studs shows fracture, this fracture occurred in the shank of the stud and not in the weld. This situation still satisfies the bend test. Quality control of the welds was achieved by randomly selecting five studs of each size and bending them less than 15°.

Figure 3-7 Drawn-Arc Welding Process Used for Stud Welding

Figure 3-8 Bend Test Performed on 1¼"-Diameter Studs

3.6.3 Casting of Test Specimens

On the day before the push-out specimens were to be cast, all shear studs were wrapped in plastic wrap to prevent form oil from getting on them. This was done in order to try and achieve the same bond between concrete and shear stud that would be seen in an actual bridge.

The formwork was then coated with form oil to help the forms release from the concrete when the forms were stripped. The flanges of the steel section were greased with WD-40 in an effort to prevent the bond of the steel to the concrete so that all of the force would be transferred through the shear studs and not as friction at the interface. Finally, the plastic wrap was removed from the shear studs, the reinforcement cage was placed into the formwork, and the outside form panel was caulked and bolted into place.

After the concrete truck arrived, a slump test was run in accordance with ASTM C143 to determine the workability of the concrete. Water was added to the concrete until a desirable slump of 3-4" was achieved. After target slump was achieved, 36 4×8 cylinders were made according to ASTM C192 as shown in Figure 3-9.

Figure 3-9 Making 4×8 Concrete Cylinders for Compression Tests

When casting the test specimens, concrete was placed in each slab by using a hopper that was maneuvered by the overhead crane. Each slab was poured in a single lift and vibrated to achieve proper consolidation. This can be seen in Figure 3-10.

Figure 3-10 Vibrating Concrete to Achieve Proper Consolidation

After placement and vibration of concrete, the surface was screeded and finished with a wooden trowel. Shortly after initial set of the concrete, the test specimens were covered with a layer of wet burlap and a layer of plastic, as shown in Figure 3-11, to retain the moisture and improve the curing conditions of the concrete. Each day for the next week, the burlap was rewet to keep the concrete moist while curing.

Figure 3-11 Concrete Curing Under Wet Burlap

3.7 Test Setup

This section gives an overview of the test frame, the capacity of the hydraulic actuator used for testing, and the pre-testing procedure used to get the specimen in place and ready for testing.

3.7.1 Load Testing Frame

A new self-reacting load frame, shown in Figure 3-12, was specifically designed for this test program in order to house the hydraulic actuator that would be used to load the specimen. The frame was designed by the author and was fabricated by FabArc Steel Supply Inc., a steel fabricator in Oxford, AL, and erected by ROPAC Inc., a steel erector located in Deatsville, AL. Both fabricator and erector are AISC-certified. Although static testing of the push-out specimens is not included here, the frame was designed to be able to test the push-out specimens up to static failure.

Figure 3-12 Load Testing Frame

3.7.2 Hydraulic Actuator

An MTS Model 244.51 fatigue rated actuator was acquired for testing these push-out specimens. The actuator, capable of utilizing load control as well as displacement control, can range from 220 kips in tension to 220 kips in compression and has a stroke range of 0 to 40 inches. An MTS Model 407 controller was used to control the actuator, and load control was used for all cyclic testing.

3.7.3 Push-Out Specimen Setup

The push-out specimen was lifted and placed into the self-reacting test frame using the laboratory 10 ton capacity overhead crane. After making sure that the actuator was plumb, care was taken to center the actuator with the center of the steel section to prevent any eccentricity and consequently any bending of the steel section causing non-uniform stress distribution. A sheet of $^{5}/_{8}$"-thick drywall measuring 12"×32" was placed under the base of each concrete slab in order to take out any irregularities in the concrete surface and provide a uniform bearing area. Steel plates were placed between the base of the actuator swivel and the top of the steel section so that the load would be as uniform as possible when it was introduced to the top of the steel section.

Aluminum angles were connected and bolted to the top of the concrete slab. Laser sensors were mounted to the aluminum angles and the laser was reflected off of another piece of aluminum angle that was mounted to the bottom of the steel section using a magnet. This configuration was used to measure the relative slip between the top of the concrete slab and the bottom of the steel section because these two locations would theoretically have no stress.

A W8×35 beam was placed at the bottom of each concrete slab and four $^{5}/_{8}$"-diameter steel bars ran between the two steel beams. These beams were used to prevent the bottom of the concrete slabs from moving out of plane and therefore putting axial forces on the shear studs. A schematic of the test setup is shown in Figure 3-13a and a photo of the setup is shown in Figure 3-13b.

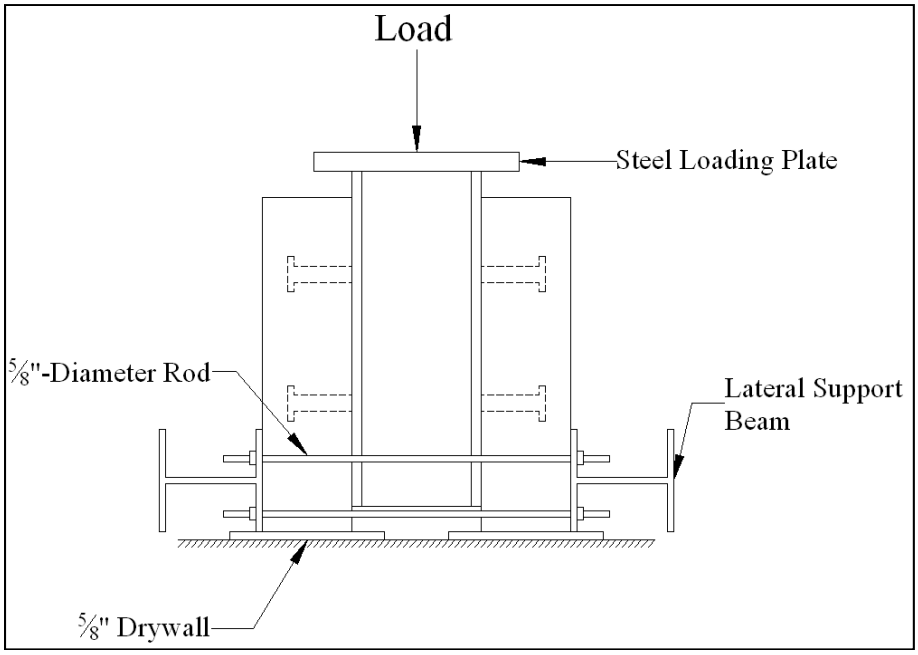

Figure 3-13a Schematic of Test Setup

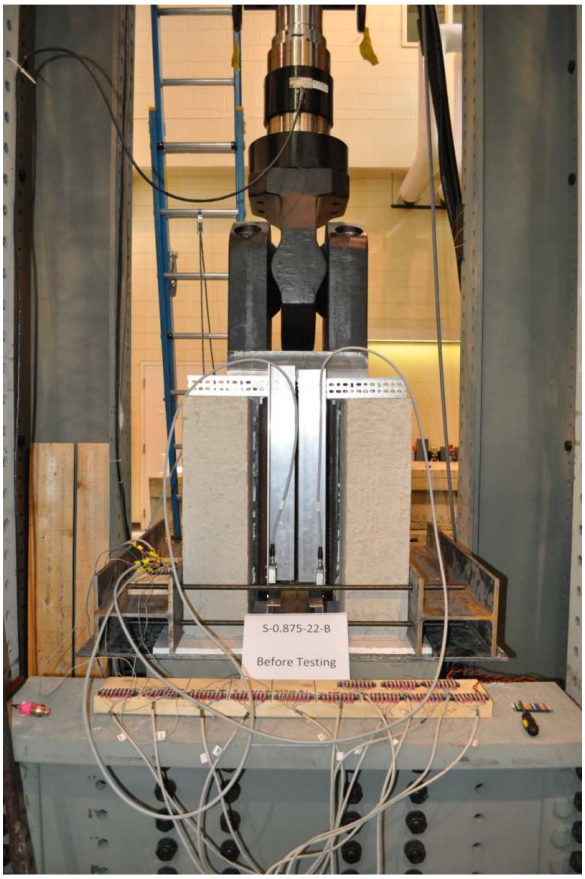

Figure 3-13b Photo of Test Setup

3.8 Instrumentation and Data Measurement

This section describes the data acquisition system and explains how data was collected as well as what sampling rate was used for data collection. Information will be given regarding how each specimen was instrumented using non-contact laser sensors to measure relative slip between the concrete and steel section and why it was chosen to measure the relative slip in this manner.

3.8.1 Sampling Rate

Using a Pacific Instruments 6000 Data Acquisition System, data was collected at a rate of 200 samples per second per channel. The first two tests were monitored closely and data was recorded for 10 seconds every 5000 cycles. Thereafter, data was recorded throughout the entire test and from those recordings, select data was exported for analysis. This was done so that the tests could be run continuously and if failure occurred overnight, no data would be lost. The number of cycles each specimen was subjected to was recorded constantly by the MTS Model 407 Controller.

3.8.2 Relative Slip

The relative slip between the concrete and steel section were measured using four non-contact laser sensors with accuracy up to 0.01mm. These laser sensors will be referred to as front left (FL), front right (FR), back right (BR), and back left (BL). The two points that were selected to measure the relative slip between were the top of the concrete slab and the bottom of the steel section. Pieces of aluminum angle were bolted together as well as bolted to the top of the concrete slabs using Redhead concrete anchors. The laser sensors were then bolted to the bottom

of the aluminum angle. Another piece of aluminum angle used to reflect the laser was attached to a magnet at the bottom of the steel section. A schematic drawing showing the instrumentation setup to measure relative slip is shown in Figure 3-14a, and a photo of the setup is shown in Figure 3-14b.

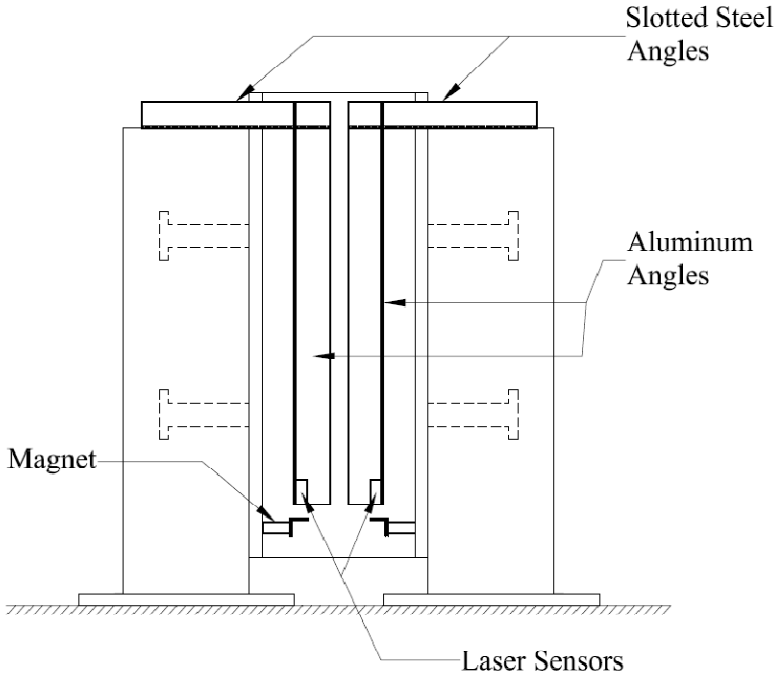

Figure 3-14a Schematic of Instrumentation Setup to Measure Relative Slip

Figure 3-14b Photo of Instrumentation for Relative Slip Measurement

3.9 Loading Procedure

When each test was started, the load was cycled slowly five to ten times between 0 and 130 kips which was approximately 40% of the static capacity to seat the specimen and break any bond between the concrete and steel flanges that might have developed. Once this was done, the load was increased to the mean load and cyclic loading was started. It was decided to change the loading frequency for some tests in order to shorten the time needed to fail the specimen. Loading was carried out using a sine wave and an example of this loading pattern run at 2 Hz is shown for specimen S-0.875-22-A in Figure 3-15. Only full load cycles were counted in the number of cycles. Cyclic loading was continued until the strength of the studs was reduced enough that the peak load in a single fatigue cycle was enough to fail the specimen statically.

For the first specimen (S-0.875-22-A), all testing was supervised and therefore was stopped overnight.

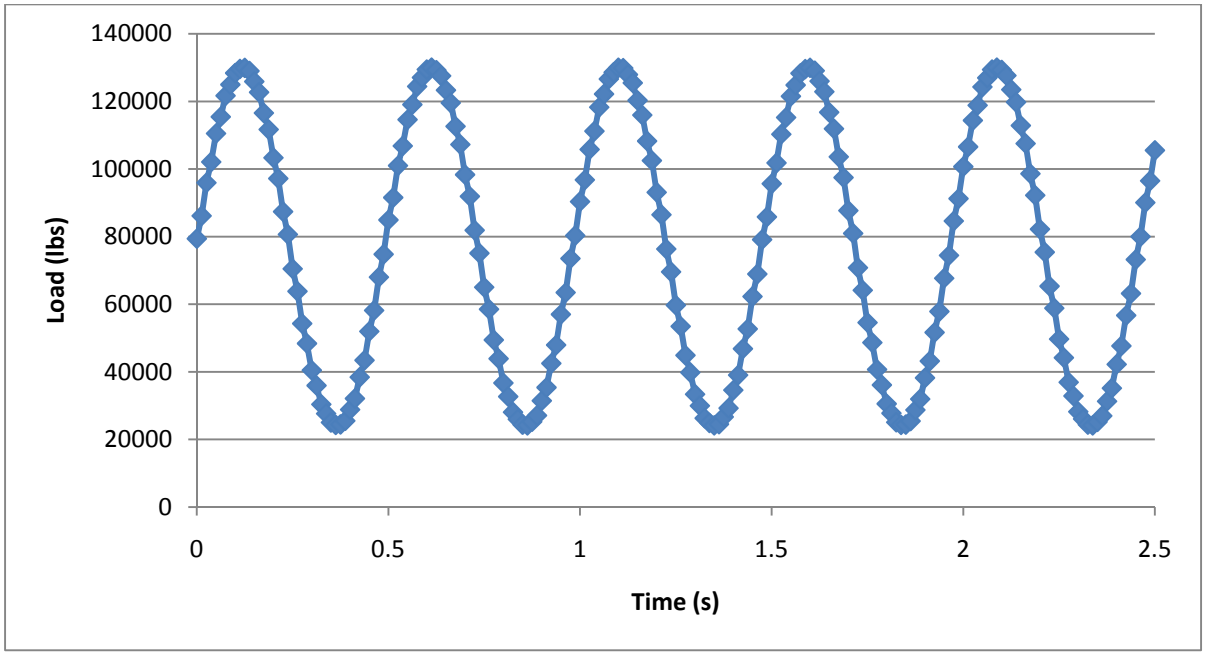

Figure 3-15 Sample Sinusoidal Loading History for S-0.875-22-A

3.10 Post Failure Procedure

When failure of the push-out specimen took place, there were three scenarios that were observed. The first was when one side, right or left, failed as a result of the peak load during cyclic loading, and the other side was able to be failed statically in order to examine the failure surface. The second was when one side, right or left, failed as a result of the peak load during cyclic loading, but the other side was unable to be failed statically because the fatigue cracks had not propagated through enough of the diameter of the studs to reduce the static strength enough to be failed by the 220 kip capacity actuator. The last scenario occurred when both right and left sides failed simultaneously, or almost simultaneously, under the peak load during cyclic loading.

When this happened, static loading was unnecessary in order to examine failure surfaces of all studs.

Once the steel and concrete slabs were separated, many of the fractured studs had concrete debris lodged in them therefore making it difficult to see the failure surface. To prevent damaging the studs and failure surfaces, compressed air was used to clean out as much of the debris as possible. Documentation of the condition of the studs was made by using a numbering convention for the studs and pictures of all failed studs were taken.

Chapter 4 RESULTS AND DATA PRESENTATION

4.1 Overview

This chapter presents the results of the test program described in the previous chapter in the form of pictures, charts, and tables. The results are presented in a table that includes specimen name, testing frequency, minimum and maximum stresses, stress range, number of cycles to failure, side of failure, and concrete batch that was used for each specimen. A section of this chapter will then be dedicated to showing how the data was developed to then be used in the subsequent charts that will be shown. A numbering convention will then be given for the studs so that the pictures shown within this chapter can be related to a specific stud on each corresponding specimen. Next, the results for each stress range tested will be given individually so that trends within each stress range can be shown. Lastly, a comparison of all of the stress ranges will be made so that conclusions and trends can be seen for the tests as a whole.

4.2 Summary of Results

The test results are summarized in Table 4-1 below. This table will be referred to throughout this chapter for information about each specimen and the parameters under which it was tested. In regards to the concrete mix that corresponds to each specimen, Mix 3 had the highest strength, Mix 1 had the intermediate strength, and Mix 2 had the lowest strength. Concrete strength and its effect on the fatigue life will be examined in more detail in Chapter 5 of this thesis.

Table 4-1 Results from Test Program

Specimen ID	Freq. (Hz)	Min. Stress (ksi)	Max. Stress (ksi)	S_r (ksi)	No. of Cycles	Concrete Mix	Side Failed
S-0.875-22-A	2	5	27	22	325,557	3	Left
S-0.875-22-B	2.25	5	27	22	80,346	2	Right
S-0.875-22-C	2.25	5	27	22	245,121	1	Both
S-0.875-22-D	2	5	27	22	91,598	1	Left
S-1.25-22-A	2.25	5	27	22	276,594	3	Right
S-1.25-22-B	2	5	27	22	177,890	2	Right
S-1.25-22-C	2.25	5	27	22	56,753	1	Left
S-1.25-22-D	2	5	27	22	138,588	2	Both
S-0.875-18-A	3	5	23	18	1,586,515	2	Left
S-0.875-18-B	3	5	23	18	2,654,243	3	Left
S-0.875-18-C	3	5	23	18	986,718	1	Left
S-0.875-18-D	3	5	23	18	235,326	1	Right
S-1.25-18-A	3	5	23	18	655,779	2	Left
S-1.25-18-B	3	5	23	18	3,852,257	3	Right
S-1.25-18-C	3	5	23	18	992,965	1	Left
S-1.25-18-D	3	5	23	18	381,667	2	Left
S-0.875-26-A	2	5	31	26	38,295	2	Both
S-0.875-26-B	2	5	31	26	56,507	3	Left
S-0.875-26-C	2	5	31	26	36,094	1	Left
S-0.875-26-D	2	5	31	26	38,101	1	Left
S-1.25-26-A	2	5	31	26	87,933	3	Both
S-1.25-26-B	2	5	31	26	11,097	2	Left
S-1.25-26-C	2	5	31	26	29,987	1	Right
S-1.25-26-D	2	5	31	26	36,583	2	Both

4.3 Definitions

As was mentioned before, data was recorded continuously for most of the tests. This was done so that the tests could be run overnight, and if failure occurred overnight, no data would be missed. Since data was only needed at discrete intervals of testing, 10 seconds of data was exported at select numbers of cycles to get an idea of the behavior of the specimen at that point in time. Depending of the frequency that was being run at that time, these 10 seconds of

exported data represents between 20 and 30 cycles. Therefore, the data that is reported for a given number of cycles represents data for a range of cycles included in the 10 second recording.

When initially setting up each test, it was mentioned that the load was cycled very slowly five to ten times in order to seat the specimen and break any residual bond between the steel and concrete. After this was done, the load was taken to zero and all of the lasers were offset so that they read a value of zero with no load. Therefore, any values for relative slip refer to the amount of displacement relative to the initial start of the test with zero load applied.

4.3.1 Maximum and Minimum Slip

When reporting the maximum and minimum slip values, this was determined by taking the maximum or minimum value for each laser sensor for the 10 seconds that were recorded. In most cases, the average of the maximum or minimum from the four different laser sensors was taken and used for analysis purposes.

4.3.2 Relative Slip Range

For the purposes of this test program, the relative slip range, Δslip, is defined as the difference between the maximum value of slip over 10 seconds of cycling and the minimum value of slip over the same 10 seconds of cycling. This was done by taking the values of maximum and minimum slip as determined above and subtracting them and then taking the values from each laser sensor and averaging them together. It must be mentioned that this is not necessarily the slip range that is taken from a single load cycle, because it is taken from data over a 10 second interval. This is shown graphically in Figure 4-1.

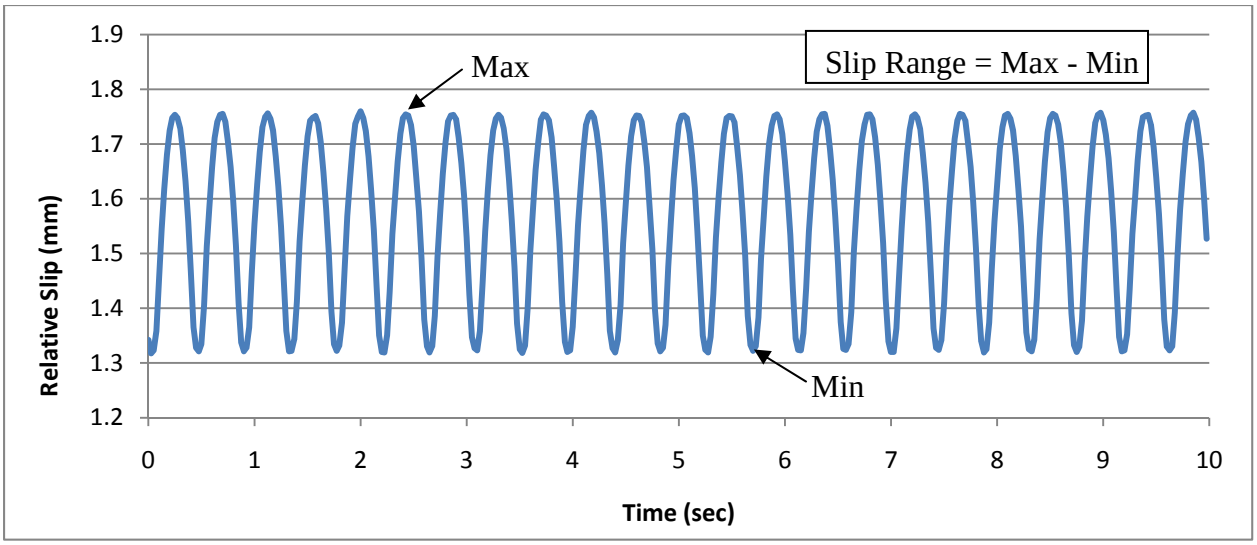

Figure 4-1 Graphical Representation of Relative Slip Range

4.3.3 Reduction in Stiffness

Information about the reduction in stiffness was gathered to see how the stiffness of the specimen degraded throughout the test. A measure of stiffness was determined by using the relative slip range, Δslip, in combination with the load range, ΔP. To determine a value for initial stiffness, the load range, which remains constant for a given test, was divided by an initial value for the slip range taken within the first 5000 cycles using the method given in the preceding section. At any given number of cycles throughout the test, the relative slip range, which increases over time, could be determined to compute the stiffness at that point in time. This number was then compared to the initial stiffness to show how much the stiffness of the specimen had reduced over time.

4.3.4 Slip Charts

The slip charts produced for this test program have typically been used in other push-out fatigue testing research (Ahn et al. 2007). Their main purpose is to give a visual representation of how the relative slip changes as the test progresses. To create these charts, data from the four

laser sensors was taken and averaged at a certain number of cycles and the relationship between load and slip was plotted for half of a cycle (minimum load up to maximum load). This process was then repeated for various numbers of cycles during the test. All of the plots were placed on the same graph and each different line on the graph represents the load vs. average relative slip relationship at different numbers of cycles which are referenced in the legend on the graph.

The two figures below give a representative schematic that shows what can be seen in these charts. N_f in the figures represents the number of cycles at failure. As the test progresses, the decrease of the slope of each line gives an idea as to the amount of reduction in stiffness that is being seen. As the plots shift toward the right as the number of cycles increases, this gives a representation of the cumulative damage that is taking place in the specimen. After examining all of the tests, two situations were seen. The first scenario observed was when the stiffness of the specimens seemed to decrease gradually as seen in Figure 4-2 where the slope of the line changes at each interval. The second scenario observed was when the stiffness stayed mostly constant throughout the test and decreased at the end of its fatigue life as shown in Figure 4-3 where the slope of the line doesn't change until the last interval.

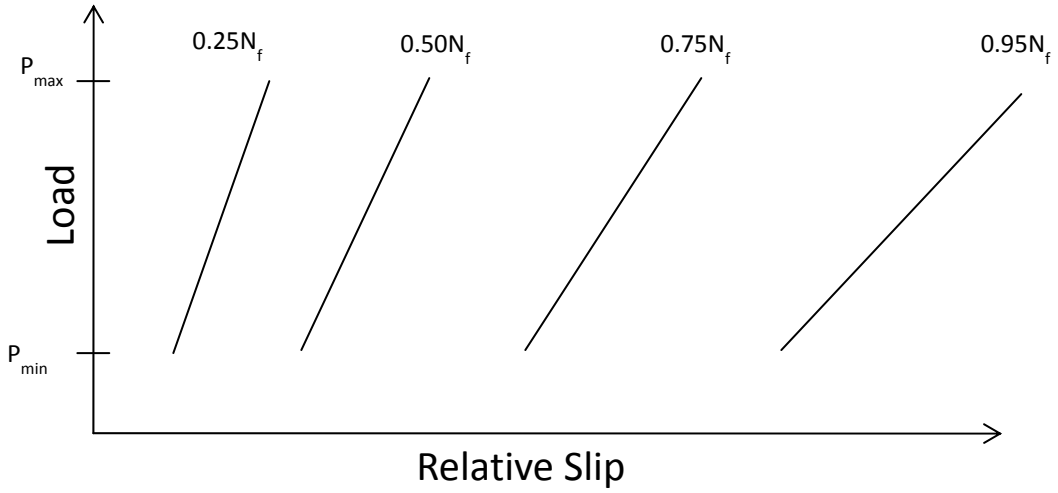

Figure 4-2 Slip Chart Schematic with Gradual Stiffness Reduction

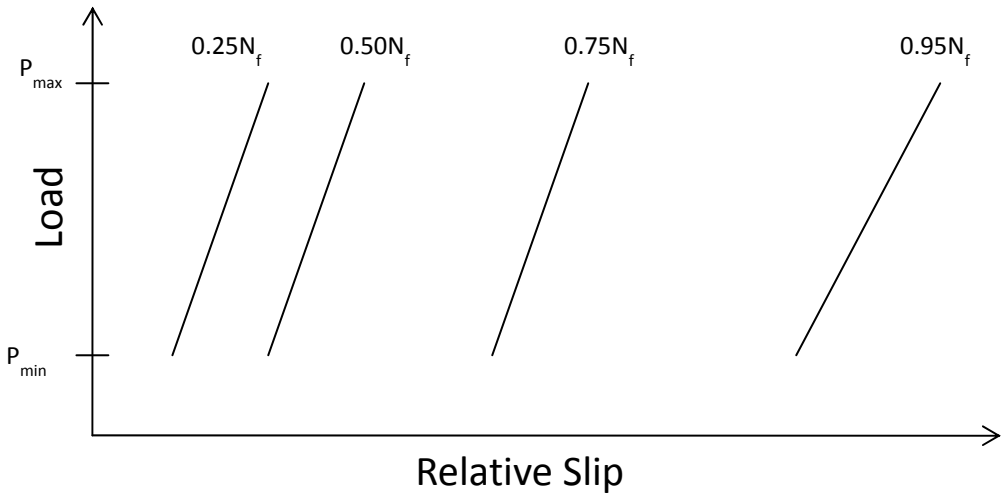

Figure 4-3 Slip Chart Schematic with Late Stiffness Reduction

4.3.5 Rate of Change of Average Maximum Slip

The purpose of showing the rate of change of the average maximum slip is to show how quickly the relative slip is growing at different intervals of testing. This is done by plotting the slope of the average maximum relative slip vs. the number of cycles. The slope of the line was computed by taking the change in maximum relative slip, Δmax_{slip}, and dividing it by the change in number of cycles between two points to give the y-coordinate. The x-coordinate was computed by simply taking the average of the number of cycles for the two points in question. This was done for each interval for which data was recorded.

4.3.6 Stud Numbering Convention

When pictures were taken of the failure surfaces of the studs, a convenient numbering convention was developed so that the studs could be labeled in the picture. Each picture includes a numbered piece of paper that can be used to determine the location of the stud on the push-out specimen that was tested. Since the $^{7}/_{8}$"-diameter push-out specimens had eight studs each and

the 1¼"-diameter push-out specimens only had four studs, the numbering convention differs slightly as can be seen in Figure 4-4.

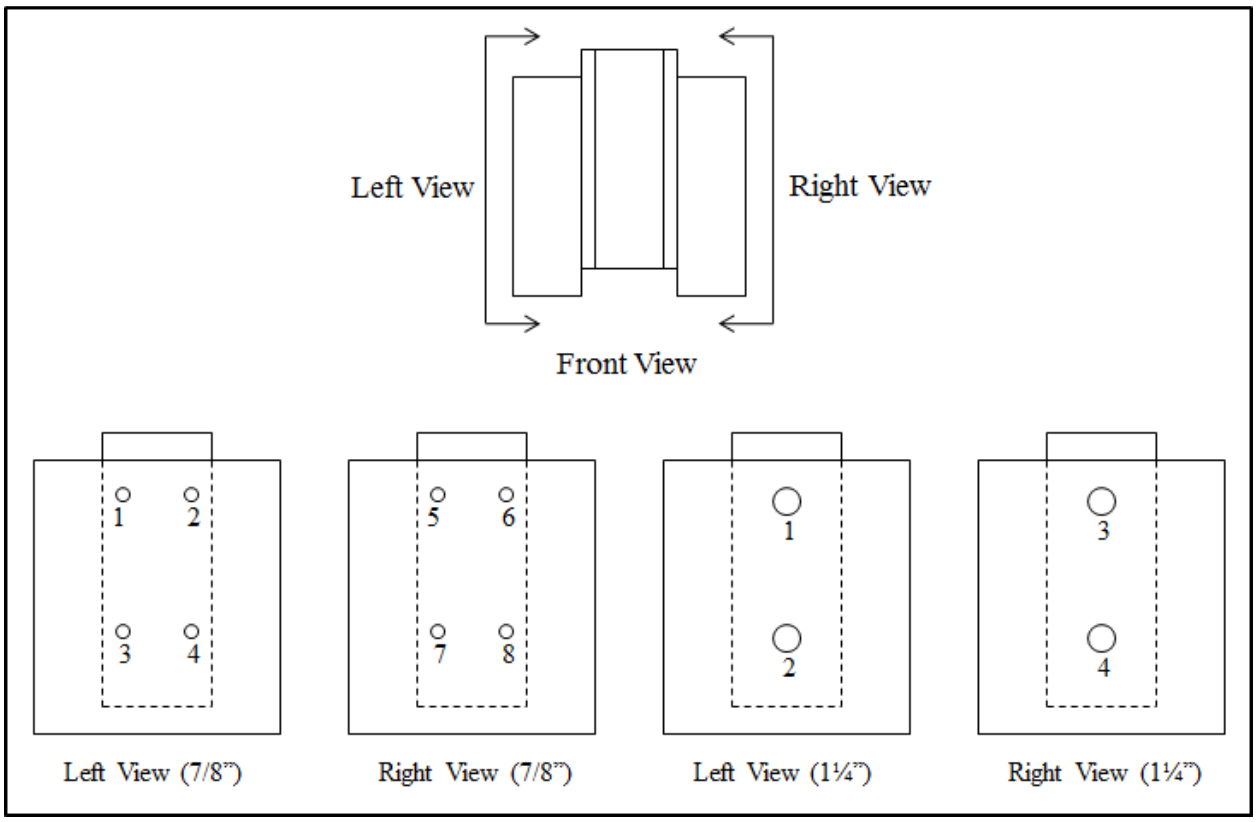

Figure 4-4 Stud Numbering Convention

4.4 Failure Modes

Although the exact failure mode of each specimen and each stud was different, some similarities could be drawn as to what failure mode took place for each stress range individually. Figure 4-5 taken from Nelson Stud Welding (Chambers 2001) gives a cross-sectional view of a welded stud that will be used for defining and giving terminology to certain regions of the weld. For the remaining sections, the weld toe will be defined as the point where the weld meets the base material, and the weld collar will be defined as the point where the weld meets the stud

material. When explaining failure modes in subsequent sections for each stress range, Figure 4-5 and its terminology will be refered to in order to catagorize the failures.

Region A: Heat-unaffected stud material
Region B: Stud heat affected zone
Region C: Cast zone
Region D: Base material heat affected zone
Region E: Heat-unaffected base material

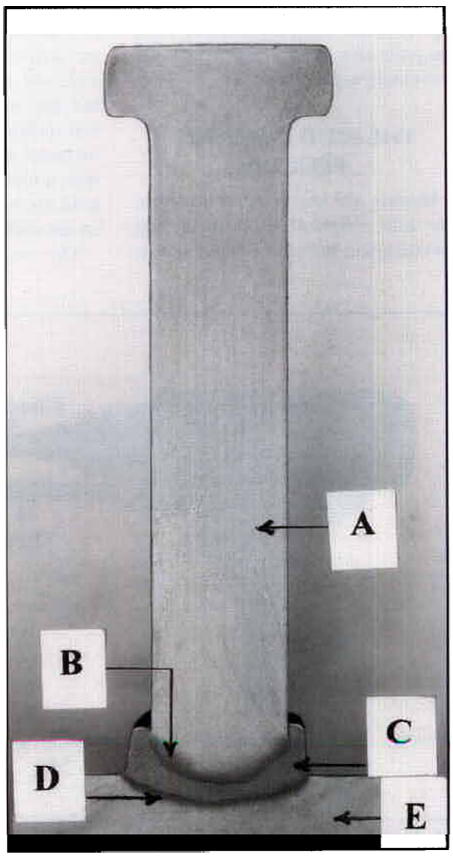

Figure 4-5 Cross-Section of Welded Stud (Chambers 2001)

4.5 Stress Range of 22 ksi

A total of eight push-out specimens were tested with a stress range of 22 ksi including four with $^{7}/_{8}$"-diameter studs and four with 1¼"-diameter studs. Sufficient data was collected for these tests with the exception of S-0.875-22-B because it failed earlier than expected and data was not being recorded continuously. Therefore, it is not included in many of the plots because the only useful data from this specimen was the number of cycles to failure.

4.5.1 Slip Results

The results from the maximum average relative slip data can be seen in Figures 4-6a and 4-6b with the only difference being that in Figure 4-6b, the x-axis represents the normalized number of cycles to failure. From Figure 4-6b where the number of cycles are normalized, it becomes apparent that the 1¼"-diameter specimens experience larger values of relative slip throughout the test before failure actually takes place.

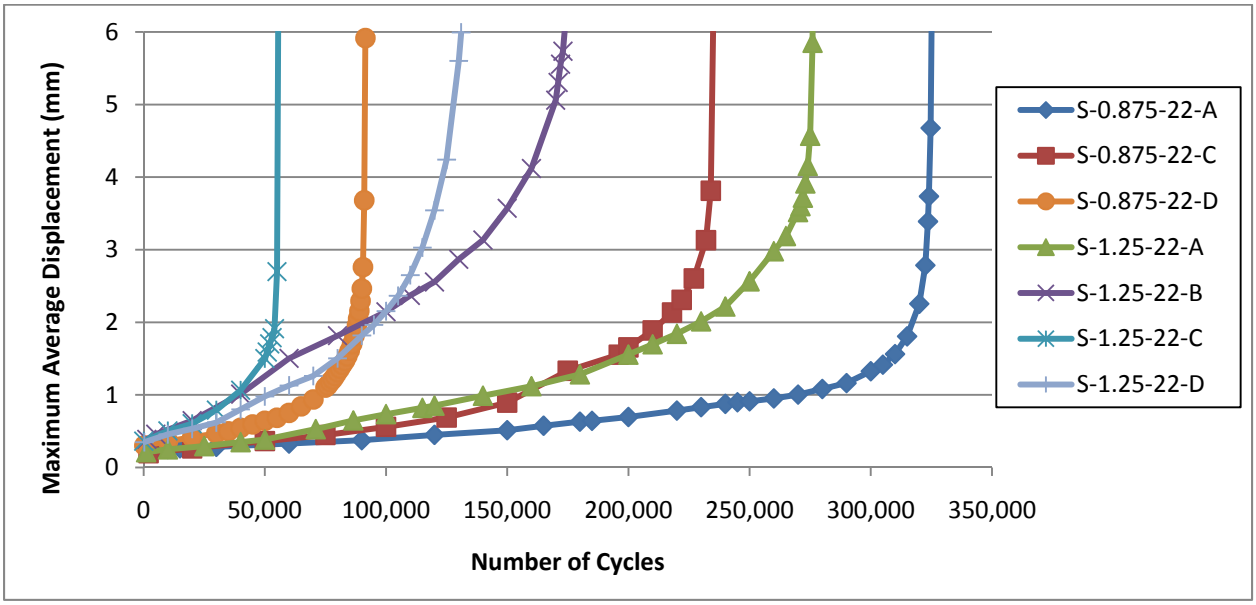

Figure 4-6a Maximum Average Relative Slip (S_r = 22 ksi)

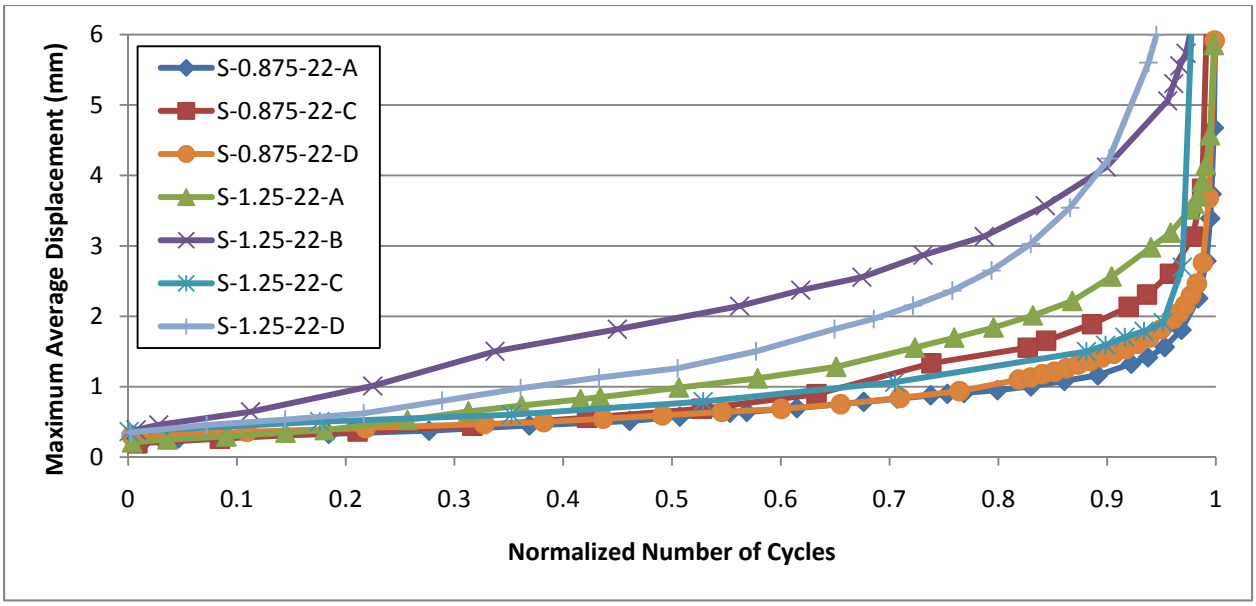

Figure 4-6b Maximum Average Relative Slip with Normalized No. of Cycles (S_r = 22 ksi)

From Figure 4-6a, it can be seen that S-1.25-22-C had a relatively short fatigue life compared to the others. The cause for this was determined to be poor fusion in the weld between the stud and base material. When looking at the fractured surfaces on this specimen, a large number of porosities were noticed. Another reason that it was believed that this specimen failed prematurely was that the opposite side of the specimen was not able to be failed statically which would signify that there was very little if any fatigue damage of the remaining studs.

A separate slip chart was created for each test that was run with the exception of S-0.875-22-B because of the lack of sufficient data. Figure 4-7 was taken from specimen S-1.25-22-A and follows the pattern shown in Figure 4-2 where the stiffness of the specimen decreases at a fairly gradual rate. By noticing how much each line shifts to the right for a certain interval of number of cycles, this plot provides a visual representation of how the relative slip increases as the number of cycles increases. The slope of each line gives insight into the stiffness of the specimen at a given number of cycles, and it can be seen that as the number of cycles increases, the slope of these lines decrease which represents a decrease in stiffness.

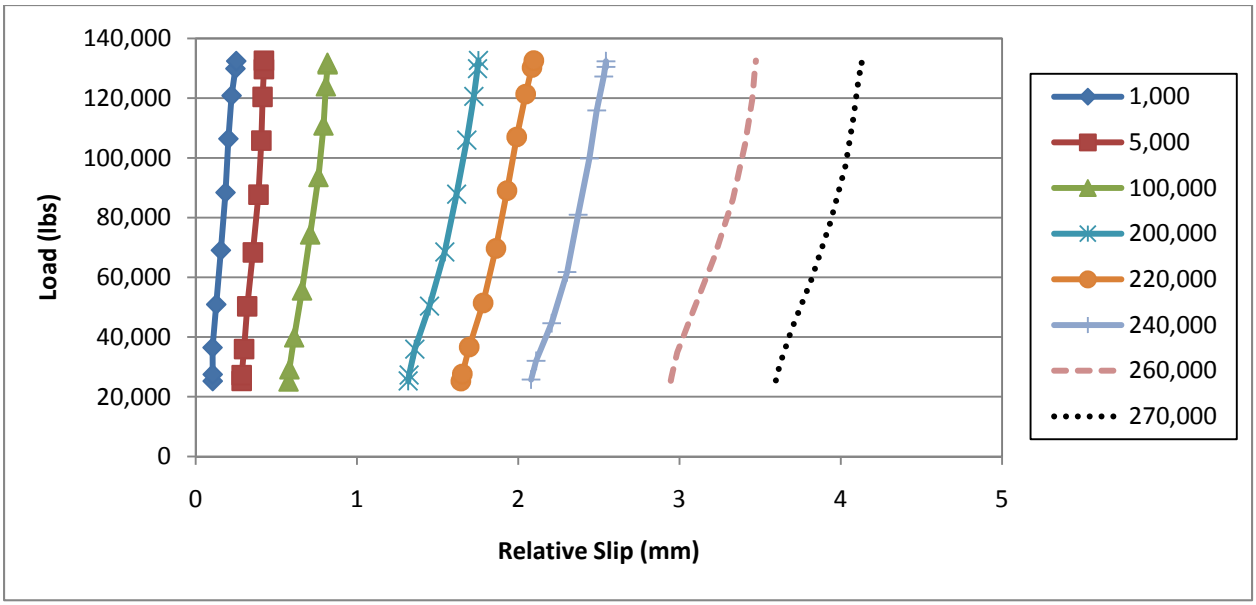

Figure 4-7 Slip Chart for S-1.25-22-A

The rate of change of the average maximum relative slip was plotted for the 22 ksi stress range in an effort to see if any conclusions could be drawn about when the fatigue crack started and how quickly it propagated. Based on the data from the 22 ksi stress range, no significant trends could be seen that gave insight into when the actual fatigue crack was initiated. The plot of this data is still included and shown in Figure 4-8.

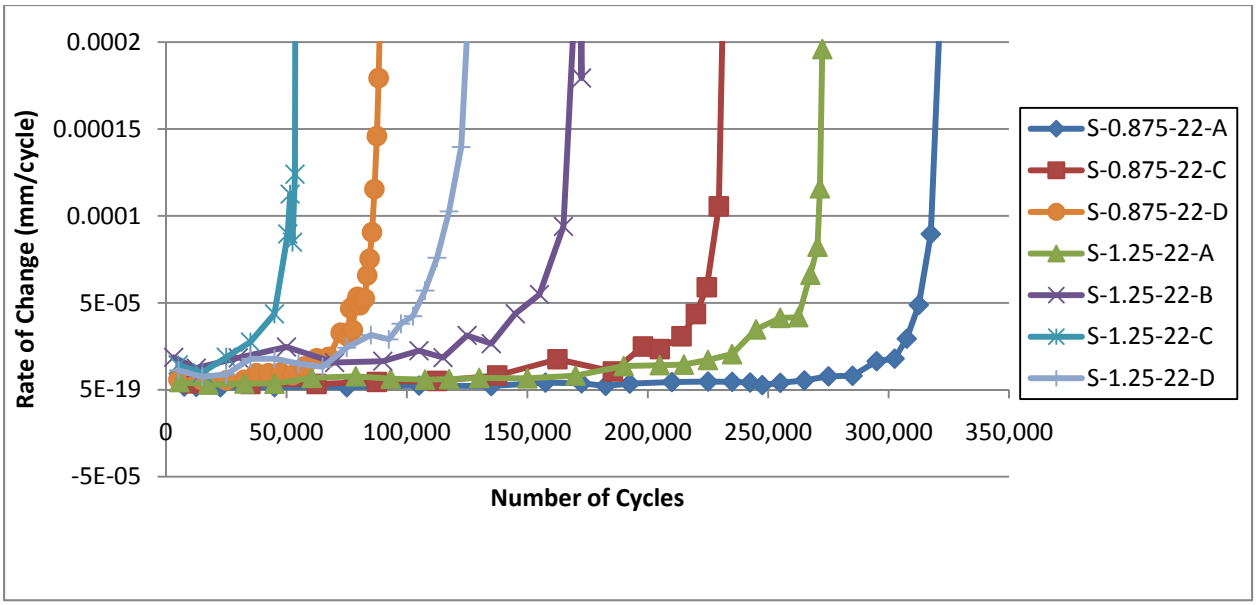

Figure 4-8 Rate of Change of Average Maximum Relative Slip (S_r = 22 ksi)

4.5.2 Stiffness Results

The following chart gives insight into how much the stiffness is being reduced over the course of the test. Figure 4-9 plots the normalized stiffness in relation to the normalized number of cycles. By normalizing both axes, the plots from each different specimen tend to lie along the same path. The line corresponding to S-1.25-22-C seems to follow a much different path than the other four, and this is probably due to the large number of porosities that were seen in the weld and resulted in a non-typical failure. The reference values that were used to normalize the stiffnesses are shown in Table 4-2.

Table 4-2 Initial Stiffness (S_r = 22 ksi)

Specimen	Initial Stiffness (kips/in)
S-0.875-22-A	20,120
S-0.875-22-C	18,670
S-0.875-22-D	14,990
S-1.25-22-A	15,980
S-1.25-22-B	11,840
S-1.25-22-C	11,890
S-1.25-22-D	12,090

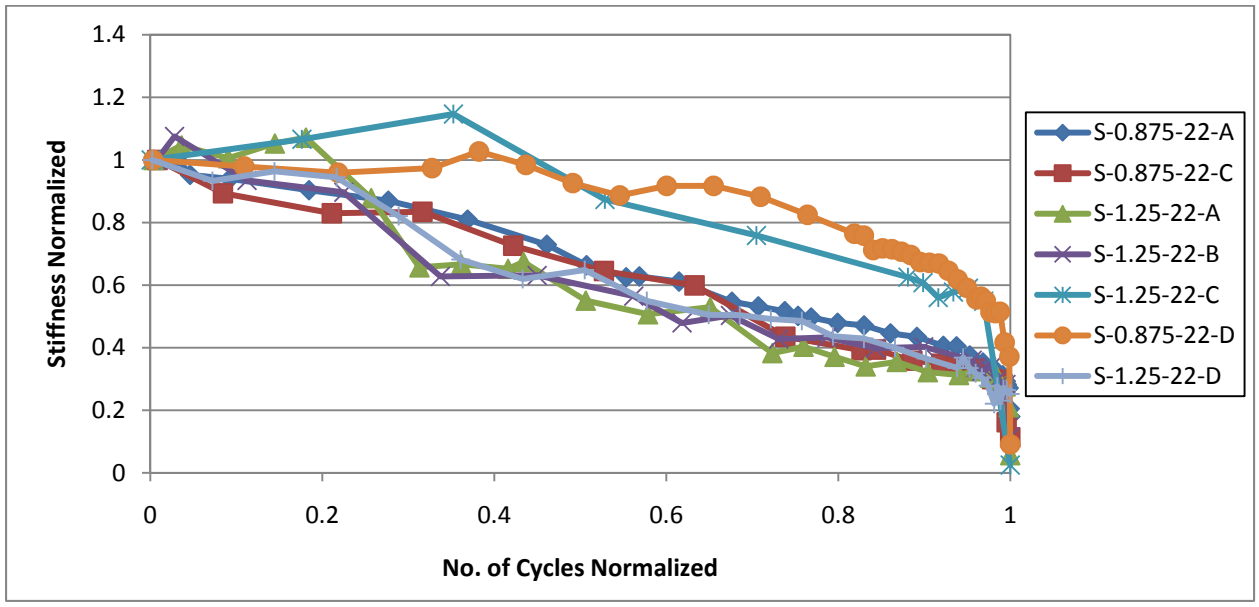

Figure 4-9 Reduction in Stiffness (S_r = 22 ksi)

The trends seen in Figure 4-9 show that the overall rate of stiffness degradation is fairly constant with the exception of the last 5% of the life of the specimen where the stiffness reduces much more rapidly. Towards the beginning of some of the tests, the graph indicates that the stiffness of the specimen increased. The reason for this phenomenon is not completely known, but it could be due to additional seating of the push-out specimen early in its life.

4.5.3 Failure Modes and Pictures

It has been widely observed that failure surfaces on shear studs when subjected to fatigue testing usually exhibit both a dull colored surface as well as a shiny colored surface. The dull surface typically is due to propagation of a fatigue crack through the steel while the shiny failure surface is due to the static failure at the end of the test when the peak fatigue load is enough to shear the rest of the stud off completely. The pictures in this section will show some of the typical failure surfaces that were observed while testing the 22 ksi stress range.

For the 22 ksi stress range, it was most common for the crack to initiate either at the weld toe or the weld collar on the bottom side of the stud and propagate through either the cast zone (Region C) or the base material heat affected zone (Region D). There is a very fine line between these scenarios and it was difficult to determine which path the cracks took. Figures 4-10 and 4-11 give good examples of the dull versus shiny failure surfaces seen for $^{7}/_{8}$" and 1 ¼"-diameter studs respectively.

Figure 4-10 Failure Surface for S-0.875-22-C (3)

Figure 4-11 Failure Surface for S-1.25-22-B (3)

Another common occurrence during the failure of the push-out specimen was for the stud to tear or peel off part of the top of the steel flange as the two were being separated. The most

noticeable place this was seen was on S-0.875-22-B on one of the top row studs as shown in Figure 4-12. The peeled off surface shown has a shiny surface indicating that this was part of the final static failure rather than propagation of a fatigue crack.

Figure 4-12 Failure Surface for S-0.875-22-B (6)

A failure mode for the 22 ksi stress range that was seen for one the 1¼"-diameter specimens that was not seen for the $^{7}/_{8}$"-diameter specimens was for there to be a fracture surface between one and two inches up the stud shank from the base of the stud. This fracture surface was very rough and had characteristics consistent with that of a very brittle failure that might have happened due to failure at the end of the test. This failure mode is shown in Figure 4-13.

Figure 4-13 Failure Surface for S-1.25-22-B (4)

It has been previously mentioned that S-1.25-22-C failed much earlier than was expected and that this was due to a large number of porosities in the weld. These unfavorable porosities are formed from gas that is built up in the weld during the welding process and are seen in Figure 4-14 as small black dots or voids on the failure surface. Although the fatigue life of this specimen was relatively short, the two distinct dull and shiny failure regions are still seen indicating that there was fatigue damage, but that it may have either started earlier or propagated more rapidly.

Figure 4-14 Failure Surface for S-1.25-22-C (1)

4.6 Stress Range of 18 ksi

A total of eight push-out specimens were tested at a stress range of 18 ksi including four with 1¼"-diameter studs and four with $^{7}/_{8}$"-diameter studs. Data was collected continuously and therefore sufficient data was available for each test. This data was then reduced so that information could be gathered on the behavior of each specimen.

4.6.1 Slip Results

The results for the maximum average relative slip can be seen in Figures 4-15a and 4-15b with the only difference being that in Figure 4-15b, the x-axis represents the normalized number of cycles to failure. Although it is not as obvious for this stress range as it was for the 22 ksi stress range, the 1¼"-diameter stud specimens experience larger relative slip before failure takes place as shown in Figure 4-15b.

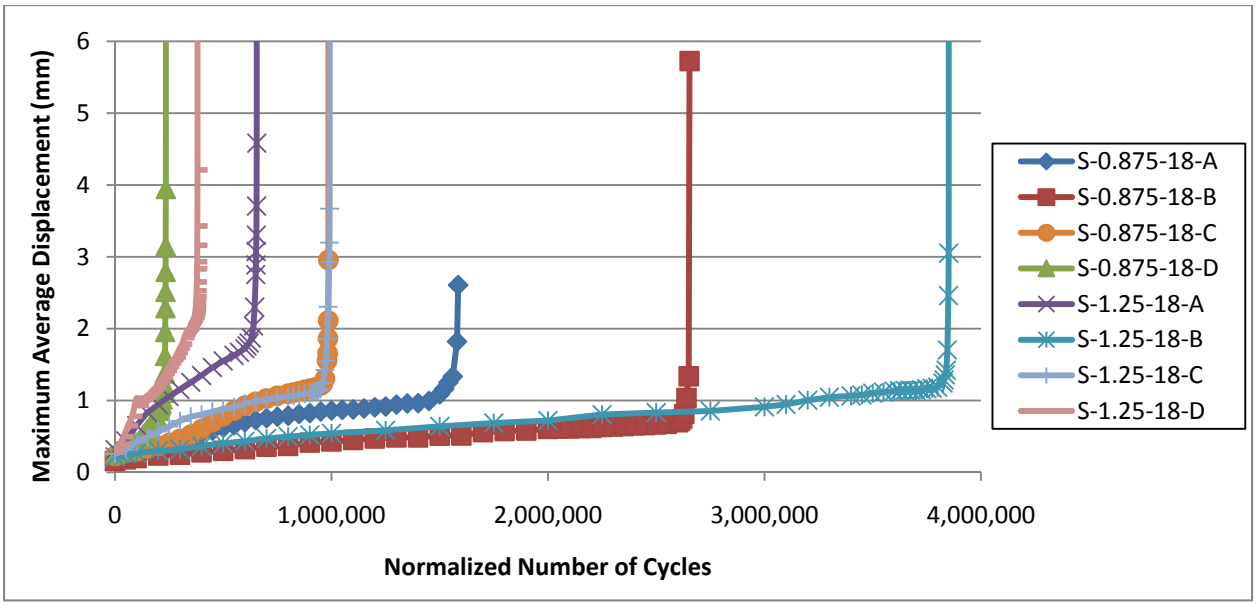

Figure 4-15a Maximum Average Relative Slip (S_r = 18 ksi)

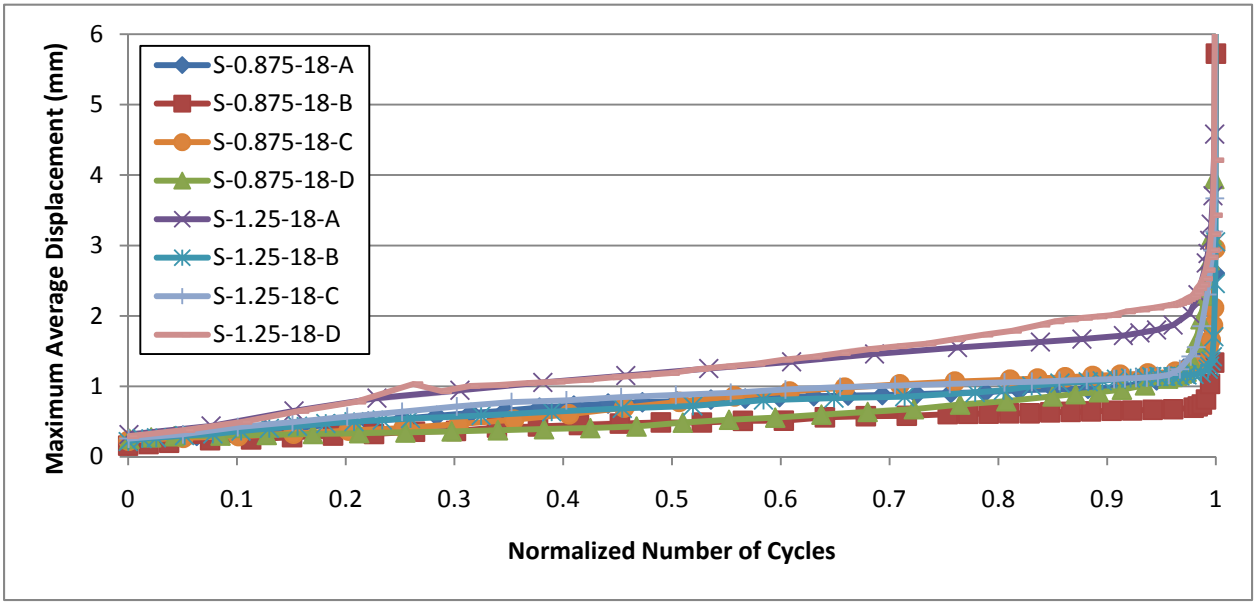

Figure 4-15b Maximum Average Relative Slip with Normalized No. of Cycles (S_r = 18 ksi)

The largest amount of scatter of the three stress ranges employed was seen in the 18 ksi stress range which had fatigue lives anywhere from approximately 230,000 to 3,850,000 cycles. As was mentioned previously, much of the scatter in the data could be attributed to the variation of the quality of the fusion between the stud and the steel section it was being welded to.

Although the amount of variability in welding is greatly reduced by using an automatic stud welder, there are still many more variables that could play a part in the quality of the fusion that is achieved.

The slip chart from specimen S-0.875-18-C is shown below to give a representation of how the specimens at the 18 ksi stress range performed. Much like the trend that was seen with the 22 ksi stress range, this plot shows that the slope of the load vs. slip line decreases at a fairly constant rate as the test progressed.

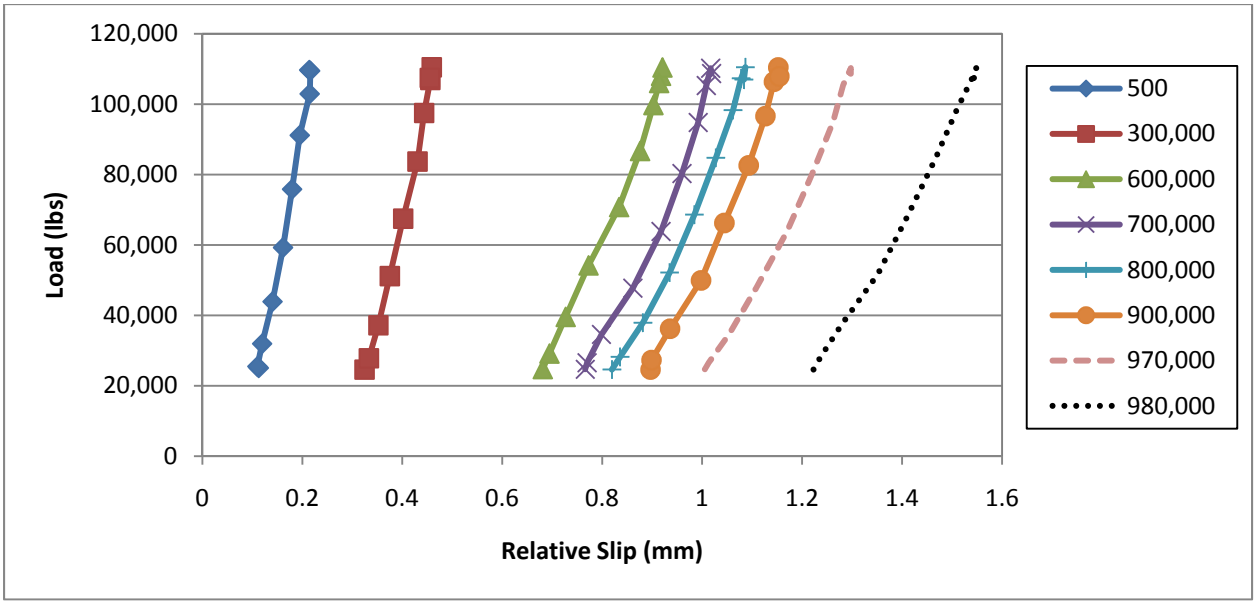

Figure 4-16 Slip Chart for S-0.875-18-C

The rate of change of the average maximum relative slip was also investigated for the 18 ksi stress range. The data from specimen S-0.875-18-D as well as S-1.25-18-D have been excluded from the following graph because their results were unreliable and inconsistent with the others. One of the most interesting observations seen in the 18 ksi stress range that was not seen as predominately in the other stress ranges was the tendency for the rate to increase towards the beginning of the test and then decrease to a constant rate of change until the end of the fatigue

life where the rate increased very sharply. This trend is the most readily apparent for specimens S-0.875-18-C and S-1.25-18-C shown in Figure 4-17.

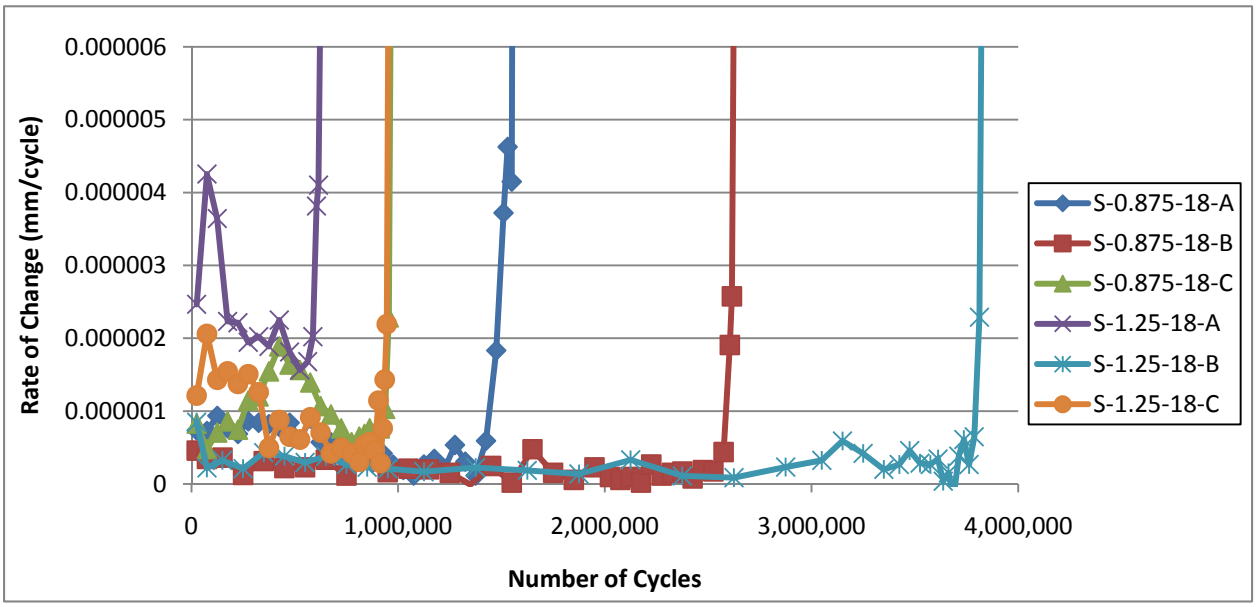

Figure 4-17 Rate of Change of Average Maximum Relative Slip (S_r = 18 ksi)

4.6.2 Stiffness Results

The graph showing the reduction in stiffness for all specimens tested at 18 ksi stress range is shown in Figure 4-18. When each test was normalized with respect to the number of cycles to failure, most of the specimens showed a similar stiffness reduction with the exception of S-0.875-18-D which in turn had the shortest fatigue life of the 18 ksi stress range group. Because of the short fatigue life that was observed in specimen S-0.875-18-D, this may have had an effect on how the specimen behaved throughout the test and might explain why its reduction in stiffness was much different than the other seven specimens. Since all of stiffnesses were normalized, Table 4-3 is shown in order to give the reference value to show the initial stiffness that each specimen was normalized with respect to.

Table 4-3 Initial Stiffness (S_r = 18 ksi)

Specimen	Initial Stiffness (kips/in)
S-0.875-18-A	18,900
S-0.875-18-B	25,910
S-0.875-18-C	17,600
S-0.875-18-D	16,230
S-1.25-18-A	12,600
S-1.25-18-B	18,310
S-1.25-18-C	14,070
S-1.25-18-D	12,750

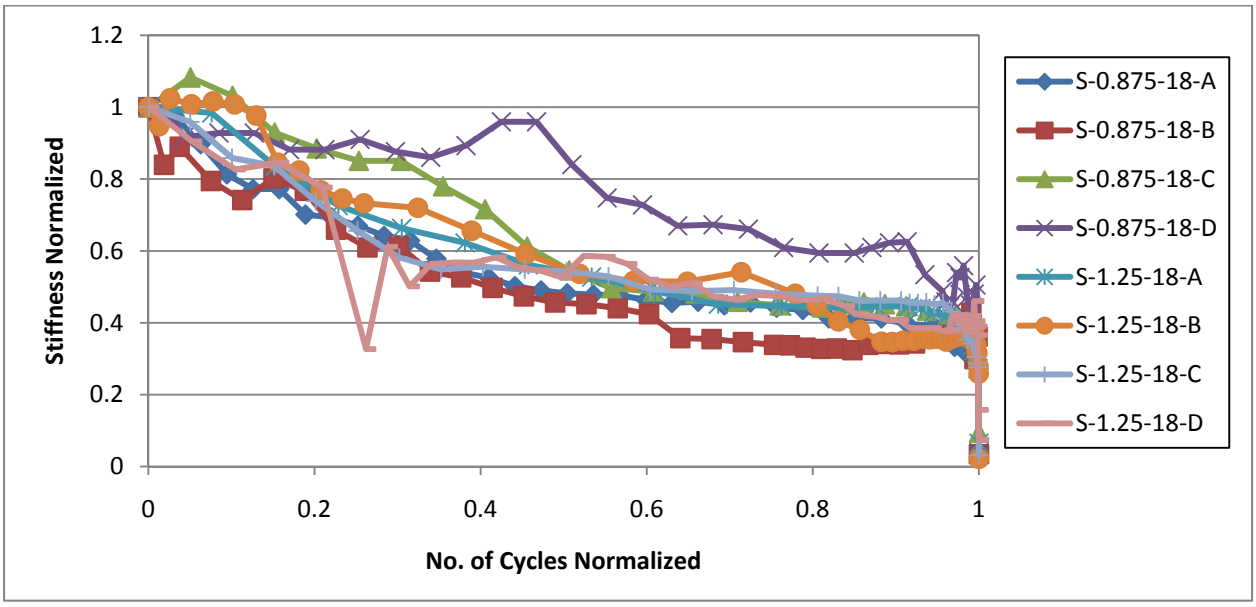

Figure 4-18 Reduction in Stiffness (S_r = 18 ksi)

4.6.3 Failure Modes and Pictures

Much like the specimens tested at a 22 ksi stress range, the specimens at 18 ksi stress range showed evidence of a dull-colored surface as well as a shiny surface that is typical of shear stud fatigue failures. It was also observed that the proportion of dull-colored surface was greatest for the 18 ksi stress range which is most likely due to this stress range having a lower maximum load during cycling which would require a larger area of the stud to be damaged before a static failure could take place at the end of the test.

The crack initiation point for the 18 ksi stress range was similar to that of the 22 ksi stress range where it was either at the weld toe or the weld collar. The main difference between these two stress ranges lies in the path that the crack propagated along. Rather than propagating through the cast zone (Region C) or the heat affected base material (Region D), the crack seemed to follow a steeper path and move into the heat-unaffected base material (Region E). From there it was also observed that the crack progressed away from the base of the stud and penetrated outward into the beam flange. As more deformations took place, the remaining section of the stud was bent over exposing this failure surface as seen in Figure 4-19

Figure 4-19 Failure Surface for S-0.875-18-A (2)

One of the most interesting differences that was observed for the 18 ksi stress range was the high tendency for a failure surface to form approximately one to two inches up the shank from the base of the stud. This occurred on at least one stud in every specimen in the 18 ksi stress range with the exception of S-0.875-18-D which in turn also had the shortest fatigue life, possibly indicating that there were other factors preventing this specimen from behaving like the

others. When this failure mode was observed, there was significant fatigue damage that initiated on the bottom side at the base of the stud, but when failure actually took place, a fatigue crack which initiated on the top side of the stud propagated through the shank and failure occurred in the shank of the stud. When this surface was examined, there were typically two distinctly different textures. The first, which covered the majority of the failure surface, was slightly rough and porous. The second was a smaller area that was shiny and sometimes exhibited significant deformations. Pictures of these failure types are shown for both 1¼" and $^{7}/_{8}$" specimens in Figures 4-20 – 4-22.

Figure 4-20 Failure Surface for S-0.875-18-C (3)

Figure 4-21 Failure Surface for S-0.875-18-C (3)

Figure 4-22 Failure Surface for S-1.25-18-B (4)

After all of the tests had been completed, it was determined that in order to confirm the location of the crack initiation, the studs that did not fail during fatigue testing should be extracted and cut in half. This process was performed on specimen S-1.25.18-D for studs #3 and #4 which were previously subjected to 381,667 cycles of fatigue loading. The studs were extracted using a concrete core rig to take a 4"-diameter core through the 7"-thick reinforced concrete slab around the shear studs. After this was done, the concrete slab could be separated from the steel section. The concrete around the stud was chiseled away leaving just the stud and steel section. A small portion of steel section that included the shear stud was cut out with a torch. Finally, a band saw was used to make a cut through the stud and steel section parallel to the web. Figures 4-23 and 4-24 show the exposed cross-section of studs #3 and #4 respectively from specimen S-1.25-18-D.

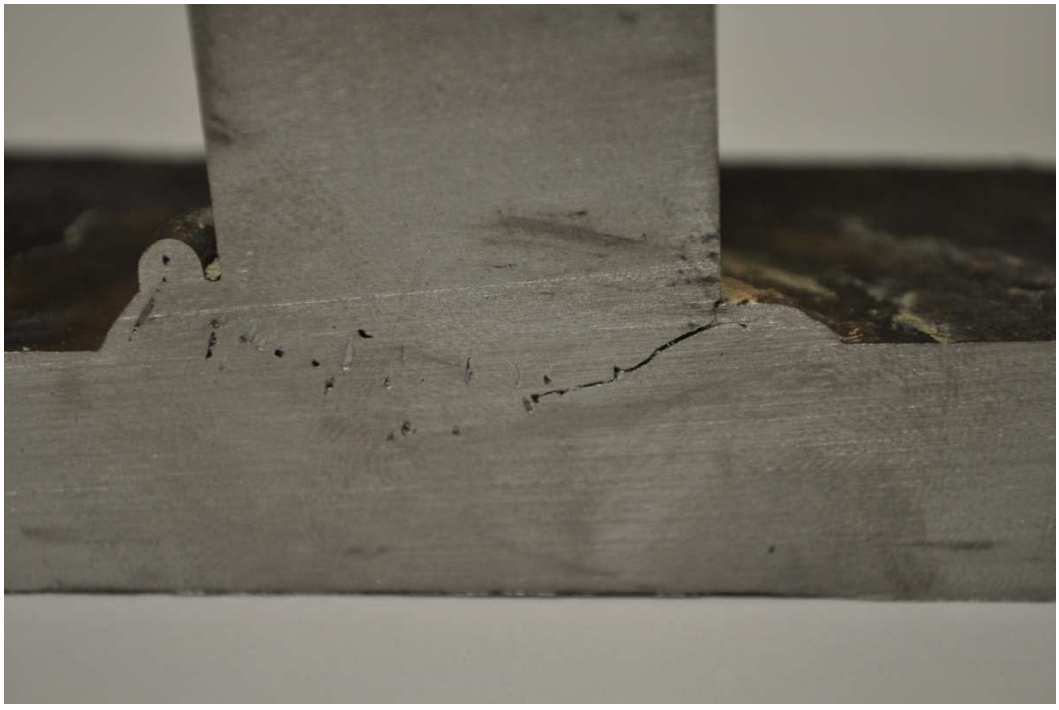

Figure 4-23 Cross-Section of Stud #3 from S-1.25.18-D

Figure 4-24 Cross-Section of Stud #4 from S-1.25-18-D

Both of these figures show evidence of the crack initiation point being at the weld collar where the weld meets the shank of the stud. From that point it seems to propagate downward into the heat-unaffected base material (Region E).

4.7 Stress Range of 26 ksi

A total of eight push-out specimens were tested at a stress range of 26 ksi including four with 1¼"-diameter studs and four with $^{7}/_{8}$"-diameter studs. Data was collected continuously and therefore sufficient data was available for each test. This data was then reduced so that information could be gathered on the behavior of each specimen.

4.7.1 Slip Results

The data that was collected for the maximum average relative slip is shown in Figures 4-25a and 4-25b with the only difference being that Figure 4-25b normalizes the number of cycles

with respect to the fatigue life. By looking at the graphs below, the same trend that was seen for the previous stress ranges is quite obvious here that the 1¼"-diameter specimens experience more relative slip throughout the test prior to failure. The possible reason behind this observation will be described in a later section that compares trends seen overall in the test program.

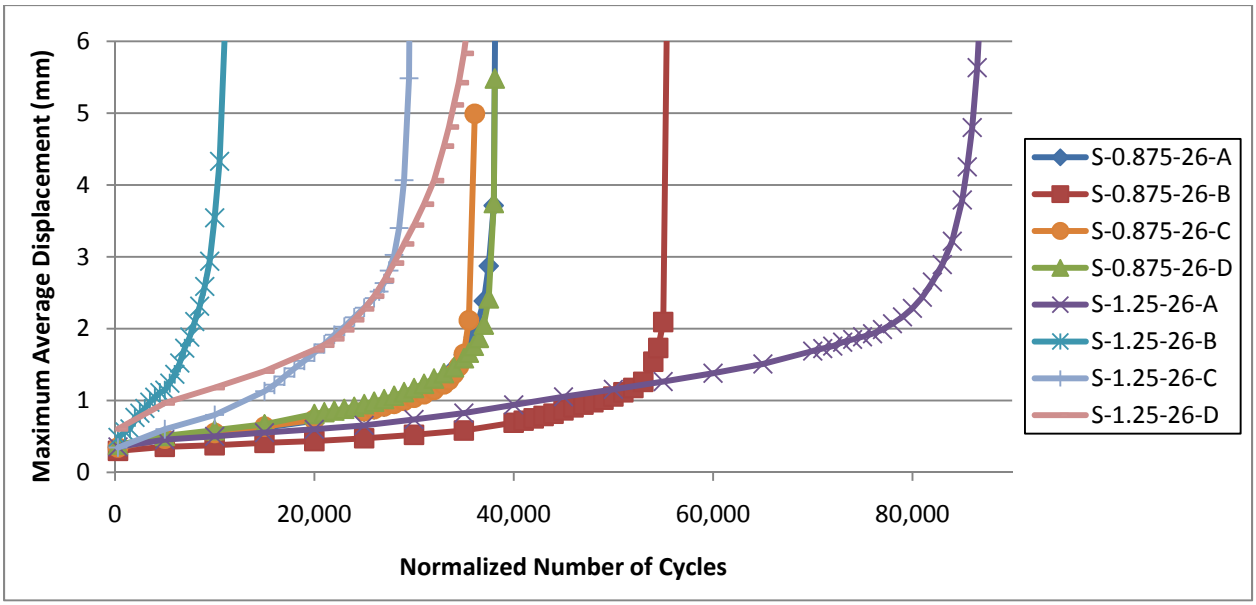

Figure 4-25a Maximum Average Relative Slip (S_r = 26 ksi)

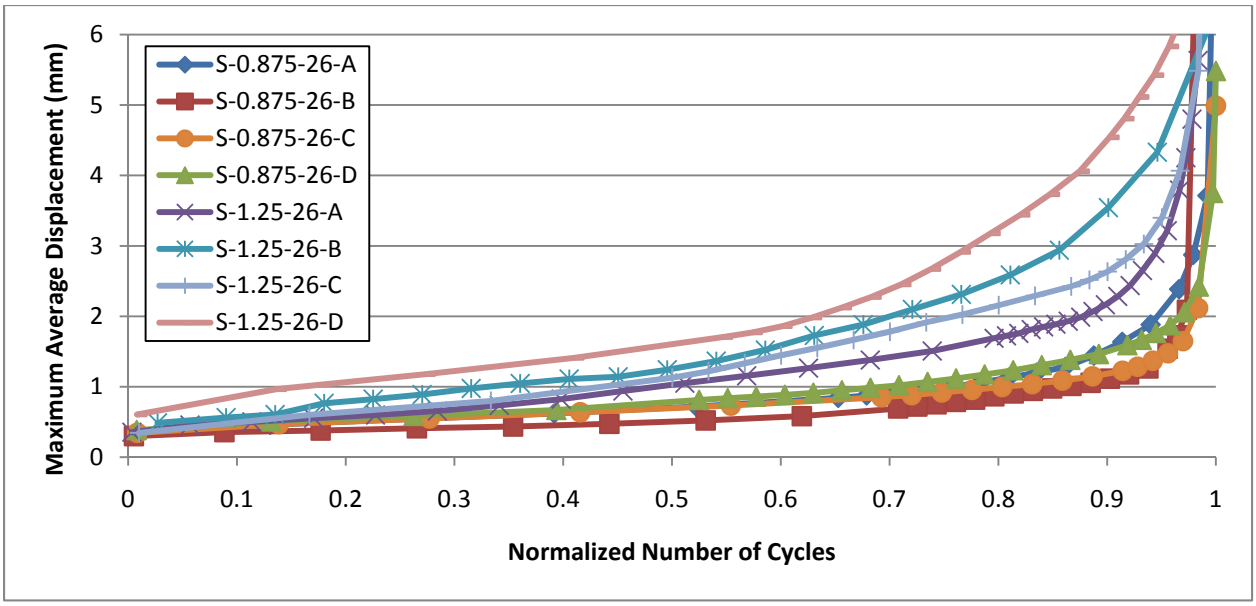

Figure 4-25b Maximum Average Relative Slip with Normalized No. of Cycles (S_r = 26 ksi)

Although the scatter of the data in the 26 ksi stress range varies from approximately 11,000 to 88,000 cycles and seems to be much smaller than that of other stress ranges, when plotted on the S-N curve with a log-log relationship, the width of the scatter for the 26 ksi and 22 ksi stress ranges are very similar.

The slip chart that was chosen as a representative sample for the 26 ksi stress range was taken from specimen S-1.25-26-D. In referring to the schematic at the beginning of this chapter, the slip charts for the 26 ksi stress range resemble Figure 4-3 where the slope of each line remains fairly constant throughout the test with the exception of a slight decrease in the slope at the end of the test. Even as more damage is accumulated as indicated by the shifting of the line to the right, the stiffness does not seem to be changing very rapidly. This lack of reduction of stiffness of the specimen will also be discussed in the section dedicated to stiffness reduction.

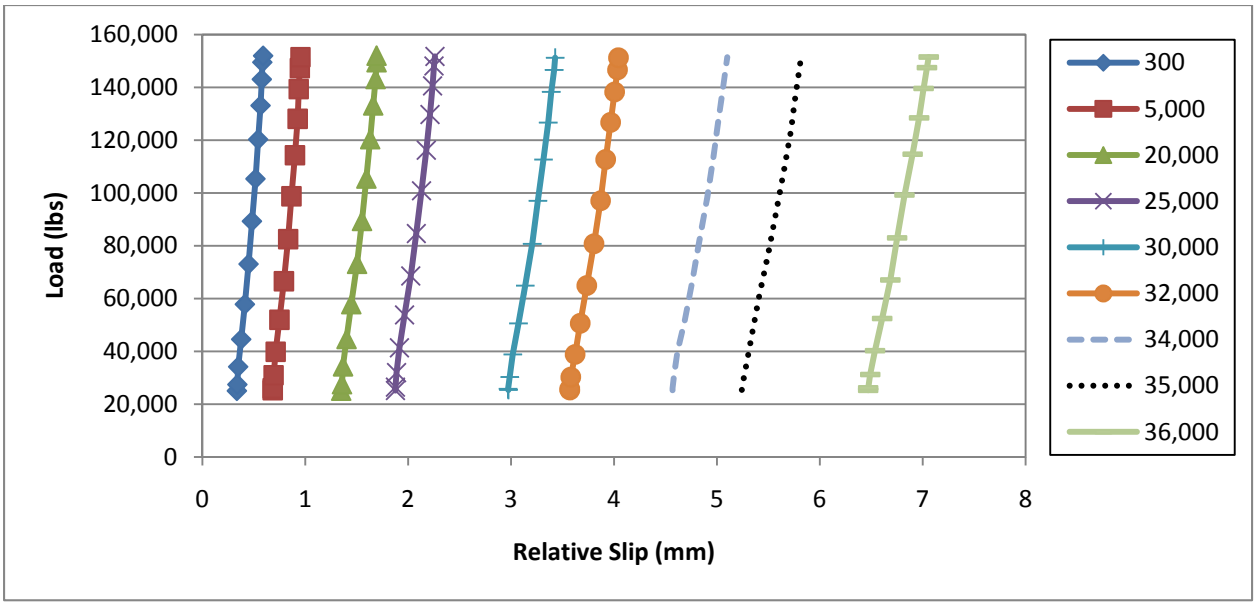

Figure 4-26 Slip Chart for S-1.25-26-D

The rate of change of the maximum average relative slip was determined for the 26 ksi stress range and is shown in Figure 4-27. All eight specimens were included with the exception of S-1.25-26-B that was excluded because its results were scattered and inconsistent with others in this stress range. This specimen also had the shortest fatigue life for this stress range which could also indicate that there were other variables that caused this specimen to behave differently than the others. The rate of change for each specimen showed a general trend that the rate decreased slightly at the beginning of the test, and then increased at the end of the test until failure. Specimens S-0.875-26-B and S-1.25-26-C showed a similarity just before the end of their fatigue lives. In the case of both specimens, there was a jump in the rate of change of the average maximum relative slip, followed by a slight decrease, and then rapid increase indicative of failure. This could indicate sudden damage of either the stud or the surrounding concrete which contributed to the failure that followed shortly.

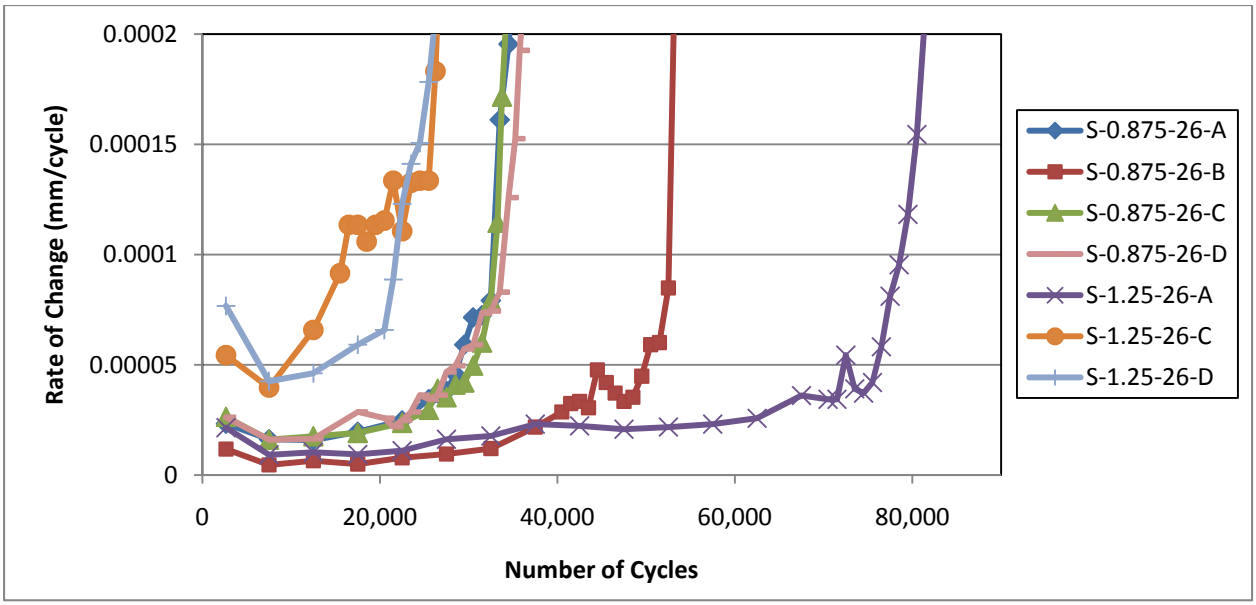

Figure 4-27 Rate of Change of Average Maximum Relative Slip (S_r = 26 ksi)

4.7.2 Stiffness Results

The results for the reduction in stiffness for each specimen tested at the 26 ksi stress range are shown in Figure 4-28. The results from this stress range are much different than those of the other stress ranges in that there does not seem to be any general path that the plots take. The graphs for each specimen in this stress range also do not seem to lose stiffness as quickly as specimens in other stress ranges. This is related to the slope of the lines in the slip chart shown previously in Figure 4-26. The slope of those lines don't change much at different intervals because as shown in Figure 4-28, the specimens tested at the 26 ksi stress range do not lose much stiffness until the end of their fatigue lives. Included in Table 4-4 are the initial stiffnesses of each specimen with which each stiffness was normalized with respect to.

Table 4-4 Initial Stiffness (S_r = 26 ksi)

Specimen	Initial Stiffness (kips/in)
S-0.875-26-A	16,560
S-0.875-26-B	17,630
S-0.875-26-C	14,430
S-0.875-26-D	16,330
S-1.25-26-A	10,030
S-1.25-26-B	12,500
S-1.25-26-C	16,990
S-1.25-26-D	11,840

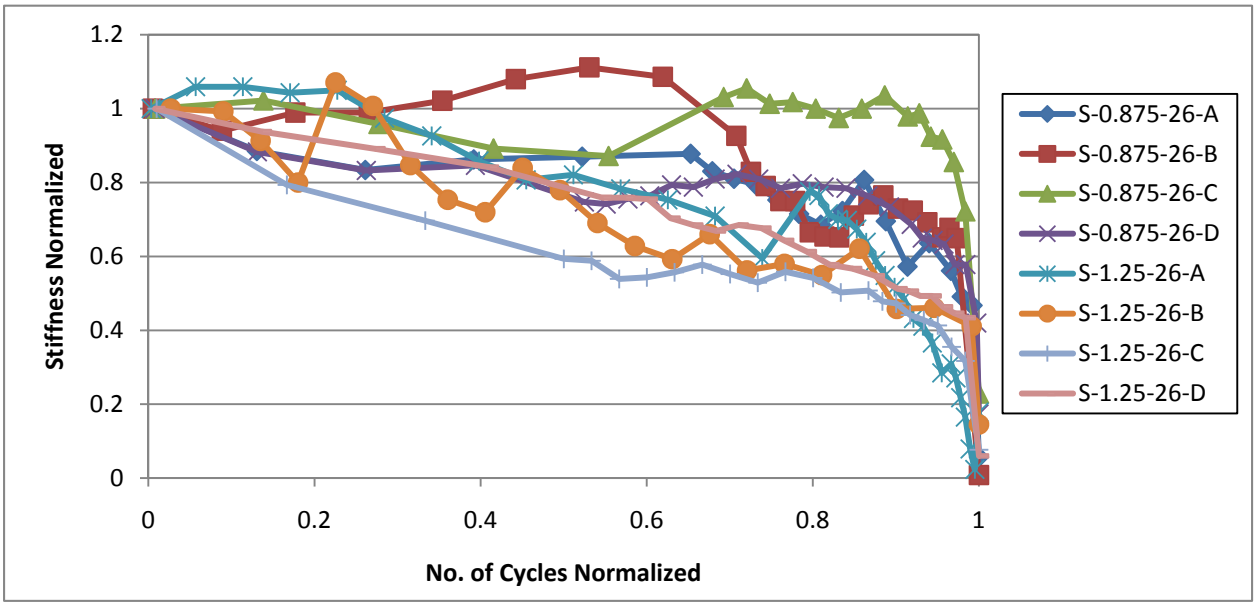

Figure 4-28 Reduction in Stiffness (S_r = 26 ksi)

4.7.3 Failure Modes and Pictures

Although there were similarities between this stress range and the others, there were also some significant differences that were observed. The 26 ksi stress range exhibited the expected combination of dull-colored surface, indicative of fatigue, as well as a shiny surface typically due to final static failure of the stud. The most notable difference for this stress range was in where the fatigue cracks began and how they propagated resulting in failure of the specimen. While examining the failure surfaces, it was observed that the crack initiation point for every exposed

stud was at the top of the weld collar. There was no evidence that showed a crack initiating at the weld toe where the weld meets the base material for any stud tested at a 26 ksi stress range. From this point of initiation, the crack followed a path along either the stud heat affected zone (Region B) or the cast zone (Region C), and after failure, the bottom half of the weld collar remained intact with the steel section. Figure 4-29 and Figure 4-30 show typical examples of this failure mode for $^{7}/_{8}$" and 1¼"-diameter specimens respectively.

Figure 4-29 Failure Surface for S-0.875-22-A (5)

Figure 4-30 Failure Surface for S-1.25-26-D (2)

4.8 Comparison of All Stress Ranges

When comparing each stress range individually, it was difficult to see the overall behavior of the specimens and draw conclusions on the test program as a whole. When all of the specimens were analyzed as a whole, the slip behavior of the different stud sizes became much more apparent. The following figures might seem cluttered with many graphs, but the main point is to show the obvious difference in how specimens with different stud diameters performed. All of the specimens with $^{7}/_{8}$"-diameter studs are shown with the same type line, and all of the specimens with 1¼"-diameter studs are shown with a different type line. Figure 4-31 shows the maximum average relative slip with the number of cycles normalized for each respective specimen. It is quite obvious when analyzing the data this way that the 1¼"-diameter specimens experienced more relative slip before failure actually took place.

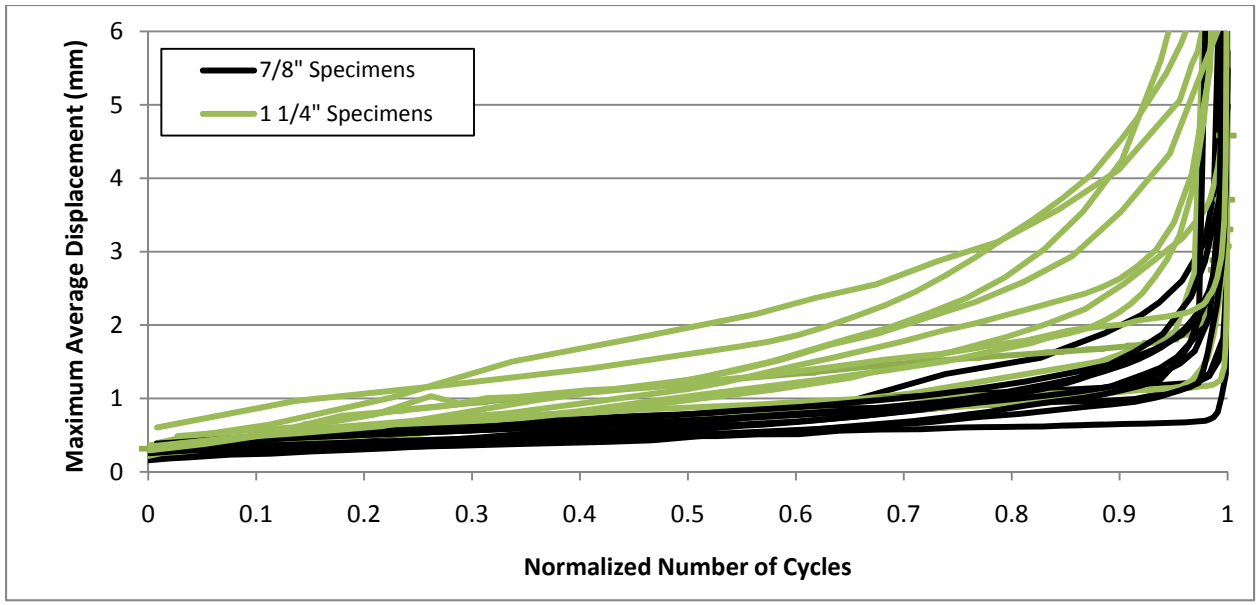

Figure 4-31 Maximum Average Relative Slip (All Stress Ranges)

The large amount of relative slip seen for the 1¼"-diameter studs is possibly explained by the higher bearing stresses that were caused by the larger diameter studs. Because half as many studs were used for the 1¼"-diameter specimens than for the $^{7}/_{8}$"-diameter specimens, a larger bearing stress is imposed on the concrete causing more significant elastic and inelastic deformations which in turn give rise to larger relative slip.

Another significant difference between the specimens with different size studs was in the amount of relative slip range that was observed. The relative slip range in this case was the difference in the maximum and minimum slip at a given number of cycles as shown in Figure 4-1. The relative slip range for the 1¼"-diameter specimens was consistently larger than that of the $^{7}/_{8}$"-diameter specimens. This is directly related to the stiffness of the specimen because for the same given load, there was a larger relative slip range for the 1¼" specimen. The reason for this could also be linked to the previous idea that the larger diameter studs impose a larger bearing stress which could cause larger elastic and inelastic deformations of the concrete. Figure 4-32 gives a graphical representation to show the obvious difference between the two stud sizes. The

$^{7}/_{8}$"-diameter specimens are shown as a single line type while the 1¼"-diameter specimens are shown as another line type.

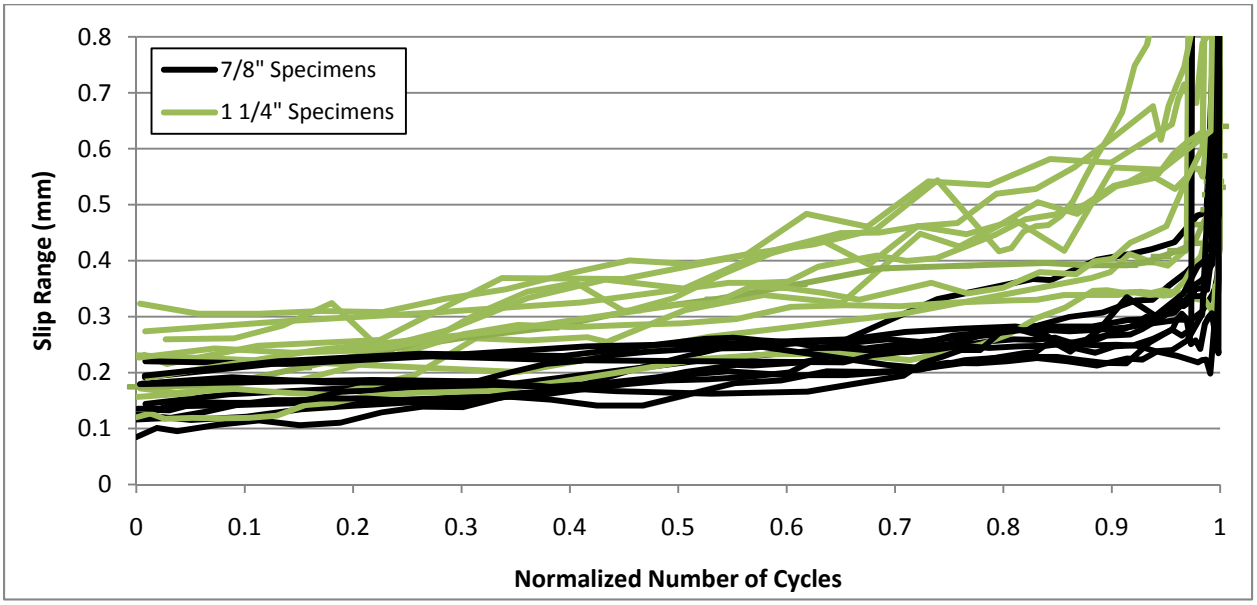

Figure 4-32 Relative Slip Range (All Stress Ranges)

Chapter 5 ANALYSIS OF RESULTS

5.1 Overview

The most common way to analyze fatigue test data is in the context of the S-N curve where S and N represent the stress range and number of cycles to failure respectively. The x-axis, which represents the number of cycles, and the y-axis, which represents the stress range are both plotted on a logarithmic scale. A regression analysis was performed to give a best fit line for the data which will then be compared to current design codes. The reason for the scatter of the test data is primarily attributed to variations in concrete strength as well as variations in weld quality and will be explained in this chapter.

5.2 Regression Analysis

A linear regression analysis was performed so that a best fit line could be compared with other design codes. The procedure that was followed for the regression analysis of all test specimens will be outlined in this section to explain exactly how the analysis was done. The analysis was then repeated for 1¼"-diameter specimens only and for $^{7}/_{8}$"-diameter specimens only. By doing this, any slight differences caused by the size of the stud can be seen.

First, the log was taken of both the stress range and the number of cycles to failure for each specimen. These points were then plotted on a graph with $\log(S_r)$ on the x-axis and $\log(N)$ on the y-axis. Microsoft Excel was used to pass a linear trendline through the data giving a mean line for the data and an equation of that mean line. The sample standard deviation of the data

was also computed to give an idea of the error between the actual data points and the mean line. In order to find the sample standard deviation of the data, the following equation was used:

$$s = \sqrt{\frac{\sum (\log(N) - \log(N)_{mean})^2}{n-1}} \quad (5\text{-}1)$$

where

s = sample standard deviation

log(N) = log of the number of cycles to failure for a given specimen

$\log(N)_{mean}$ = log of the number of cycles from the mean line equation

n = number of samples

After following this procedure three times, the following equations and sample standard deviations were obtained for the mean line of all specimens, 1¼" specimens, and $^{7}/_{8}$" specimens respectively.

$$\log(N) = -8.9932\log(S_r) + 17.272 \qquad s = 0.307 \quad (5\text{-}2)$$

$$\log(N) = -9.3305\log(S_r) + 17.697 \qquad s = 0.332 \quad (5\text{-}3)$$

$$\log(N) = -8.6560\log(S_r) + 16.847 \qquad s = 0.290 \quad (5\text{-}4)$$

The main focus behind this research has been to develop design criteria for 1¼"-diameter shear studs for use in composite highway bridge girders. The best way to compare the effects of stud diameter on the fatigue life is to use the regression analysis that was done for each stud size individually and compare their mean equations and sample standard deviations. By shifting each of these mean curves by 1.96 sample standard deviations, an approximate design equation is developed that gives a 97.5% confidence interval, or a 2.5% probability of failure. The data

points, mean curves, design curves, and current AASHTO LRFD (2007) design curve are shown in Figure 5-1 for comparison purposes.

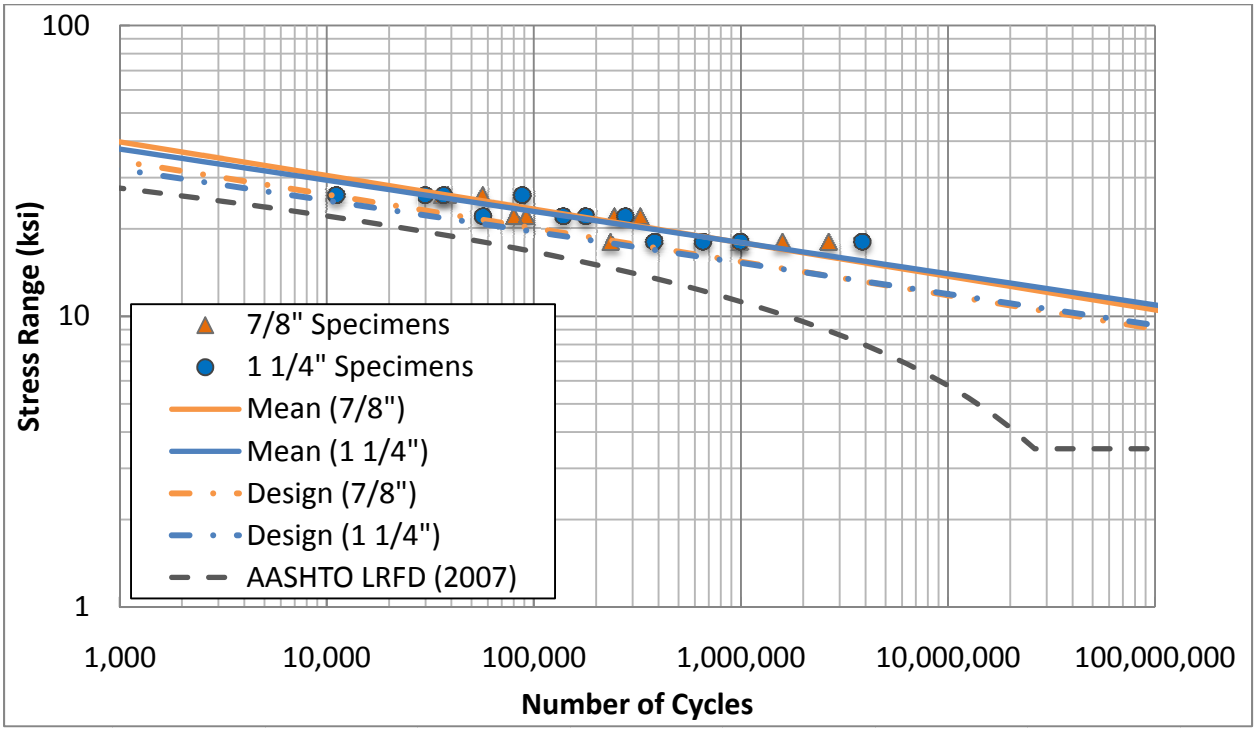

Figure 5-1 S-N Curve for Comparison of Stud Diameters

Even with the amount of scatter that was observed in the test data, the mean curves for both the $^{7}/_{8}$" and 1¼"-diameter specimens are almost identical as can be seen in Figure 5-1. Based on this test program, and given the scatter in the test data, it would be reasonable to say that 1¼"-diameter studs have essentially the same fatigue life as $^{7}/_{8}$"-diameter studs.

Before proposing new design equations for AASHTO LRFD for the fatigue life of shear studs, full-scale beam tests should be performed to show how results from push-out tests compare to results from a full-scale beam test. In the meantime, these test results show that 1¼"-diameter shear studs can safely be used to achieve composite action in highway bridge girders by using the design equation currently given in AASHTO (2007).

5.3 Comparison of Results to Design Codes

In this section, graphical comparisons as well as tabular comparisons will be made between results from this test program and the design curves for AASHTO LRFD Bridge Design Specifications (AASHTO 2007), Eurocode 4 (CEN 2005), BS 5400 (BSI 1980), and JSCE (2009). Because the BS 5400 (BSI 1980) and JSCE (2009) take the concrete strength into account for their design equations, the nominal strength of the concrete of 4000 psi and stud dimensions for the $^{7}/_{8}$"-diameter studs were used to calculate the static strengths. Figure 5-2 shows the four design curves from the different codes, a mean curve from the test results, and a design curve for the test results that was obtained by shifting the mean curve by 1.96 sample standard deviations. So that a fair comparison is made amongst the different codes, these curves were all based on the design curves for each respective code. The only curve that cannot be directly compared to the design codes is the curve for the mean of the test results. This curve is solely based on the mean of the data and gives a 50% probability of failure.

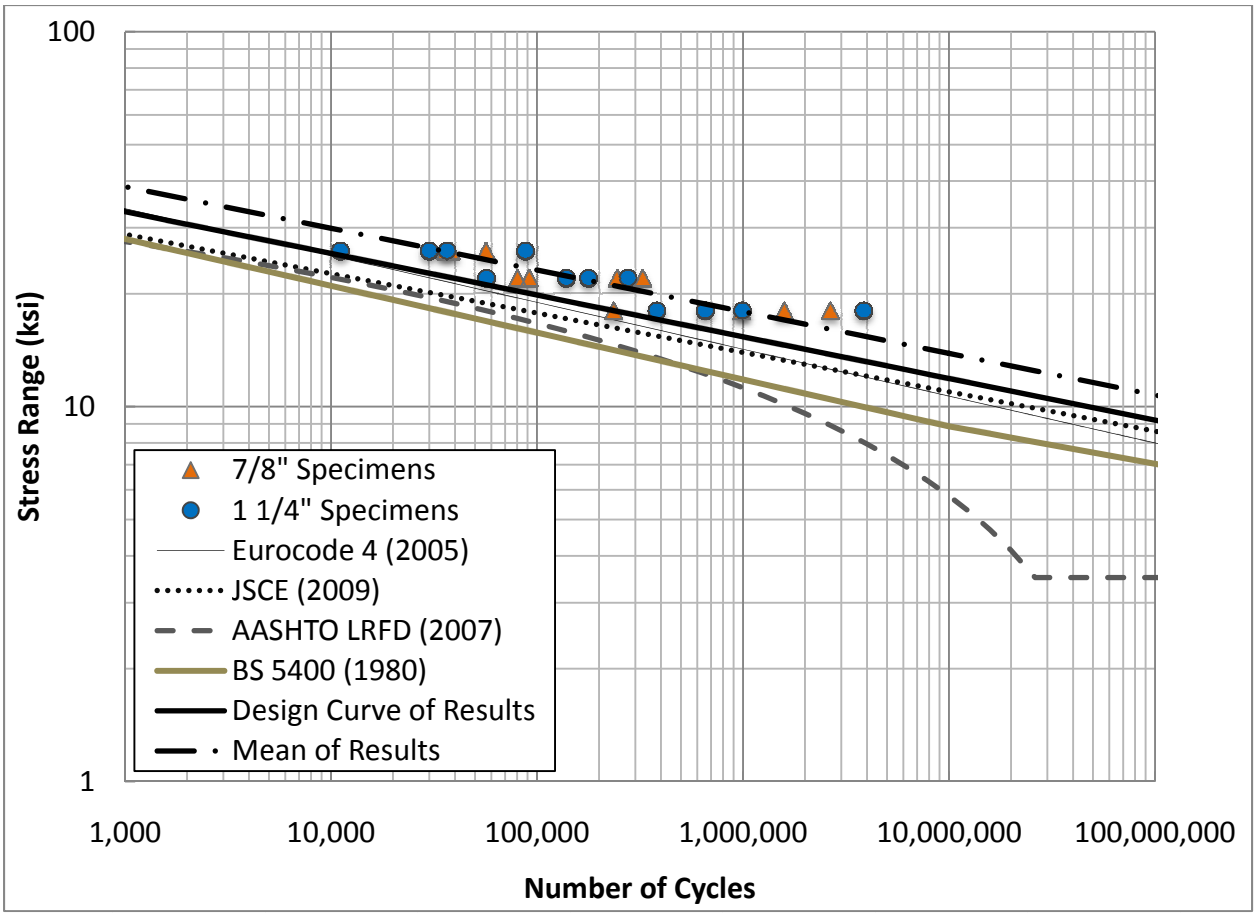

Figure 5-2 Graphical Comparison of Results to Design Codes

The equations that the design lines in Figure 5-2 were derived from were also used to give numerical values to show the differences in design codes. For given stress ranges of 5, 10, and 15 ksi, the expected number of cycles for each design and for the mean curve from the test data are tabulated in Table 5-1.

Table 5-1 Tabulated Comparison of Results to Design Codes

Stress Range (ksi)	AASHTO LRFD (2007)	Eurocode 4 (2005)	JSCE (2009)	BS 5400 (1980)	Design Line of Results	Mean Line of Results
5	13,900,000	4,310,000,000	17,600,000,000	3,070,000,000	24,200,000,000	96,800,000,000
10	1,680,000	16,800,000	23,900,000	3,790,000	47,500,000	190,000,000
15	203,000	656,000	502,000	147,000	1,240,000	4,960,000

By using both Figure 5-2 and Table 5-1 it is quite apparent that there are significant differences in design codes. The design curve from AASHTO (2007) shows the largest difference mainly due to the downward curve. This becomes the most significant when designing at lower stress ranges as can be seen from the values in Table 5-1. Also, it is important to note that designing at the lower stress ranges for a larger number of cycles is the applicable region of design for most interstate highway bridges in the U.S.

5.4 Test Data Scatter

Because of the nature of fatigue testing, there is always a large scatter in the data, but much of the scatter from this test program is thought to be explained by two factors. The first factor is the variation in concrete strength. The second factor that explains the scatter of the data is the variation in the quality of the weld fusion between the stud and the beam flange. Some of the specimens that had short fatigue lives compared to other specimens tested at the same stress range showed evidence of incomplete fusion at the interface between the stud and beam flange. This could have resulted in much faster propagation of fatigue cracks which caused the specimen to fail much earlier resulting in a wide scatter of the data.

As was explained previously in Chapter 2, concrete strength is thought to have little to no impact or influence on the fatigue life of shear studs. Neither the AASHTO (2007) nor Eurocode 4 (CEN 2005) equations for fatigue life include concrete strength as one of the parameters, and the JSCE (2009) did not include concrete strength until a recent code revision in 2009.

Although concrete strength was not a variable to be tested for this research program, because the specimens had to be poured at three different times resulting in three different

concrete strengths, the test matrix was set up so that the influence of concrete strength could be examined.

Mix 1 was the first concrete batch that was poured and resulted in being the intermediate strength concrete. Mix 2 was the second concrete batch that was poured and resulted in being the lowest strength concrete. Finally, Mix 3 was the third concrete batch that was poured and resulted in being the highest strength concrete. For the remainder of this section, these mixes will be referred to based on strength as highest strength (HS), intermediate strength (IS) and lowest strength (LS).

All push-out tests were conducted when their concrete age was between 6 months and 1 year. Between this time, the strength of the concrete does not change much and therefore compressive strength will be assumed to be equal to that of the 6 month compression tests. Average values for both the moist-cured and lab-cured strength at 6 months are given in Table 5-2 for each concrete batch.

Table 5-2 Six-Month Average Concrete Strengths

Concrete Batch	6 Month Moist-Cured (psi)	6 Month Lab-Cured (psi)
Highest Strength (HS)	8130	5460
Intermediate Strength (IS)	7550	5100
Lowest Strength (LS)	6560	4360

To show the role that concrete strength plays in fatigue life of push-out specimens, an S-N curve was plotted with the different data points representing the highest strength (HS), intermediate strength (IS), and lowest strength (LS) concrete. One observation to be noted from Figure 5-3 is that the highest strength (HS) concrete batch resulted in the longest fatigue life for each size stud and each stress range. There is still a large amount of scatter in the data which makes it hard to draw definite conclusions, but it can't be ignored that the concrete strength

could have an influence on the fatigue life. Overall, the concrete strength does seem to have a small influence on the fatigue life of push-out specimens, but in order to gain more understanding of this effect, a more comprehensive test program should be carried out and focused solely on varying the concrete strength.

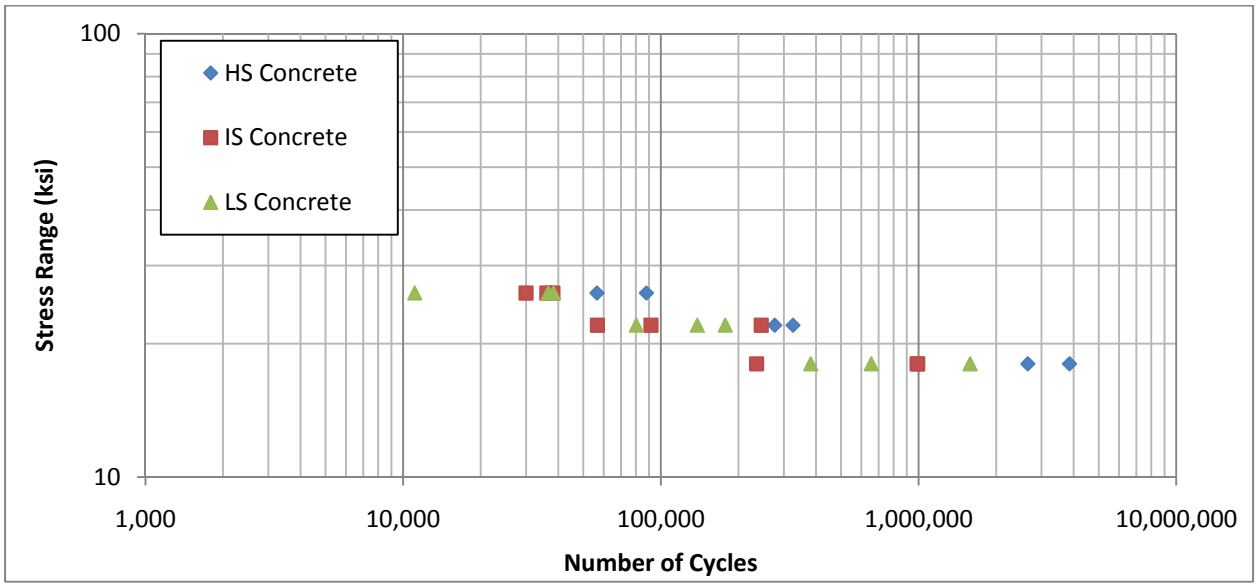

Figure 5-3 S-N Curve Showing Influence of Concrete Strength

Chapter 6 SUMMARY, CONCLUSIONS, AND RECOMMENDATIONS

6.1 Summary

Many highway bridge decks in the United States are nearing the end of their design life and are in need of being replaced. Due to the large volume of vehicular traffic using these bridges daily, replacing the concrete decks without interruption of the flow of traffic presents a difficult challenge. One of the factors that makes removing the old bridge deck so difficult is the large number of shear studs that hold the concrete bridge deck to the steel girders. By using larger diameter shear studs, fewer shear studs would be required for design therefore saving time and labor in both rehabilitation efforts and new construction.

In this thesis, experimental research was performed at Auburn University on push-out specimens to evaluate the fatigue life of large diameter shear studs in comparison to standard diameter shear studs that are currently used in composite highway bridges. Large diameter studs are seldom used and therefore require testing to determine their adequacy before being included in design codes.

Based on the research presented within this thesis, it was found that there is no significant difference in the fatigue life of the large diameter and standard diameter shear studs. There was, however, a large discrepancy in the fatigue life predicted by AASHTO (2007) and the actual results that were generated, especially for low stress ranges. From the information gathered from this test program, it was determined that large diameter shear studs can be designed according to the current design criteria in AASHTO (2007).

6.2 Conclusions

The research contained in this thesis compares the fatigue life of push-out specimens with $^{7}/_{8}$"-diameter studs to push-out specimens with 1¼"-diameter shear studs. It also compares the results from this test program to four design codes. After these comparisons were performed, the following conclusions were made:

- By using an electric current of approximately 2700 amps and a weld time of approximately 1.8 seconds, 1¼"-diameter shear studs can be welded with the same quality as that of $^{7}/_{8}$"-diameter shear studs.
- The linear regression equations for the $^{7}/_{8}$"-diameter and 1¼"-diameter specimens were essentially the same, but the standard deviation was slightly larger for the 1¼"-diameter specimens.
- At higher stress ranges, the fatigue crack usually initiated at the weld collar. At lower stress ranges the fatigue crack more frequently initiated at the weld toe and propagated down into the base material.
- The semi-log fatigue design equation in AASHTO (2007) significantly underestimates the fatigue life of shear studs, especially at low stress ranges.
- The compressive strength of the concrete was found to have an influence on the fatigue life of shear studs.
- The fatigue design equation in AASHTO (2007) can safely be used for designing composite highway bridges using 1¼"-diameter shear studs.

6.3 Recommendations

Based on the results from the test program and the conclusions made above, the following recommendations are suggested to the Alabama Department of Transportation (ALDOT):

- When using large diameter studs, use the same geometry of 1¼"-diameter shear studs provided in Appendix A. Further geometrical requirements in AASHTO (2007) must also be satisfied.
- For automatically welding 1¼"-diameter headed shear studs, use a stud welder capable of providing a current of approximately 2700 amps and a weld time of approximately 1.8 seconds to achieve weld quality similar to what was used for this test program.
- The fatigue design provisions in AASHTO (2007) can safely be used to design large diameter shear studs.

In addition, the following recommendations of further research were determined:

- Perform fatigue testing of full scale composite beams to determine if there are any significant differences when compared to push-out specimens
- Perform static testing on push-out specimens to determine if the use of large diameter studs has any effect on the ultimate strength.
- It is recommended to carry out a more comprehensive test program to evaluate the effect of concrete strength on the fatigue life of shear studs.
- Re-evaluate the semi-log model used for fatigue design of stud shear connectors in AASHTO (2007).

References

AASHTO (1996) *AASHTO Standard Specifications for Highway Bridges*, 16th edition. Washington, D.C.

AASHTO (1998). *AASHTO LRFD Bridge Design Specifications*, 2nd edition. Washington, D.C.

AASHTO (2004). *AASHTO LRFD Bridge Design Specifications*, 3rd edition. Washington, D.C.

AASHTO (2007). *AASHTO LRFD Bridge Design Specifications*, 4th edition. Washington, D.C.

Ahn, J. H., Kim, S. H., and Jeong, Y. J. (2007). "Fatigue experiment of stud welded on steel plate for a new bridge deck system." *Steel and Composite Structures*, 7(5), 391-404.

Badie, S. S., Tadros, M. K., Kakish, H. F., Splittgerber, D. L., and Baishya, M. C. (2002). "Large shear studs for composite action in steel bridge girders." *Journal of Bridge Engineering ASCE*, 7(3), 195-203.

BSI (1980). BS5400 steel, concrete and composite bridges. Part 10: *Code of practice for fatigue*. London, England.

BSI (2005). BS5400 steel, concrete and composite bridges. Part 5: *Code of practice for design of composite bridges*. London, England.

Bro, Markus., and Westberg, Marie. (2004). *Influence of Fatigue on Headed Stud Connectors in Composite Bridges*. M.S. Thesis, Lulea University of Technology.

CEN (1993). 1993-1-9 Eurocode 3. Design of steel structures, *Fatigue*.

CEN (1997). 1994-2 Eurocode 4. Design of Composite Steel and Concrete Structures., *General rules and rules for bridges*.

CEN (2005). 1994-2 Eurocode 4. Design of Composite Steel and Concrete Structures., *General rules and rules for bridges*.

Chambers, H. A., (2001). “Principles and Practices of Stud Welding.” *PCI Journal.* 46-58.

Champney, C., and Hsu, C. (2009). “Stud Welding of Shear Connectors on Bridges.”

Fisher, J. W., Kulak, G. L., and Smith, I. F. C. (1998). “A Fatigue Primer for Structural Engineers.” National Steel Bridge Alliance.

Hallam, M. W. (1976). "The behavior of stud shear connectors under repeated loading." *Research Report No. R281,* School of Civil Engineering, The University of Sydney.

Hanswille, G., Porsch, M., and Ustundag, C. (2007). "Resistance of headed studs subjected to fatigue loading Part I: Experimental study." *Journal of Constructional Steel Research*, 63(4), 475-484.

JSCE Committee on Hybrid Structures (Subcommittee on Standard Specifications), *Standard Specifications for Hybrid Structures*, JSCE, 2009 (in Japanese).

JSSC (1995). *Fatigue Design Recommendations for Steel Structures*. Gihodo Shuppan.

Lee, P. G., Shim, C. S., and Chang, S. P. (2005). "Static and fatigue behavior of large stud shear connectors for steel-concrete composite bridges." *Journal of Constructional Steel Research*, 61, 1270-1285.

Mainstone, R. J., and Menzies, J. B. (1967a). "Shear connectors in steel-concrete composite beams for bridges. 1. Static and fatigue tests on push-out specimens." *Concrete*, 1(9), 291-302.

Oehlers, D. J. (1990). "Deterioration in strength of stud connectors in composite bridge beams." *Journal of Structural Engineering ASCE*, 116(12), 3417-3431.

Roberts, T. M., and Dogan, O. (1998). "Fatigue of welded stud shear connectors in steel-concrete-steel sandwich beams." *Journal of Constructional Steel Research*, 45(3), 301-320.

Roderick, J. W., and Ansourian, P. (1976). "Repeated loading of composite beams." *Research Report No. R280*, School of Civil Engineering, The University of Sydney.

Slutter, R. G., and Fisher, J. W. (1966). "Fatigue strength of shear connectors." Highway *Research Record No. 147*, National Research Council, Washington, D.C.

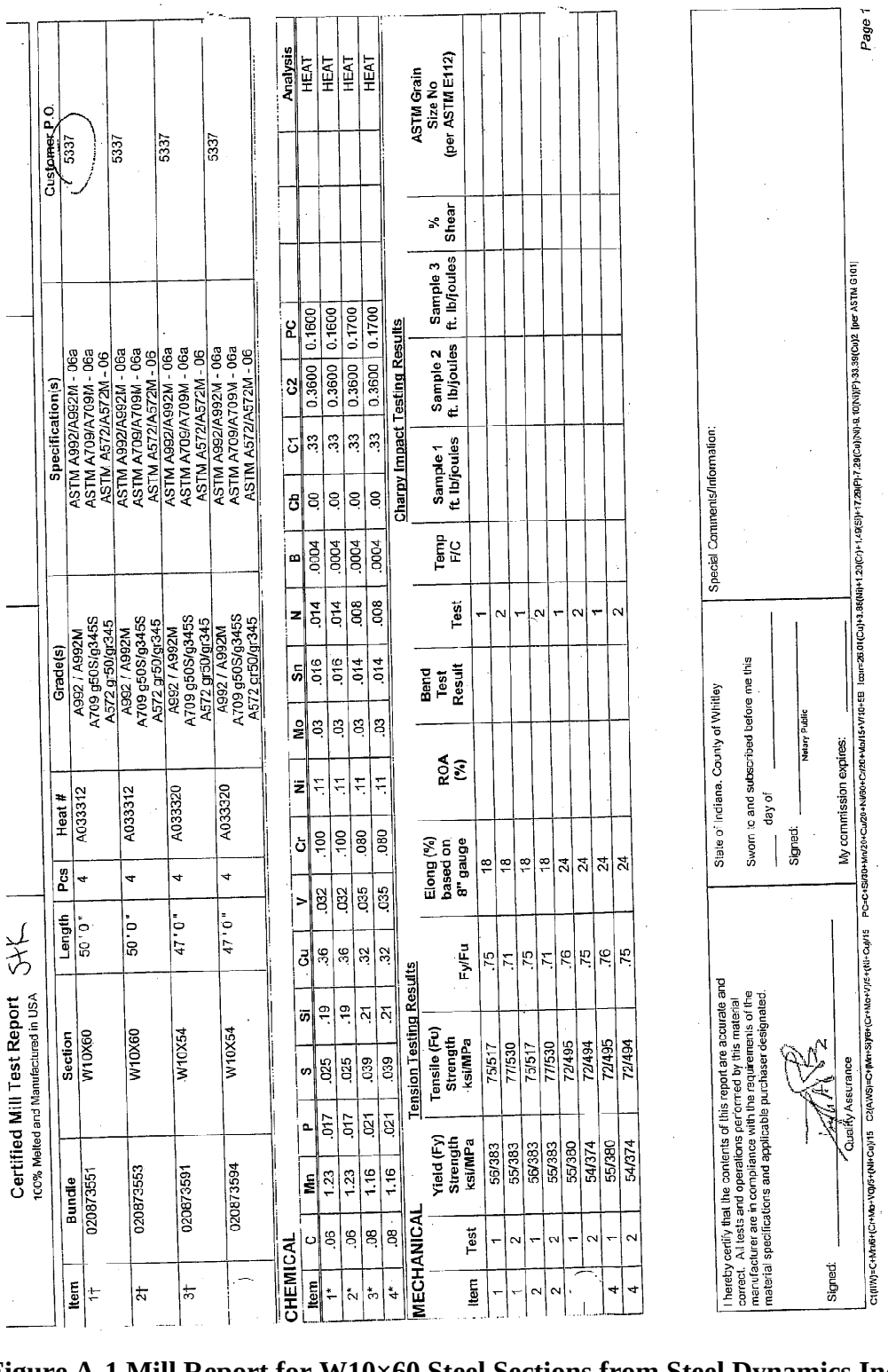

Certified Mill Test Report SK

100% Melted and Manufactured in USA

Item	Bundle	Section	Length	Pcs	Heat #	Grade(s)	Specification(s)	Customer P.O.
1†	020873551	W10X60	50' 0"	4	A033312	A992 / A992M A709 gr50S/gr345S A572 gr50/gr345	ASTM A992/A992M - 06a ASTM A709/A709M - 06a ASTM A572/A572M - 06	5337
2†	020873553	W10X60	50' 0"	4	A033312	A992 / A992M A709 gr50S/gr345S A572 gr50/gr345	ASTM A992/A992M - 06a ASTM A709/A709M - 06a ASTM A572/A572M - 06	5337
3†	020873591	W10X54	47' 0"	4	A033320	A992 / A992M A709 gr50S/gr345S A572 gr50/gr345	ASTM A992/A992M - 06a ASTM A709/A709M - 06a ASTM A572/A572M - 06	5337
4*	020873594	W10X54	47' 0"	4	A033320	A992 / A992M A709 gr50S/gr345S A572 gr50/gr345	ASTM A992/A992M - 06a ASTM A709/A709M - 06a ASTM A572/A572M - 06	5337

CHEMICAL

Item	C	Mn	P	S	Si	Cu	V	Cr	Ni	Mo	Sn	N	B	Cb	C1	C2	PC			Analysis
1*	.06	1.23	.017	.025	.19	.36	.032	.100	.11	.03	.016	.014	.0004	.00	.33	0.3600	0.1600			HEAT
2*	.06	1.23	.017	.025	.19	.36	.032	.100	.11	.03	.016	.014	.0004	.00	.33	0.3600	0.1600			HEAT
3*	.08	1.16	.021	.039	.21	.32	.035	.080	.11	.03	.014	.008	.0004	.00	.33	0.3600	0.1700			HEAT
4*	.08	1.16	.021	.039	.21	.32	.035	.080	.11	.03	.014	.008	.0004	.00	.33	0.3600	0.1700			HEAT

MECHANICAL — Tension Testing Results — Charpy Impact Testing Results

Item	Test	Yield (Fy) Strength ksi/MPa	Tensile (Fu) Strength ksi/MPa	Fy/Fu	Elong (%) based on 8" gauge	ROA (%)	Bend Test Result	Test	Temp F/C	Sample 1 ft. lb/joules	Sample 2 ft. lb/joules	Sample 3 ft. lb/joules	% Shear	ASTM Grain Size No (per ASTM E112)
1	1	55/383	75/517	.75	18			1						
1	2	55/383	77/530	.71	18			2						
2	1	56/383	75/517	.75	18			1						
2	2	55/383	77/530	.71	18			2						
3	1	55/380	72/495	.76	24			1						
3	2	54/374	72/494	.75	24			2						
4	1	55/380	72/495	.76	24			1						
4	2	54/374	72/494	.75	24			2						

I hereby certify that the contents of this report are accurate and correct. All tests and operations performed by this material manufacturer are in compliance with the requirements of the material specifications and applicable purchaser designated.

Signed: _____ Quality Assurance

State of Indiana, County of Whitley

Sworn to and subscribed before me this ____ day of _____

Signed: _____ Notary Public

My commission expires: _____

Special Comments/Information:

Page 1

C1(IIW)=C+Mn/6+(Cr+Mo+V)/5+(Ni+Cu)/15 C2(AWS)=C+(Mn+Si)/6+(Cr+Mo+V)/5+(Ni+Cu)/15 PC=C+Si/30+Mn/20+Cu/20+Ni/60+Cr/20+Mo/15+V/10+5B Ideal=25.01(Cu)+3.86(Ni)+1.23(Cr)+1.(-95.5)+17.28(P)-7.29(Cu)(Ni)-9.10(Ni)(P)-33.39(Cu)2 [per ASTM G101]

Figure A-1 Mill Report for W10×60 Steel Sections from Steel Dynamics Inc.

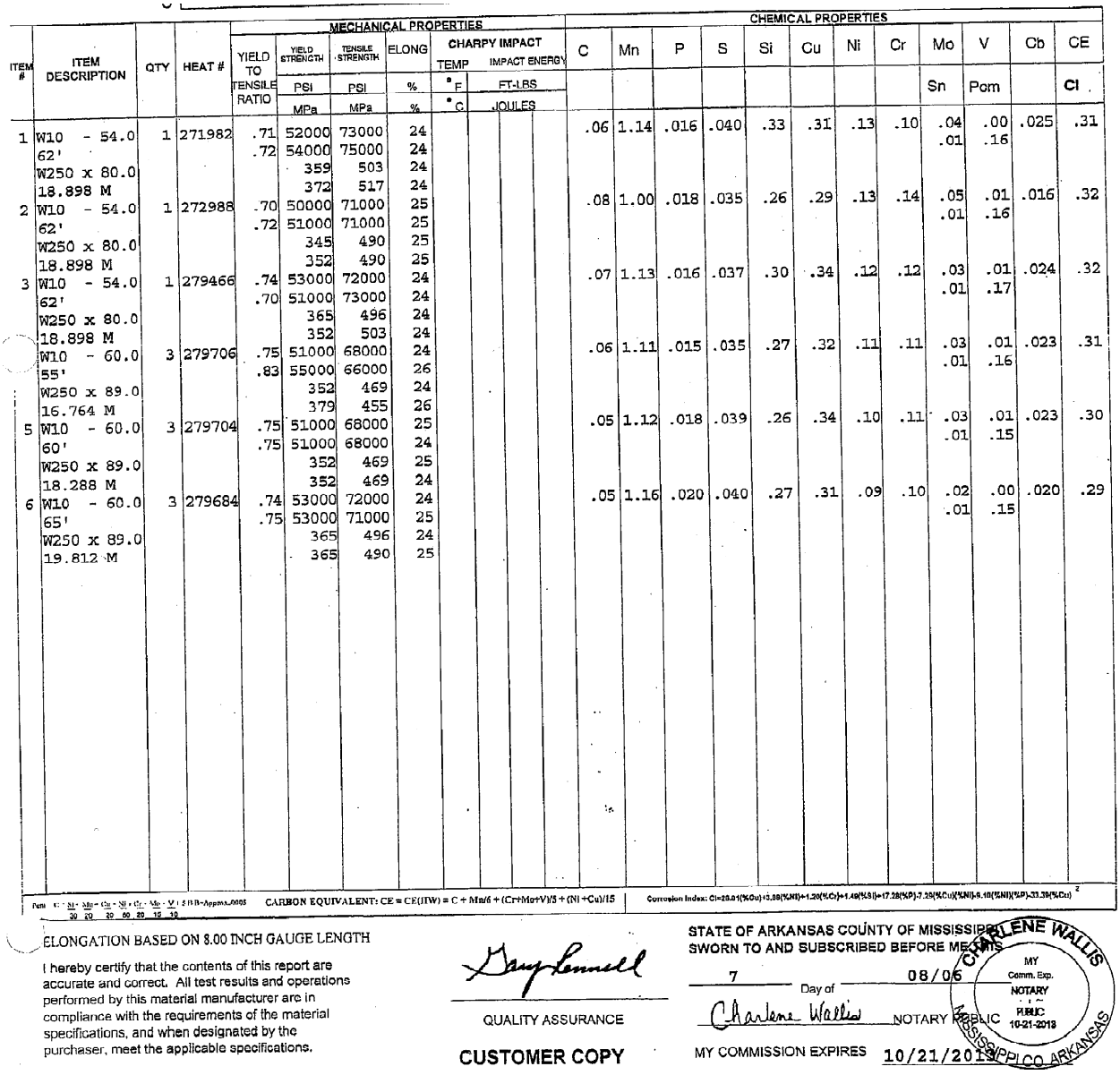

ITEM #	ITEM DESCRIPTION	QTY	HEAT #	MECHANICAL PROPERTIES: YIELD TO TENSILE RATIO	YIELD STRENGTH PSI / MPa	TENSILE STRENGTH PSI / MPa	ELONG % / %	CHARPY IMPACT TEMP °F / °C	CHARPY IMPACT ENERGY FT-LBS / JOULES	CHEMICAL PROPERTIES: C	Mn	P	S	Si	Cu	Ni	Cr	Mo / Sn	V / Pcm	Cb	CE / Cl
1	W10 - 54.0	1	271982	.71	52000	73000	24			.06	1.14	.016	.040	.33	.31	.13	.10	.04	.00	.025	.31
	62'			.72	54000	75000	24											.01	.16		
	W250 x 80.0				359	503	24														
	18.898 M				372	517	24														
2	W10 - 54.0	1	272988	.70	50000	71000	25			.08	1.00	.018	.035	.26	.29	.13	.14	.05	.01	.016	.32
	62'			.72	51000	71000	25											.01	.16		
	W250 x 80.0				345	490	25														
	18.898 M				352	490	25														
3	W10 - 54.0	1	279466	.74	53000	72000	24			.07	1.13	.016	.037	.30	.34	.12	.12	.03	.01	.024	.32
	62'			.70	51000	73000	24											.01	.17		
	W250 x 80.0				365	496	24														
	18.898 M				352	503	24														
	W10 - 60.0	3	279706	.75	51000	68000	24			.06	1.11	.015	.035	.27	.32	.11	.11	.03	.01	.023	.31
	55'			.83	55000	66000	26											.01	.16		
	W250 x 89.0				352	469	24														
	16.764 M				379	455	26														
5	W10 - 60.0	3	279704	.75	51000	68000	25			.05	1.12	.018	.039	.26	.34	.10	.11	.03	.01	.023	.30
	60'			.75	51000	68000	24											.01	.15		
	W250 x 89.0				352	469	25														
	18.288 M				352	469	24														
6	W10 - 60.0	3	279684	.74	53000	72000	24			.05	1.16	.020	.040	.27	.31	.09	.10	.02	.00	.020	.29
	65'			.75	53000	71000	25											.01	.15		
	W250 x 89.0				365	496	24														
	19.812 M				365	490	25														

Pcm = C + Si/30 + Mn/20 + Cu/20 + Ni/60 + Cr/20 + Mo/15 + V/10 + 5B ASTM A-Approx.0005

CARBON EQUIVALENT: CE = CE(IIW) = C + Mn/6 + (Cr+Mo+V)/5 + (Ni+Cu)/15

Corrosion Index: CI=26.01(%Cu)+3.88(%Ni)+1.20(%Cr)+1.49(%Si)+17.28(%P)-7.29(%Cu)(%Ni)-9.10(%Ni)(%P)-33.39(%Cu)^2

ELONGATION BASED ON 8.00 INCH GAUGE LENGTH

I hereby certify that the contents of this report are accurate and correct. All test results and operations performed by this material manufacturer are in compliance with the requirements of the material specifications, and when designated by the purchaser, meet the applicable specifications.

QUALITY ASSURANCE

CUSTOMER COPY

STATE OF ARKANSAS COUNTY OF MISSISSIPPI
SWORN TO AND SUBSCRIBED BEFORE ME THIS
7 Day of 08/06
Charlene Wallis NOTARY PUBLIC
MY COMMISSION EXPIRES 10/21/2013

CHARLENE WALLIS MY Comm. Exp. NOTARY PUBLIC 10-21-2013 MISSISSIPPI CO. ARKANSAS

Figure A-2 Mill Report for W10×60 Steel Section from Nucor-Yamato Steel Co.

PO-7129
Stock

NUCOR
PLATE MILL

P.O.Box 279
Winton, NC 27986
(252) 356-3700

Mill Test Report

Page 1

NUCOR It's our Nature.

Issuing Date : 08/24/2009 B/L No. : 237407 Load No. : 239128 Our Order No. : 74977/1 Cust. Order No. : FSE-16230

Vehicle No: 8256

Specification : 0.7500" x 120.000" x 240.000"
ASTM A572 Grade 50-07/ASTM A709 Grade 50-09/AASHTO M270-50
Type 2

Sold To : Macsteel Service Centers USA Inc
2005 GRASSLAND PARKWAY
ALPHARETTA,GA 30004

Ship To : FERRO UNION SOUTHEAST, INC.
2005 GRASSLAND PARKWAY
ALPHARETTA,GA 30004

Marking :

Heat No	C	Mn	P	S	Si	Cu	Ni	Cr	Mo	Al(tot)	V	Nb	Ti	N	Ca	B	Sn	CEQ	PCM
9104300	0.18	1.00	0.016	0.004	0.19	0.25	0.08	0.13	0.02	0.009	0.028	0.002	0.001		0.0013	0.0003	0.012	0.41	0.27

Tensile Test								Charpy Impacts											
Plate Serial No	Pieces	Tons	Dir.	(psi) Yield	(psi) Tensile	Elongation % in 2"	Elongation % in 8"	Dir.	1	(%) shear	2	(%) shear	3	(%) shear	Ave.	(%) shear	Size	Temp	Min Ave.
9104300-01	2	6.12	T	54,700	78,200		16.2												
			T	51,500	65,600		20.9												
9104300-04	5	15.31	T	54,700	78,200		16.2												
			T	51,500	65,600		20.9												

Manufactured to fully killed practice by Electric Arc Furnace. Welding or weld repair was not performed on this material.
Mercury has not been used in the direct manufacturing of this material. Produced as continuous cast discrete plate as-rolled, unless otherwise noted in Specification.
Yield by 0.5EUL method unless otherwise specified. Ceq = C+(Mn/6)+((Cr+Mo+V)/5)+((Cu+Ni)/15)
Pcm = C+(Si/30)+(Mn/20)+(Cu/20)+(Ni/60)+(Cr/20)+(Mo/15)+(V/10)+5B
Melted and manufactured in the USA. ISO 9001-2000 certified (#006461) by SRI Quality System Registrar (#0985-09). PED 97/23/EC 7/2 Annex 1, Para. 4.3 Compliant.
DIN 50049 3.1.B/EN 10204 3.1B(2004), DIN EN 10204 3.1(2005) compliant. For ABS grades only, Quality Assurance certificate 06-MMPQA-383

We hereby certify that the contents of this report are accurate and correct. All test results and operations performed by the material manufacturer are in compliance with the applicable specifications, including customer specifications.

T. A. Depretis

T. A. Depretis, Metallurgist

08/24/2009 11:43:04 AM

Figure A-3 Mill Report for ¾" Thick Steel Plate for Bend Testing Studs

Appendix A-2: Shear Stud Specifications

CERTIFICATION

THIS IS TO CERTIFY THAT THE WELD STUDS SUPPLIED TO YOUR
PURCHASE ORDER 19815 , SHIPMENT NO. 140754 DATED 02/18/2010
HAVE BEEN MANUFACTURED IN ACCORDANCE WITH STANDARD AASHTO/AWS D1.1/D1.5-04
SPECIFICATIONS, OF MATERIAL CONFORMING TO ASTM-A108-07/A29 LOW CARBON STEEL
HAVING THE FOLLOWING CHEMICAL COMPOSITION AND PHYSICAL PROPERTIES:

HEAT NO.	415130
GRADE	C1015
CARBON	.150 %
MANGANESE	.490 %
PHOSPHOROUS	.012 %
SULPHUR	.008 %
REFERENCE	TW06-146
ULTIMATE	68118 PSI
	470 N/mm2
YIELD	52839 PSI
	364 N/mm2
REDUCTION OF AREA	59.0
ELONGATION	25.0

415130
STUDS PASSED BEND TEST.
MACHINED SPECIMEN.

MECHANICAL PROPERTIES ABOVE ARE DERIVED FROM FINISHED PRODUCT.
TFP CORP. CERTIFIES THAT THIS IS A COPY OF THE ORIGINAL MECHANICAL
CERTIFICATION ON FILE, THAT THIS PRODUCT IS MELTED AND MANUFACTURED
IN THE U.S.A., AND IS FREE FROM MERCURY CONTAMINATION.

BY:
TRU-WELD DIVISION
TFP CORPORATION

Figure A-4 Certification and Chemical Composition of 1¼"- Diameter Studs

CERTIFICATION

THIS IS TO CERTIFY THAT THE WELD STUDS SUPPLIED TO YOUR
PURCHASE ORDER 19815 , SHIPMENT NO. 140754 DATED 02/18/2010
HAVE BEEN MANUFACTURED IN ACCORDANCE WITH STANDARD AASHTO/AWS D1.1/D1.5-04
SPECIFICATIONS, OF MATERIAL CONFORMING TO ASTM-A108-07/A29 LOW CARBON STEEL
HAVING THE FOLLOWING CHEMICAL COMPOSITION AND PHYSICAL PROPERTIES:

HEAT NO.	10023530
GRADE	C1015
CARBON	.160 %
MANGANESE	.470 %
PHOSPHOROUS	.006 %
SULPHUR	.012 %
REFERENCE	TW09-250
ULTIMATE	70677 PSI
	487 N/mm2
YIELD	56957 PSI
	393 N/mm2
REDUCTION OF AREA	58.7
ELONGATION	29.7

10023530
STUDS PASSED BEND TEST.

MECHANICAL PROPERTIES ABOVE ARE DERIVED FROM FINISHED PRODUCT.
TFP CORP. CERTIFIES THAT THIS IS A COPY OF THE ORIGINAL MECHANICAL
CERTIFICATION ON FILE, THAT THIS PRODUCT IS MELTED AND MANUFACTURED
IN THE U.S.A., AND IS FREE FROM MERCURY CONTAMINATION.

BY: Susan Ballew

TRU-WELD DIVISION
TFP CORPORATION

Figure A-5 Certification and Chemical Composition of $^{7}/_{8}$"- Diameter Studs

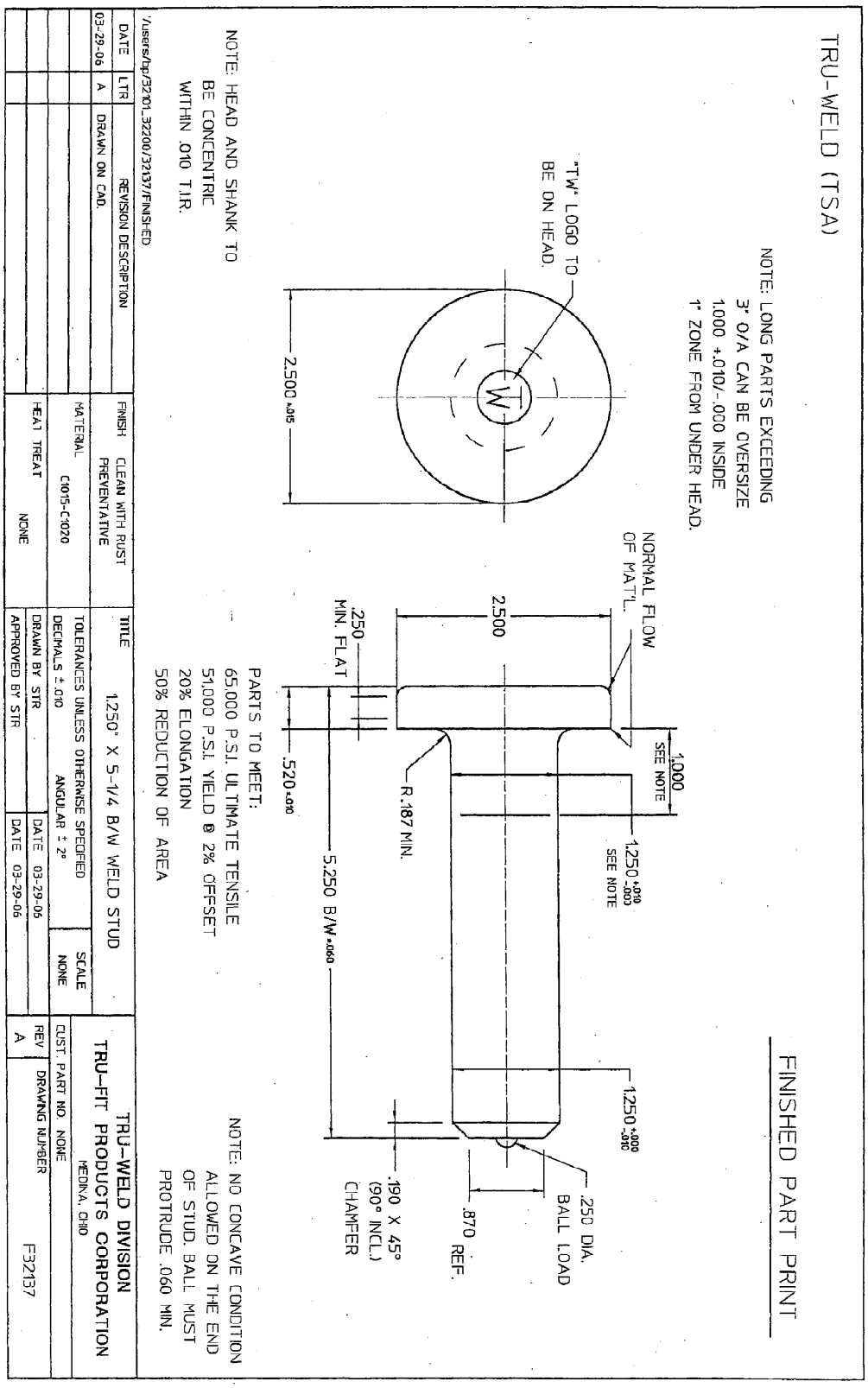

Figure A-6 Geometric Specifications for 1¼"- Diameter Stud